Department of Electrical and Computer Engineering
Lisbon, Portugal

Faculty of Electronics and Information Technology
Warsaw, Poland

Impact of the directional channel in adaptive beamforming for UMTS-FDD in macro-cells

Tomasz Szymański

Lisbon, Portugal
September 2002

Under the supervision of:

Prof. Luis M. Correia

Department of Electrical and Computer Engineering
Instituto Superior Tecnico, Technical University of Lisbon
Portugal

Acknowledgments

Firstly I want to thank Professor Luis M. Correia for giving me chance to work in his team, having always time, patience and sharing his professional and human wisdom.

Thanks to João Gil for help, sharing his work and knowledge, not only about antenna technology, but also about life and entertainment.

I want to thank to all my colleagues who surrounded me with friendly and nice atmosphere, which was of great importance for me during such long stay abroad. In particular I want to thank to my “roommate” Jorge and Gabriela for keeping delightful spirit and helping me every time when I needed, but also others that I am not able to mention all.

I want to thank Agnieszka for love, patience, trust and everything that she has done for me during this time, and to my family for belief, support and love that they were constantly showing me despite thousands of kilometres separating us.

I want to thank to dr Tomasz Buczkowski and dr Tomasz Kosiło for making this studies possible and their great help.

Finally I want to thank to “Fundacja Wspierania Rozwoju Radiokomunikacji i Technik Multimedialnych” for support with scholarship which made this studies possible.

Thanks to all other people that I met or already known, but I didn’t mentioned by name.

Abstract

The report deals with non-blind adaptive beamforming using linear and circular antenna arrays in macro-cellular scenarios for the UMTS FDD mode. Wideband directional channel model, based on the Geometrically Based Single Bounced Model has been implemented to simulate the transmission environment. Applied Conjugate Gradients adaptive algorithm sets the weights for a beamformer consisting of uniform linear or circular arrays. Several scenarios, characterised by different mobile terminal placement and groupings, mobile to base station distance or radius of scatterers around each mobile terminal have been examined. Simulations mainly aim to investigate the impact of various parameters on the beamforming gain, giving an overall view on the conditions favouring the use of smart antennas or obstructing it. It has been verified that distance between mobile terminal and base station has an impact on the beamforming, as well as the number of users and radius of scatterers region around the mobile, however terminal placement and grouping having the major influence on beamforming gain. Since the distance modifies the beamforming gain values by the order of several dB, as well as the number of users and scattering circle radius do (inside the limits of the values used in simulations), terminal placement and grouping can modify beamforming gain values by 20-30 dB, which emphasises the importance of the latter parameter in beamforming applications.

Keywords

UMTS, Smart antennas, Beamforming, Conjugate Gradient, Wideband Directional Channel Model,

Table of Contents

List of Figures

List of Tables

List of Acronyms

π/4- DQPSK	π/4-Differencial Quadrature Phase Shift Keying
3G	Third Generation
3GPP	3rd Generation Partnership Project
AF	Array Factor
AoA	Angle of Arrival
BG	Beamforming Gain
BER	Bit Error Rate
BoD	Bandwidth on Demand
BS	Base Station
BU	Bad Urban
CDMA	Code Division Multiple Access
CG	Conjugate Gradient
CGNR	CG Normal Equation Residual
CLPC	Closed Loop Power Control
CN	Core Network
COST	European Co-operation in the Field of Scientific and Technical Research
DCIR	Directional Channel Impulse Response
DECT	Digital Enhanced Cordless Telephone
DesS	Desired Signal
DL	Downlink
DoA	Direction-of-Arrival
DPCCH	Dedicated Physical Control Channel
DPDCH	Dedicated Physical Data Channel
DS-CDMA	Direct Sequence Code Division Multiple Access
ETSI	European Telecommunications Standards Institute
FDD	Frequency Division Duplex
FDMA	Frequency Division Multiple Access
FER	Frame Error Rate
FM	Frequency Modulation
FSK	Frequency Shift Keying
GAA	Gaussian Angle of Arrival
GBSB	Geometrically Based Single Bounce
GBSBCM	Geometrically Based Single Bounce Circular Model
GBSBEM	Geometrically Based Single Bounce Elliptical Model
GPS	Global Positioning System
GPs	General Parameters
GSM	Global System for Mobile Communications

GWSSUS	Gaussian Wide Sense Stationary Uncorrelated Scattering
HPBW	Half-Power Bandwidth
HS-DPCCH	High Speed DPCCH
IMT-2000	International Mobile Telecommunications 2000
IS-95	Interim Standard – 95
ITU	International Telecommunication Union
LCMV	Linear Constrained Minimum Variance
LMS	Least Mean Squares
LoS	Line of Sight
LPs	Local Parameters
MAC	Medium Access Control
ME	Mobile Equipment
MMSE	Minimum Mean Square Error
MSC	Multi Sidelobe Canceller
MT	Mobile Terminal
NB	Narrowband
NDesI	Non-Desired Interference
OLPC	Open Loop Power Control
OVSF	Orthogonal Variable Spreading Factor
PC	Power Control
PCS	Personal Communication System
PDF	Probability Density Function
PHS	Personal Handyphone System
PSK	Phase Shift Keying
QAM	Quadrature Amplitude Modulation
QoS	Quality of Service
RE	Radio Environment
RF	Radio Frequency
RLC	Radio Link Control
RLS	Recursive Least Squares
RNC	Radio Network Controller
RNS	Radio Network Subsystem
RRC	Radio Resource Control
SAP	Service Access Point
SCORE	Self COherence REstoral
SDMA	Space Division Multiple Access
SF	Spreading Factor
SINR	Signal-to-Interference-plus-Noise-Ratio
SIR	Signal-to-Interference-Ratio
SMI	Sample Matrix Inversion
SNoI	Signal-Not-of-Interest

SNR	Signal-to-Noise-Ratio
SoI	Signal-of-Interest
TDD	Time Division Duplex
TDMA	Time Division Multiple Access
ToA	Time of Arrival
TPC	Transmit Power Control
TU	Typical Urban
UCA	Uniform Circular Array
UE	User Equipment
UL	Uplink
ULA	Uniform Linear Array
UMTS	Universal Mobile Telecommunications System
USIM	User Services Identity Module
UTRA	Universal Terrestrial Radio Access (3GPP), UMTS Terrestrial Radio Access (ETSI)
UTRAN	Universal Terrestrial Radio Access Network
VCIR	Vector Channel Impulse Response
WB	Wideband
WCDMA	Wideband Code Division Multiple Access
WDCM	Wideband Directional Channel Model

List of Symbols

α	step size of conjugate gradient algorithm
β	R-orthogonality factor.
l	wavelength
q	azimuthal angle
f	horizontal angle
Δt	ToA spread
Δf_{NB}	narrowband AoA spread
Δf_{WB}	wideband AoA spread
$(\ldots)^{\mathrm{H}}$	Hermitan transpose
f_0	MT angular position
f_{BW}	angle distribution
s_{dB}	Standard deviation
m_{dB}	mean value
∇f	gradient of the function f
$\tau_{\max}$	maximum time delay
y_{n}	phase excitation (relative to the array to the centre) of the nth element
f_{n}	angular position of nth element of UCA on x-y plane
Δ_{R}	radial range
$\mathbf{a}$	steering vector
$\mathbf{b}$	cross-correlation vector between the input data and desired signal
B_w	bandwidth
c	speed of light
C_{ch}	channelisation code
$\mathbf{c}_{\mathrm{l}}$	lth DesS code or sequence
c_{long}	long scrambling sequence
c_{short}	short scrambling sequence
d	distance
$\boldsymbol{d}$	desired/reference signal
$f(\mathbf{w})$	cost function
$\mathbf{g}$	direction vector
G_{bf}	Beamforming Gain
G_p	Processing Gain
$\mathbf{h}(\mathrm{t})$	impulse response vector
i	iteration index
K	number of concretisations
k	code number

k_{Boltz}	Boltzman constant
L	number of MT-BS links
M	number of array elements
N	number of matrix elements
N_s	number of baseband signal samples
N_{th}	noise power
pc_fact	Power Control factor
P_{DesS}	Desired Signal Power
P_{NDesI}	Non-Desired Interference Powers
$\mathbf{R}$	correlation matrix of the input data vector
$\mathbf{r}$	residual vector
r_{a}	antenna radius
r_{max}	radius of scatterers region
$S_{\mathrm{dpch,n}}$	scrambling code
t_n	time instant n
$\mathbf{U}$	channel matrix
$\mathbf{w}$	weights vector
X	average SINR/BG
$\mathbf{x}$	input signal vector
$x_{k,l}$	SINR or BG of lth link at kth concretisation
$\mathbf{y}$	output signal vector

1 Introduction

Mobile Communication is of interest to more and more people nowadays. The main idea is to provide services to every user, in every place of the world at every time of the day and night. Universal Mobile Telecommunications System (UMTS) is the next step in developing mobile communications after the success of Global System for Mobile Communications (GSM), and many engineers are working on making it a better, more intelligent, more efficient and reliable system than previous ones. Smart technologies are one of many ways to improve the system, at the antenna, receiver, and at the baseband processing levels, to gain capacity, coverage or quality.

Using smart antennas combined with adaptive algorithms to improve received, and transmitted signal quality, is one of the main problems for engineers to solve, because of the many advantages that it can provide. UMTS as a Wideband Code Division Multiple Access (WCDMA) system is in opposition to Frequency Division Multiple Access (FDMA) or Time Division Multiple Access (TDMA), noise-limited system, which means that although for FDMA limitation for number of users or coverage is the number of available radio channels, for WCDMA the limitation is noise level, or to be more precise Signal-to-Interference-plus-Noise-Ratio (SINR). For this reason, it is so important to gain as much as possible from the signals that one wants to receive/transmit, and suppress or cancel the ones that one does not need.

The target of this work is to simulate and analyse what scenario parameters, particularly channel parameters, are the most important in terms of beamforming, and which order of gains one can expect.

To achieve this target some initial assumptions and choices had to be made: UMTS has been assumed as the system that will be used in simulations. As a result of a closer analysis of this system, some issues were identified as important: one has to use proper frequencies, codes, and power control mechanisms. After that, one has to learn about the transmission medium, namely radio channel, that will be used, and how to model, or which model to use to take into account needed parameters. Already knowing the system and medium, one can analyse the beamformer system, meaning proper type of antenna, proper algorithm, depending on available input signals. Finally one has to learn how to feed the antenna, and the overall view is complete.

The work presented here explores utilisation of Adaptive Beamforming in UMTS in macro-cell environments for some specific scenario. The simulation environment has been prepared in MATLAB® for UMTS FDD mode, and a number of simulations has been performed. General conclusions are drawn on the basis of obtained results, main features, and characteristics of used scenarios have been identified as well as importance or triviality of parameters used.

The work presented in this report is the development and supplement to the work of João Gil concerning beamforming for UMTS-TDD mode [GiCo01a], [GiCo02a], [GiCo02b], [GiCo02c], [GiCo02d], [GiMC01].

This report is organised as follows. Chapter 2 describes theoretical aspects of all needed elements, starting from UMTS across Wideband Channel models, smart antennas and adaptive algorithms, and finishing with theory of antenna arrays. Chapter 3 contains all issues related with implementation of consecutive parties of the system for simulation; one can also find here a description of the analysis procedure and scenarios used. Chapter 4 brings a complete analysis of obtained results divided in Uniform Linear and Circular Arrays analysis, comparison of both, and some general observations. In Chapter 5, overall conclusions have been drawn, with a summary of the whole work. In Annexes, one can find detailed information on issues referred earlier in this work.

The analysis performed in this work supplements the work of João Gil in the same area for the UMTS-FDD mode, giving a more complete view on the impact of the directional channel and its parameters in beamforming. It is also helpful for those who also address similar problems, in terms of comparison of obtained results and methods or tools used. As a result of changing the UMTS mode, several issues have been added to João Gil's work. The most important feature was adapting the program to operate with large numbers of users, and making the number of users changeable in a dynamic way. Moreover, the code generator has been added, which generates a combination of channelisation and scrambling codes for a specified number of users. The large computational burden, which is the consequence of the long code sequences used, forced a number of improvements, including the use of CG as MATLAB® internal function, to achieve better performance and shorter simulation time. Finally, some analysis tools have been added to process the acquired results.

2 Theoretical Aspects

2.1 UMTS Description

2.1.1 General Aspects

Since the 80', when the requirement for creating an uniform international system for mobile communications has been announced, many people have been working on ideas, architecture and components for that purpose. Wide-ranging projects concerning the detailed preparation of a new mobile communications system, which should be complementary to GSM and then replace it in future, has started also in Europe. This system is called UMTS. Its main target is to join new solutions in the field of interface and radio access with new services architecture, integrating stationary and mobile telephony at least on the services and applications level. The main target of UMTS is to supply personalised, globally accessible multimedia services, executed with high bit rate in local and wide mobile telecommunications network environment.

In order to meet the expectations of the services to be supported, the following requirements to the system were defined [HoTo01]:

- Bit rates up to 2 Mbps
- Variable bit rate to offer bandwidth on demand
- Multiplexing of services with different quality requirements on a single connection, e.g., speech, video and packet data
- Delay requirements from delay-sensitive real-time traffic to flexible best-effort packet data.
- Quality requirements from 10% frame error rate to 10^{-6} bit error rate
- Coexistence of second and third generation systems, and inter-system handovers for coverage enhancements and load balancing
- Support of asymmetric Uplink (UL) and Downlink (DL) traffic (e.g., web browsing causes more loading to downlink than to uplink)
- High spectrum efficiency
- Coexistence of Frequency Division Duplex (FDD) and Time Division Duplex (TDD) modes.

Most of these expectations are already solved, or are currently being solved, in order to meet the demands of users, and to be applied from the very first system deployment.

2.1.2 UMTS Architecture

The structure of a Third Generation (3G) network can be modelled in many ways. Below two of them are introduced in order to outline the basic structure of the network.

A basic architectural split is between the user equipment (terminals) and the infrastructure [3GPP01a]. This results in two domains: the User Equipment Domain and the Infrastructure Domain. Domain is the highest-level group of physical entities, and reference points are defined between domains.

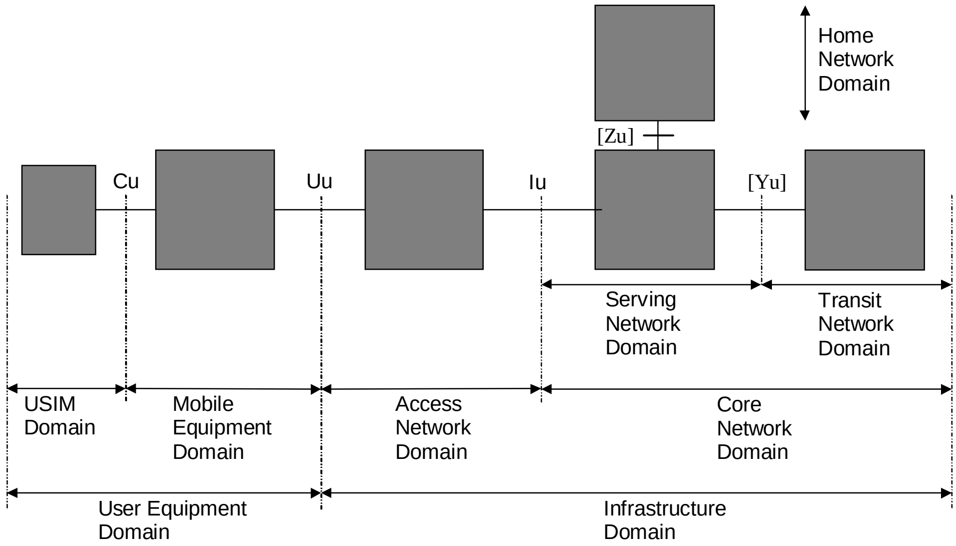

Figure 2.1 – UMTS domains and reference points (extracted from [3GPP01a]).

User equipment is the equipment used by the user to access UMTS services, which is done via a radio interface to the infrastructure. The infrastructure consists of the physical nodes, which perform the various functions required to terminate the radio interface and to support the telecommunication services requirements of the users, and it is a shared resource that provides services to all authorised end users within its coverage area. The reference point between the User Equipment Domain and the Infrastructure Domain is termed the “Uu” reference point (UMTS radio interface).

The user equipment is further sub-divided into the Mobile Equipment (ME) Domain and the User Services Identity Module (USIM) Domain. The Mobile Equipment performs radio transmission and contains applications. The USIM contains data and procedures, which unambiguously and securely identify itself, and these functions are typically embedded in a stand-alone smart card. This device is associated to a given user, and as such it allows to identify this user regardless of the ME he uses. The reference point between the ME and the USIM is termed the “Cu” reference point.

The Infrastructure Domain is further split into the Access Network Domain, which is characterised by being in direct contact with the User Equipment and the Core Network Domain. The Access Network Domain consists of the physical entities that manage the resources of the access network, and provides the user with a mechanism to access the Core Network Domain. The Core Network Domain consists of the physical entities that provide support for the network features and telecommunication services. This support includes functionalities such as the management of user location information, control of network features and services, the transfer (switching and transmission) mechanisms for signalling and for user generated information. The reference point between the Access Network Domain and the Core Network Domain is termed the “Iu” reference point.

The Core Network Domain is sub-divided into the Serving Network Domain, the Home Network Domain and the Transit Network Domain. The Serving Network Domain represents the core network functions that are local to the user’s access point, thus their location changes when the user moves. It is responsible for routing calls and transport user data/information from source to destination; it has the ability to interact with the home domain to cater for user specific data/services and with the transit domain for non user specific data/services purposes. The Home Network Domain represents the core network functions that are conducted at a permanent location regardless of the location of the user’s access point. It contains at least permanently user specific data and is responsible for management of subscription information; it may also handle home specific services, potentially not offered by the Serving Network Domain. The Transit Network Domain is the core network part located on the communication path between the Serving Network Domain and the remote party. If, for a given call, the remote party is located inside the same network as the originating UE, then no particular instance of the transit domain is activated. The reference point between the Serving Network Domain and the Home Network Domain is termed the [Zu] reference point. The reference point between the Serving Network Domain and the Transit Network Domain is termed the [Yu] reference point.

The network architecture [KALN01] is shown in Figure 2.2. The 3G network terminal is called User Equipment (UE) and it contains two separate parts, Mobile Equipment and UMTS Service Identity Module.

The UTRAN (Universal Terrestrial Radio Access Network) is divided into Radio Network Subsystems (RNSs). One RNS consists of a set of radio elements and their corresponding controlling element. In UTRAN the radio element is Node B, or Base Station

(BS), and the controlling element is the Radio Network Controller (RNC). The RNSs are connected to each other over access network-internal interface Iur.

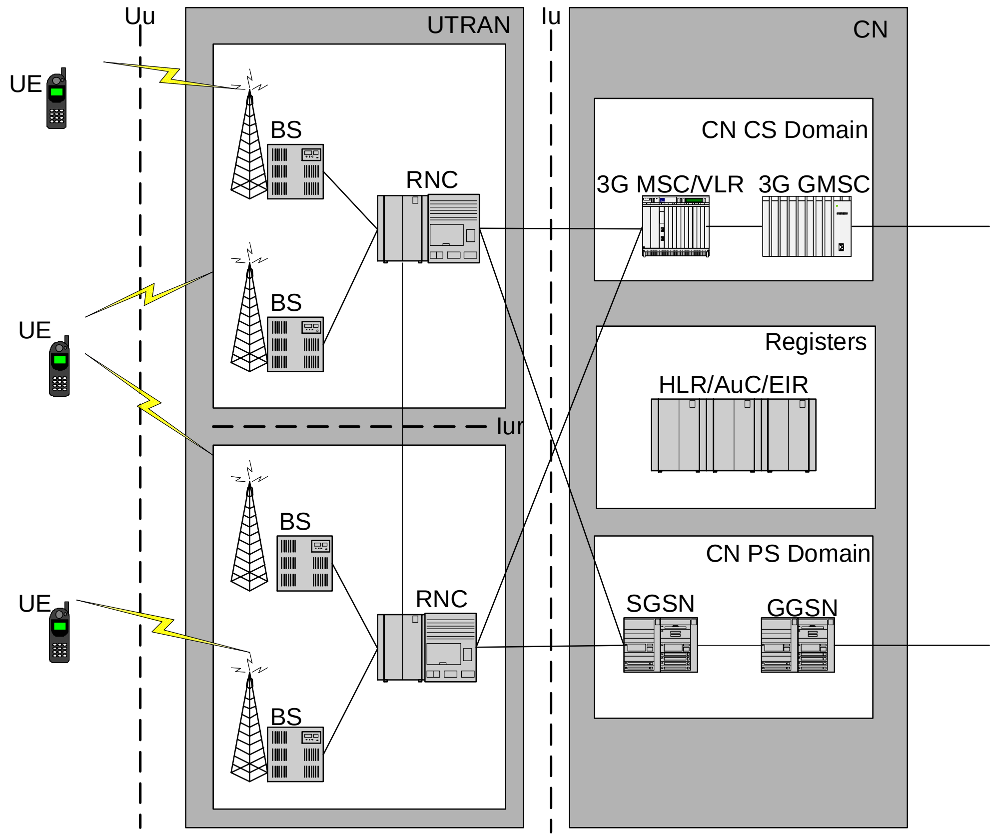

Figure 2.2 – UMTS network architecture (extracted from [KALN01])

The Core Network (CN) covers all network elements needed for switching and subscriber control. Registers maintain static subscription and security information. Between the UE and UTRAN the open interface is Uu, which in UMTS is physically realised with WCDMA technology. The other major open interface is Iu located between the UTRAN and CN.

In UMTS there are three types of channels [3GPP01c]: logical channels, transport channels and physical channels. Three types of channels are related with the layer structure of the system.

Figure 2.3 shows the UTRA (Universal Terrestrial Radio Access) radio interface protocol architecture around the physical layer (Layer 1). The physical layer interfaces the Medium Access Control (MAC) sub-layer of Layer 2 and the Radio Resource Control (RRC) layer of Layer 3. The ellipses between different layer/sub-layers indicate Service Access Points (SAPs). The physical layer offers different transport channels to MAC, and it is required to support variable bit rate transport channels to offer bandwidth-on-demand services, and to be able to multiplex several services to one connection. A transport channel is characterised by how the information is transferred over the radio interface.

MAC offers different logical channels to the Radio Link Control (RLC) sub-layer of Layer 2, characterised by the type of information transferred. Logical channels are classified into two groups: control channels, which are used to transfer control plane information, and traffic channels, for user plane information.

Physical channels are defined in the physical layer. In the FDD mode, a physical channel is characterised by the code, frequency, and in the UL by the relative phase (I/Q); in the TDD mode, the physical channel is also characterised by the timeslot. Two types of physical channels exist: dedicated channels and common channels; the main difference between them is that a common channel is a resource divided among all or a group of users in a cell, whereas a dedicated channel resource, identified by a certain code on a certain frequency, is reserved for a single user only. The physical layer is controlled by the RRC.

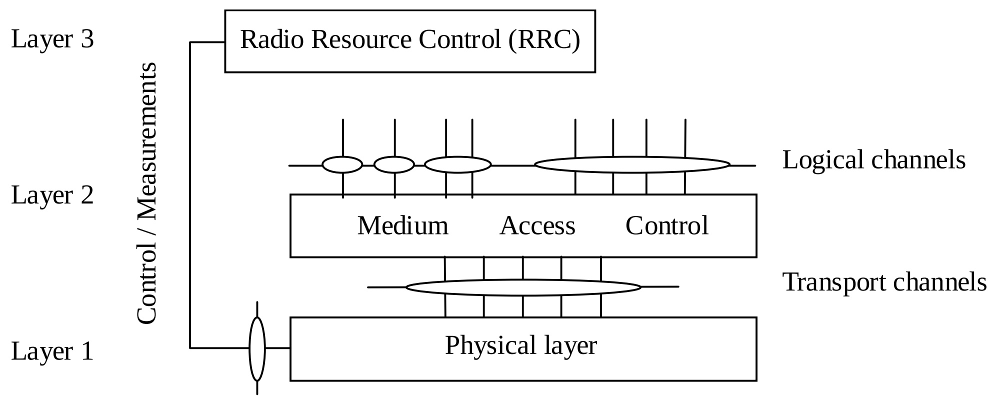

Figure 2.3 – Radio interface protocol architecture around the physical layer (extracted from [3GPP01c]).

2.1.3 Wideband Code Division Multiple Access

In the standardisation fora, WCDMA technology has emerged as the most widely adopted third generation air interface [HoTo01]. WCDMA is a wideband Direct-Sequence Code Division Multiple Access (DS-CDMA) system, which means that user information bits are spread over a wide bandwidth by multiplying the user data with quasi-random bits (called chips) derived from CDMA (Code Division Multiple Access) spreading codes. In order to support very high bit rates (up to 2 Mbps), the use of a variable spreading factor and multicode connections is supported. The chip rate of 3.84 Mcps used leads to a carrier bandwidth of approximately 5 MHz. The inherently wide carrier bandwidth of WCDMA supports high user data rates, and also has certain performance benefits, such as increased multipath diversity.

The concept of obtaining Bandwidth on Demand (BoD) is well supported, because WCDMA supports highly variable user data rates. Frames of 10 ms duration are used, during which the user data rate is kept constant, however, the data capacity among users can change from frame to frame.

WCDMA supports two basic modes of operation: FDD and TDD. In the FDD mode, separate 5 MHz carrier frequencies are used for UL and DL respectively, whereas in TDD only one 5 MHz carrier is time-shared between UL and DL. The FDD mode is the main mode to be used by UMTS, while the TDD mode was added in order to complement the basic WCDMA system with the unpaired spectrum allocations of the International Telecommunications Union (ITU) for the International Mobile Telecommunications (IMT-2000) systems.

There is no need for a global time reference, such as Global Positioning System (GPS) because WCDMA supports the operation of asynchronous BSs. WCDMA employs coherent detection on UL and DL based on the use of pilot symbols or common pilot. The use of coherent detection is new for public CDMA systems, and will result in an overall increase of coverage and capacity on the UL.

The air interface has been crafted in such a way that advanced CDMA receiver concepts, such as multiuser detection and smart adaptive antennas, can be deployed by the network operator as options to increase capacity and/or coverage. Table 2.1 shows some basic features of the system.

Table 2.1 – Main WCDMA parameters (extracted from [HoTo01]).

Multiple access method	DS-CDMA
Duplexing method	FDD / TDD
Base station synchronisation	Asynchronous operation
Chip rate	3.84 Mcps
Frame length	10 ms
Service multiplexing	Multiple service with different quality of service requirements multiplexed on one connection
Multirate concept	Variable spreading factor and multicode
Detection	Coherent using pilot symbols or common pilot
Multiuser detection, smart antennas	Supported by the standard, optional in the implementation

The system has been given in Europe the following frequency bandwidths [HoTo01]:

- Paired bands, FDD
  - 1920 – 1980 MHz – UL
  - 2110 – 2170 MHz – DL
- Unpaired bands, TDD
  - 1900 – 1920 MHz – UMTS TDD mode
  - 2010 – 2025 MHz – UMTS TDD mode
- Satellite bands, FDD
  - 1980 – 2010 MHz – UL
  - 2170 – 2200 MHz – DL

12 radio channels for FDD, predicted to be the main UMTS mode supporting the majority of services, and 7 radio channels for TDD, being the additional mode supporting mainly services with asymmetrical traffic characteristics, will be available for UMTS. Duplex separation of 190 MHz between UL and DL in FDD mode is predicted, which should be taken into account, when considering path differences of transmitted and received signals.

The above-mentioned frequency bands correspond to European countries. The spectrum allocation including other countries is shown on the Figure 2.4.

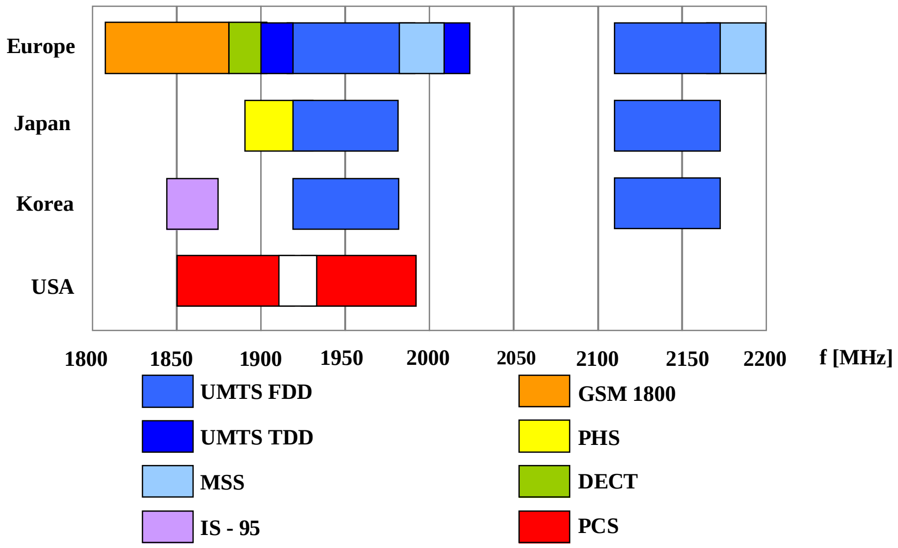

Figure 2.4 – Spectrum allocation in Europe, Japan, Korea, USA (extracted from [HoTo01]).

Two main operations performed in the code domain are spreading and scrambling [HoTo01]. The spreading operation is the multiplication of each user data bit by a sequence of code bits. The increase of the signalling rate by a spreading factor corresponds to a widening of the occupied spectrum of the spread user data signal; due to this, CDMA systems are more generally called spread spectrum systems. Despreading (operation opposite to the spreading one) restores bandwidth, which was previously used by the signal. In addition to spreading, part of the process in the transmitter is the scrambling operation, which is needed to separate terminals or BSs from each other. Scrambling is used on top of spreading, so it does not change the signal bandwidth, but only makes the signals from different sources separable from each other. Figure 2.5 shows the relation of the chip rate in the channel to spreading and scrambling; as the chip rate is already achieved in the spreading by the channelisation codes, the symbol rate is not affected by the scrambling.

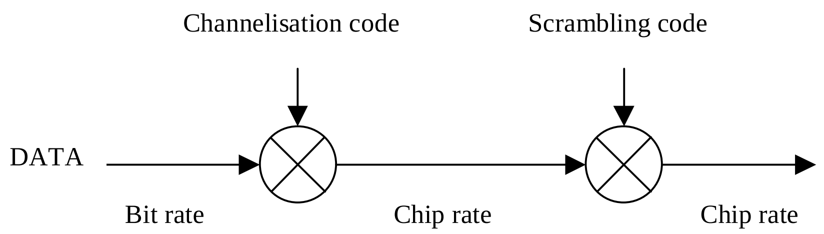

Figure 2.5 – Relation between spreading and scrambling (extracted from [HoTo01]).

Transmissions from a single source are separated by channelisation codes, i.e. DL connections within one sector and the dedicated physical channel in the UL from one terminal. Spreading/channelisation codes have orthogonal properties, and are used for separating information transmitted from a single source, i.e. different connections within one cell in DL, where the own interference is also reduced, and dedicated physical data channels from one UE in the reverse direction.

Channelisation codes are based on the Orthogonal Variable Spreading Factor (OVSF) technique. The use of OVSF codes allows the spreading factor to be changed and orthogonality between different spreading codes of different lengths to be maintained. The codes are picked from the code tree, which is illustrated in Figure 2.6.

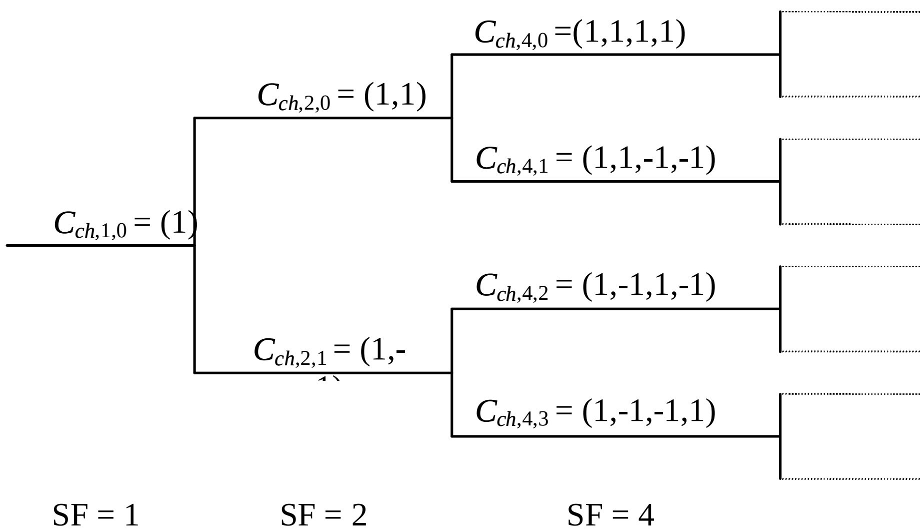

Figure 2.6 – Code-tree for generation of OVSF codes (extracted from [3GPP01b]).

In Figure 2.6, the channelisation codes are uniquely described as $C_{ch,\mathrm{SF},k}$, where SF is the spreading factor of the code and k is the code number, $0 \le k \le$ SF-1. Each level in the code tree defines channelisation codes of length SF. The generation method for the channelisation code is defined as [3GPP01b]:

$$C_{ch,1,0} = 1 \tag{2.1}$$

$$\begin{bmatrix} C_{ch,2,0} \\ C_{ch,2,1} \end{bmatrix} = \begin{bmatrix} C_{ch,1,0} & C_{ch,1,0} \\ C_{ch,1,0} & -C_{ch,1,0} \end{bmatrix} = \begin{bmatrix} 1 & 1 \\ 1 & -1 \end{bmatrix} \tag{2.2}$$

$$\begin{bmatrix} C_{ch,2^{(n+1)},0} \\ C_{ch,2^{(n+1)},1} \\ C_{ch,2^{(n+1)},2} \\ C_{ch,2^{(n+1)},3} \\ \vdots \\ C_{ch,2^{(n+1)},2^{(n+1)}-2} \\ C_{ch,2^{(n+1)},2^{(n+1)}-1} \end{bmatrix} = \begin{bmatrix} C_{ch,2^n,0} & C_{ch,2^n,0} \\ C_{ch,2^n,0} & -C_{ch,2^n,0} \\ C_{ch,2^n,1} & C_{ch,2^n,1} \\ C_{ch,2^n,1} & -C_{ch,2^n,1} \\ \vdots & \vdots \\ C_{ch,2^n,2^n-1} & C_{ch,2^n,2^n-1} \\ C_{ch,2^n,2^n-1} & -C_{ch,2^n,2^n-1} \end{bmatrix} \tag{2.3}$$

The leftmost value in each channelisation code word corresponds to the chip transmitted first in time.

The second operation is the scrambling operation, where a scrambling code is applied to the spread signal; by this, the resultant signals on the *I*- and *Q*-branches are multiplied by complex-valued scrambling code, where *I* and *Q* denote real and imaginary parts, respectively. The scrambling codes are used to separate different cells in DL and different terminals in UL direction. Detailed information about spreading codes is included in [3GPP01b].

Scrambling and channelisation codes may be useful for signal identification in beamforming algorithms. In some situations, a combination of channelisation and scrambling codes, for both intra-cell and inter-cell reduction, may be needed: channelisation codes work for the former one, inside the same cell; scrambling codes work for cell distinction, especially among close cells. One also needs to perform beamforming at the BS to reduce the interference from MTs (Mobile Terminals) and BSs within other cells, i.e., inter-cell interference.

The functionalities and characteristics of the scrambling and channelisation codes are summarised in Table 2.2.

Table 2.2 – Functionality of the channelisation and scrambling codes (extracted from [HoTo01]).

	Channelisation code	Scrambling code
Usage	UL: Separation of physical data and control channels from same terminal DL: Separation of downlink connections to different user within one cell	UL: separation of terminal DL: Separation of sectors (cells)
Length	4-256 chips (1.0-66.7 μs) Downlink also 512 chips	UL: 10 ms = 38400 chips or 66.7 μs = 256 chips (can be used with advanced base station receivers) DL: 10 ms = 38400 chips
Number of codes	Number of codes under one scrambling code = spreading factor	UL: several millions DL: 512
Code family	Orthogonal Variable Spreading Factor	Long 10 ms code: Gold code Short code: Extended S(2) code family
Spreading	Yes, increases transmission bandwidth	No, does not affect transmission bandwidth

2.1.4 Power Control

Power Control (PC) is perhaps one of the most important aspects in CDMA [HoTo01]. Without using an accurate PC mechanism, this multiple access technique would not operate, the main reasons being the near-far problem, interference dependent capacity of the WCDMA, and the limited power resource. Unlike FDMA and TDMA, which are bandwidth-limited multiple access schemes, WCDMA is an interference-limited multiple access one. In FDMA and TDMA, PC is applied to reduce inter-cell interference within the cellular system that arises from frequency reuse, while in WCDMA the purpose of PC is mainly to reduce the intra-cell interference.

In WCDMA, PC is employed in both UL and DL. DL PC is basically for minimising the interference to other cells and compensating for other cells interference, as well as achieving acceptable Signal-to-Interference-Ratio (SIR). The main target of the UL PC is to mitigate the near-far problem[1], by making the transmission power level received from all terminals as equal as possible at the home cell, for the same QoS (Quality of Service).

To manage PC properly in the WCDMA FDD mode, the system uses two different mechanisms:

---

[1] In near-far situations, the signal of the MT that is close to the serving BS may dominate over the signal of the MTs that are far away from the same BS.

- Open Loop Power Control (OLPC)
- Closed Loop Power Control (CLPC), including inner and outer loops

In the OLPC, which is basically used for UL power adjusting, the UE adjusts its transmission power based on an estimate of the received signal level from the BS. It is used in WCDMA only to provide a coarse initial power setting of the MT at the beginning of a connection.

In CLPC in the UL, the BS performs frequent estimates of the received SIR and compares it to a target SIR. If the measured SIR is higher than the target, the BS will command the MT to lower the power; if it is too low, it will command the MT to increase its power. The BS commands the UE to either increase or decrease its transmission power with a cycle of 1.5 kHz by 1, 2, or 3 dB step-sizes. The above-mentioned method is called Inner Loop part of the CLPC, which is the fastest loop in WCDMA power control mechanism. Another variant of the CLPC is the Outer Loop Power Control mechanism, see Figure 2.7; this mechanism adjusts the target SIR setpoint in the BS according to the needs of the individual radio link, and aims at a constant quality, usually defined as a certain target Bit Error Rate (BER) or Frame Error Rate (FER), [KALN01].

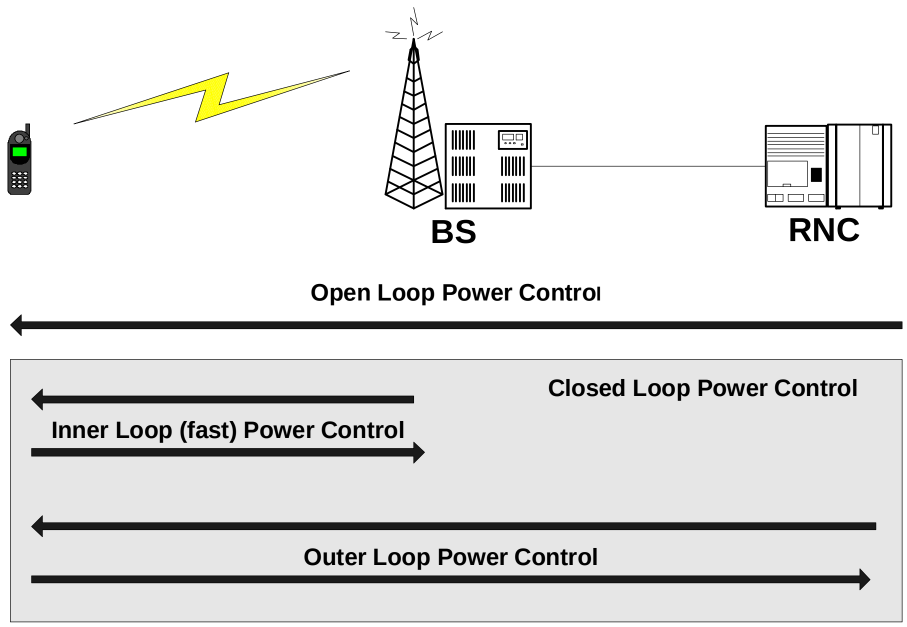

Figure 2.7 – WCDMA power control mechanisms (extracted from [KALN01]).

It should be noticed that PC affects beamforming, thus, it should be considered and implemented even in a simple way for simulation purposes. CDMA systems as UMTS require PC to ensure that all of the signals arriving at a BS are at approximately the same power level. The use of beamforming helps to isolate signals from different users, reducing the PC requirements, but on the other hand, the PC sets SIR levels that beamforming is supposed to assure.

2.2 Wideband Channel Models

2.2.1 Introduction

In order to address problems dealing with beamforming and smart antennas, one should firstly understand well the structure of the radio channel. At the present, with the introduction of techniques and features that depend on the spatial distribution of mobile sources and channel obstacles, wideband temporal and spatial information is required for relevant channel models.

Depending on the number of parameters used to build various channel models, one can divide them into: non-directional and directional ones. Non-directional, classical, channel models provide information on signal power level distributions and Doppler shifts of the received signal. Early channel models accounted only for the time-varying amplitude and phase of channel; fundamental channel models have led to the present-day theories of spatial diversity from both MT and BS perspectives. Directional channel models include both spatial and temporal features design of wideband models; these are built upon classical understanding of multipath fading and Doppler spread, by additionally including concepts such as time delay spread and Direction-Of-Arrival (DoA).

In a wireless system, a signal transmitted trough the channel interacts with the environment in a very complex way. There are reflections from large objects, diffraction of the electromagnetic waves around objects, and signal scattering. The result of these complex interactions is the presence of many signal components, or multipath signals, at the receiver. Longer paths result in delayed versions of the desired signal arriving at the receiver. When the difference in delays between the different multipath components, quantified by the time delay spread, is large, symbols spread into one another, leading to inter symbol interference at the receiver.

Given a plane wave incident from a direction (q, f), the DoA denoted by the angle pair (q, f) describes the direction from where the plane wave arrives. Unless otherwise noted, it is assumed that multipath components arrive at the BS in the horizontal plane, i.e., $q = \pi/2$, so that the azimuthal direction, f, completely specifies the DoA.

In the subsequent part of this section only Geometrically Based Single Bounce (GBSB) Models will be presented in detail, as these will be used in simulations. Description of relevant directional channel models is introduced in Annex A.

2.2.2 Geometrically Based Single Bounce Models

The concept of the GBSB Statistical Channel Models [LiRa99] is based on the definition of scatterer/cluster planar spatial PDF (Probability Density Function). The PDF delimiting region is discussed in what follows, driving to two different models: the GBSB Circular Model (GBSBCM) and the GBSB Elliptical Model (GBSBEM), which are based on a scatterer region of circular and elliptical shapes, respectively.

The GBSBCM is applicable to macro-cell environments, where it is assumed that the BS is above rooftop level, higher than potential scatterers, and Line of Sight (LoS) is absent. The MT is surrounded by a circular scatterer region of radius r_{max} centred at the MT, Figure 2.8.

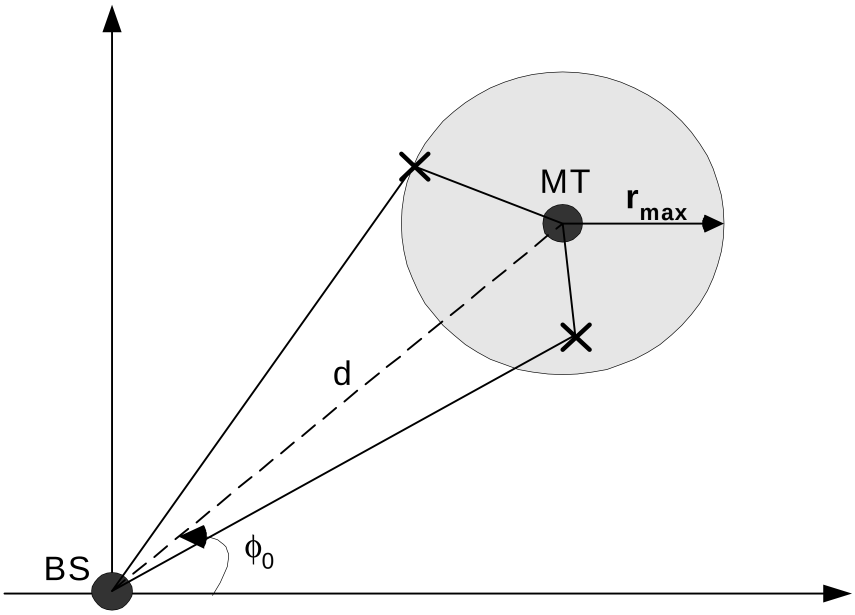

Figure 2.8 – Geometry for the GBSBCM scattering region (extracted from [ZoMa00]).

The GBSBEM is applicable to the micro-cell environments, being assumed that in this case BS antennas are relatively low-height, below rooftop level, hence, scattering will be present in the surrounding of an existing LoS path. This means that multipath scattering is as likely near both the BS and the MT, therefore, the scattering region is chosen to be an ellipse whose foci are the BS and MT. The ellipse size is confined to the street width, Figure 2.9. The mathematical simplicity of the model allows for deriving both joint and marginal statistics for AoA (Angle of Arrival) and ToA (Time of Arrival), which are important to specify and predict adaptive antenna performance. Also, it makes less complex simulations possible, since scatterers are placed randomly according to the chosen PDF.

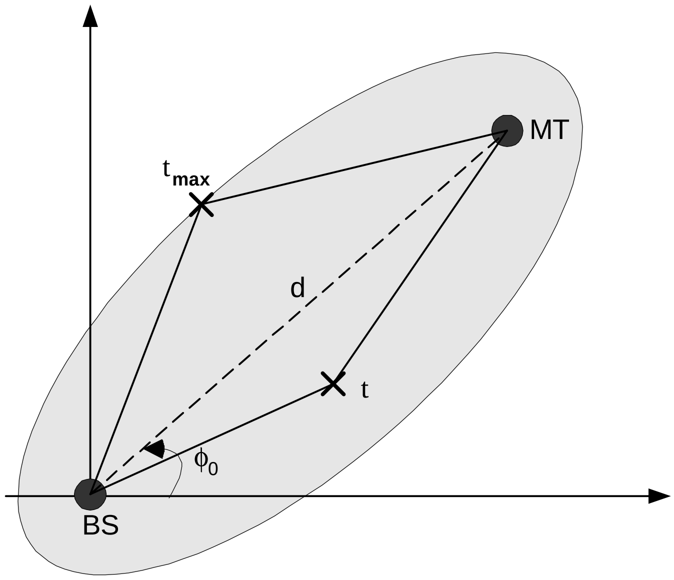

Figure 2.9 – Geometry for the GBSBEM scattering region (extracted from [ZoMa00]).

Scatterers are assumed to be omnidirectional re-radiating elements and assigned complex scattering coefficients. It is also assumed that, when multipath signals travel between MT and BS, only single scatterer reflection occurs, therefore, no other effects such as rough surface scattering, diffraction, and multiple bounce by surfaces and volumes are accounted for. Furthermore, the models to be used substitute single scatterers by clusters, comprising a group of scatterers, following a uniform spatial distribution, and scatterers within each cluster following a Gaussian distribution around the central point, Figure 2.10. The number of scatterers within each cluster follows Poisson distribution.

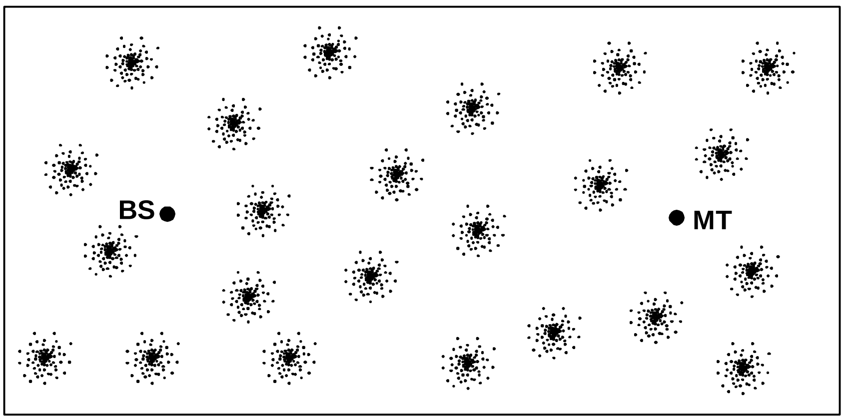

Figure 2.10 – Spatial distribution of clusters of scatterers (extracted from [ZoMa00]).

The scatterers’ reflection coefficients are also random variables, assumed uniformly distributed in amplitude and phase within intervals [0,1] and [0,2π[, respectively.

One of the inherent limitations comes from the fact that all scatterers and incoming waves are assumed to be at the horizontal level, hence, no information on elevation angle is considered. Nevertheless, such approximation is considered valid, considering that a large spatial discrimination exists in the horizontal plane, while at the vertical plane it is very small.

The GBSBCM joint ToA (t) and DoA (f) PDF, for both BS and MT, are [LiRa99]:

$$p_{t,f}(t,f)=\frac{\left(d^2-t^2c^2\right)\left(d^2c+t^2c^3-2t\,c^2d\cos\left(f-f_0\right)\right)}{4p\,r_{\max}{}^2\left(d\cos\left(f-f_0\right)-t\,c\right)^3} \tag{2.4}$$

where c is the speed of light, and d and f_0 are defined in Figure 2.8. The validity regions for the BS and MT cases are, respectively:

$$\frac{\left(d^2-t^2c^2\right)\left(d^2c+t^2c^3-2t\,c^2d\cos\left(f-f_0\right)\right)}{t\,c-d\cos\left(f-f_0\right)}\leq 2r_{\max} \tag{2.5}$$

$$\frac{d^2-t^2c^2}{d\cos\left(f-f_0\right)-t\,c}\leq 2r_{\max} \tag{2.6}$$

Out of these regions, the PDF's value is zero, which means that there are no scatterers.

For the GBSBEM, the joint PDF observed at the BS (or MT) is given by [LiRa99]:

$$p_{t,f}(t,f)=\begin{cases}\dfrac{\left(d^2-t^2c^2\right)\left(d^2c+t^2c^3-2t\,c^2d\cos\left(f-f_0\right)\right)}{p\,t_{\max}c\sqrt{t_{\max}{}^2c^2-d^2}\left(d\cos\left(f-f_0\right)-t\,c\right)^3} & ,\dfrac{d}{c}\leq t\leq t_{\max}\\ 0 & ,\text{elsewhere}\end{cases} \tag{2.7}$$

where d and f_0 are defined in Figure 2.9.

Note that the above PDF is independent of the scattering/clustering density, for it assumes a continuous scattering distribution. However, in a simulation case, cluster density should be a parameter to take into account [ZoMa00].

For the simulation purposes intended in these two models, a set of parameters must be defined. Excluding the scattering region shape, which is determined by the environment type (micro- or macro-cells) and the MT-BS distance, other parameters concerning scatterer and cluster specific properties are listed below:

- region boundaries (t_{max} or r_{max})
- cluster distribution – Uniform within the scattering region
- cluster characteristics
    - distribution of scatterers within the clusters – Gaussian
    - cluster dimensions (Gaussian standard deviation)
    - cluster density
    - number of scatterers in each cluster – determined by a Poisson distribution
    - average number of scatterers in each cluster

- scatterer characteristics
  - scattering coefficient amplitude distribution – Uniform, within [0,1]
  - scattering coefficient phase distribution – Uniform, within [0,2π[
- path attenuation coefficient
- presence or absence of LoS in the macro-cell case

For the present work, these parameters have been set according to [ZoMa00], [MPKZ01].

Two presented models are chosen for simulations, because of their simplicity, combined with suitable set of parameters corresponding to types of scenarios to be simulated (micro- or macro-cells). Use of more complex models does not seem to be necessary particularly taking into the account usually much larger computational burden, while using these models. GBSB models are the hybrid ones, giving the advantages of being quite precise as geometrical models are, remaining also quite simple, which is the characteristic feature of the statistical models. This mixture results in relatively fast and precise environment to perform simulations.

2.3 Smart Antennas and Adaptive Algorithms

2.3.1 Antennas

In the past, wireless systems were deployed using fixed antenna systems, with antenna patterns that were carefully engineered to achieve desired coverage characteristics, but that could not change to react dynamically to changing traffic requirements. Smart antennas are a new technology for wireless systems that use a fixed set of antenna elements in an array. The signals from these antenna elements are combined to form a movable beam pattern that can be steered, to the desired direction that tracks mobile units as they move, using either digital signal processing, or Radio Frequency (RF) hardware. This allows the smart antenna system to focus RF resources on a particular subscriber, while minimising the impact of noise, interference, and other effects that can degrade signal quality.

Smart antenna systems can include features of both: adaptive antenna and switched beam technologies [LiRa99], Figure 2.11. An adaptive antenna is an array of antennas, with patterns dynamically adjusted in terms of noise, interference, and multipath. Adaptive array antennas can adjust their whole pattern to track portable users, and are used to enhance received signals, or to form beams for transmission. An adaptive antenna can adjust its antenna pattern to enhance the desired signal, null or reduce interference, and collect correlated multipath power, as it is shown in Figure 2.11b.

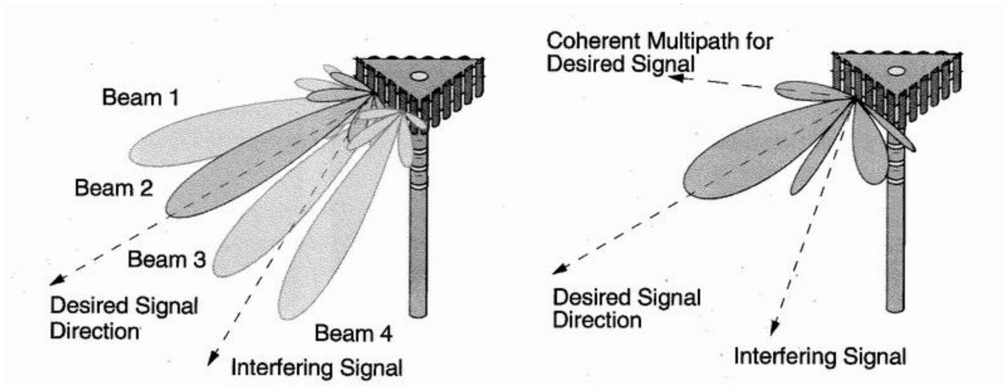

a) Switched Beam System b) Adaptive Antenna System

Figure 2.11 – Two smart antennas technologies: a) Switched Beam System, b) Adaptive Antenna System (extracted from [LiRa99]).

In an adaptive array, as shown in Figure 2.12, the weight vector $w_{k,i}$ is adjusted, or adapted, to maximise the quality of the signal that is available to the demodulator for signal k at time index i.

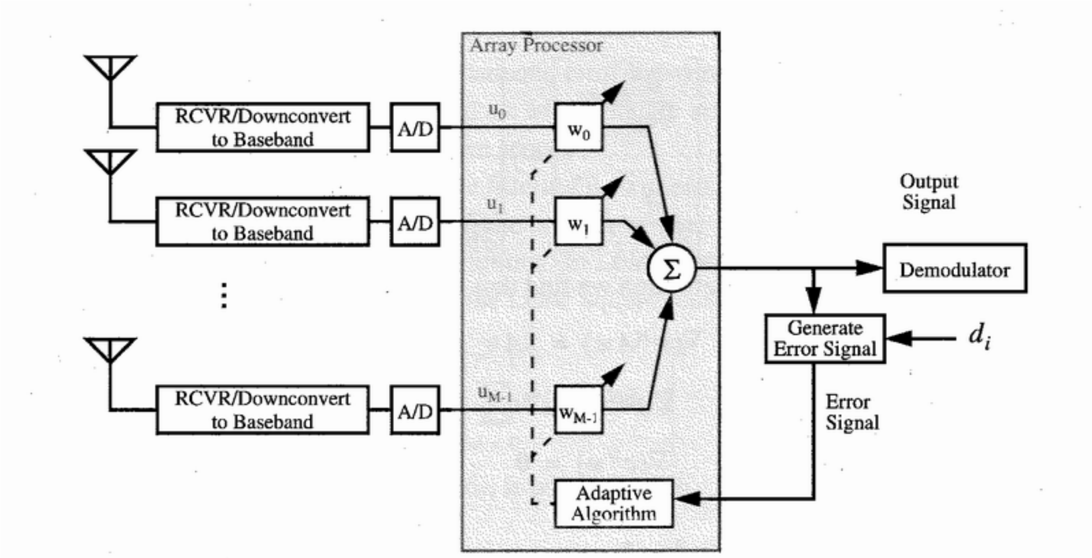

Figure 2.12 – A baseband digital signal processing adaptive array structure (extracted from [LiRa99]).

In optimal beamforming techniques, the pattern is adapted to minimise some cost function. Typically, this cost function is inversely associated with the quality of the signal at the array output, so that, as the cost function is minimised, the quality of signal is maximised at the array output.

Switched beam systems use a number of fixed beams at an antenna site, the receiver/transmitter selecting the beam that provides the greatest signal enhancement and interference reduction. Switched beam systems may not offer the degree of performance improvement offered by adaptive systems, but they are often much less complex and are easier to retro-fit to existing wireless technologies. As it is shown in Figure 2.10-a, beam 2 is selected for the desired signal.

Smart antennas offer a broad range of ways to improve wireless system performance. In general, smart antennas have the potential to provide enhanced range and reduced infrastructure costs in early deployments, as well as enhanced link performance, as the system is built-out, and increased system capacity [LiRa99]:

- By placing the main lobe of an antenna array towards the direction of the Signal-of-Interest (SoI), while simultaneously placing nulls in the Signal-Not-of-Interest (SNoI) direction (if possible), the SINR of the received/transmitted signal is maximised.
- Smart antennas provide enhanced coverage through range extension, hole filling, and better building penetration, i.e. given the same transmitter power output at the BS and MT, the range is increased by increasing the gain of the BS antenna.
- In early deployment, in order to meet initial coverage requirements, a number of BSs must be installed without customer revenue to support these BSs, hence smart antennas can ease this problem by allowing larger early cell sizes.
- Robustness to system perturbations and reduced sensitivity to non-ideal behaviour is provided. CDMA systems require PC to ensure that all of the signals arriving at a BS are at approximately the same power level, therefore, smart antennas help to isolate UL signals from different users, reducing PC requirements or mitigating the impact of imperfect PC.
- Link quality can be improved through multipath management, i.e., since multipath in radio channels can result in fading or time dispersion, smart antennas help to mitigate the impact of multipath or even exploit the diversity inherent in multipath.
- Smart antennas can improve system capacity. In CDMA systems, if smart antennas are used to allow subscribers to transmit less power for each link, then the multipath access interference is reduced, which increases the number of simultaneous subscribers that can be supported in each cell.
- Smart antennas can also be used to spatially separate signals, allowing different subscribers to share the same spectral resources, provided that they are spatially separable at the BS. Space Division Multiple Access (SDMA) allows multiple users to operate in the same cell, on the same frequency/time slot provided, using the smart antenna to separate the signals.

2.3.2 Algorithms

A generic adaptive beamforming system is shown in Figure 2.13. The choice of the weight vector ***w*** is based on the statistics of the signal vector ***x(t)*** received at the array. The objective of beamforming is to optimise the beamformer response with respect to a prescribed criterion, so that the output ***y(t)*** contains minimal contribution from noise and interference. Vector $\boldsymbol{d}^*(t)$ denotes a reference signal if such signal is required.

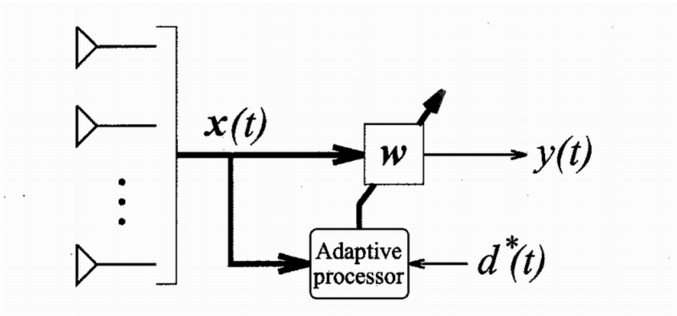

Figure 2.13 – A generic adaptive beamforming system (extracted from [LiLo96]).

There are a number of criteria for choosing the optimum weights [LiLo96]:

- Minimum Mean-Square Error (MMSE) attempts to minimise the difference between the array output and some desired signal.
- Maximum Signal-to-Noise-Ratio (Max SNR) maximises the actual signal-to-noise ratio at the array output.
- Linear Constrained Minimum Variance (LCMV) minimises the variance at the output of the array.
- Multiple Sidelobe Canceller (MSC), which goal is to choose the auxiliary channel weights to cancel the main channel interference component.

The choice of a particular criterion is not critically important in terms of performance, but it is important in terms of what information about the incoming signal is available, Table 2.3. The choice of adaptive algorithms for deriving adaptive weights is highly important, in that it determines both the speed of convergence and hardware complexity required to implement the algorithm. The MSC approach is simple, but it requires absence of desired signal from auxiliary channels for weight determination. Two of the techniques, the Max SNR approach, which maximises SNR in the array output, and the LCMV approach, require knowledge of DoA of the desired signal, which is not typically known in mobile and wireless systems. The MMSE approach attempts to minimise the difference between array output and some desired signal.

Table 2.3 – Summary of optimum beamformers (extracted from [VeBu88]).

Type	MSC	MMSE	Max SNR	LCMV
Inputs	$\mathbf{x}_a$ – auxiliary data $\mathbf{y}_m$ – primary data	$\mathbf{x}$ – array data $\mathbf{y}_d$ – desired signal	$\mathbf{x}=\mathbf{s}+\mathbf{n}$ $\mathbf{s}$ – signal component $\mathbf{n}$ – noise component	$\mathbf{x}$ – array data $\mathbf{C}$ – constraint matrix $\mathbf{f}$ – response vector
Output	$\mathbf{y}=\mathbf{y}_m\text{-}\mathbf{w}_a^H\mathbf{x}_a$	$\mathbf{y}=\mathbf{w}^H\mathbf{x}$	$\mathbf{y}=\mathbf{w}^H\mathbf{x}$	$\mathbf{y}=\mathbf{w}^H\mathbf{x}$
Criterion	$\min_{\mathbf{w}} E\left\{\left\vert\mathbf{y_m}-\mathbf{w_a^H x_a}\right\vert^2\right\}$	$\min_{\mathbf{w}} E\left\{\left\vert\mathbf{y}-\mathbf{y_d}\right\vert^2\right\}$	$\max_{\mathbf{w}} \frac{\mathbf{w^H R_s w}}{\mathbf{w^H R_n w}}$	$\min_{\mathbf{w}}\left\{\mathbf{w^H R_x w}\right\}\text{s.t.}\mathbf{C^H w}=\mathbf{f}$
Optimum Weights	$\mathbf{w}=\mathbf{R}_a^{-1}\mathbf{r}_{ma}$ where: $\mathbf{r}_{ma}=\mathrm{E}\{\mathbf{x}_a\mathbf{y}_m^*\}$ $\mathbf{R}_a=\mathrm{E}\{\mathbf{x}_a\mathbf{x}_a^H\}$	$\mathbf{w}=\mathbf{R}_x^{-1}\mathbf{r}_{xd}$ where: $\mathbf{r}_{xd}=\mathrm{E}\{\mathbf{x}\mathbf{y}_d^*\}$ $\mathbf{R}_x=\mathrm{E}\{\mathbf{x}\mathbf{x}^H\}$	$\mathbf{R}_n^{-1}\mathbf{R}_s\mathbf{w}=\lambda_{max}\mathbf{w}$ where: $\mathbf{R}_s=\mathrm{E}\{\mathbf{s}\mathbf{s}^H\}$ $\mathbf{R}_n=\mathrm{E}\{\mathbf{n}\mathbf{n}^H\}$	$\mathbf{w}=\mathbf{R}_x^{-1}\mathbf{C}[\mathbf{C}^H\mathbf{R}_x^{-1}\mathbf{C}]^{-1}\mathbf{f}$ where: $\mathbf{R}_x=\mathrm{E}\{\mathbf{x}\mathbf{x}^H\}$
Advantages	Simple	Direction of desired signal can be unknown	True maximisation of SNR	Flexible and general constrains
Disadvantages	Requires absence of desired signal from auxiliary channels for weight determination	Must generate reference signal	Must know R_s and R_n, solve generalised eigen-problem for weights; DoA of desired signal must be known	Computation of constrained weight vector; must know DoA of desired component

Algorithms that require reference signal/training sequence are referred to as non-blind algorithms. The reference signal is generated upon the knowledge of the characteristics of the desired signal and closely represents it, or at least correlates with it to a certain extent. Non-blind algorithms, despite requiring a reference signal, are characterised by fast convergence and are easy to implement. Other techniques that do not require training sequences, referred to as blind adaptive algorithms, work by attempting to restore some known property to the received signal. In the case where an explicit reference signal is not available, blind adaptive beamforming has to be used.

Non-blind adaptive beamforming is highly suitable for a WCDMA system, because the spreading/channelisation code can be used as reference for beamforming. If an explicit reference signal is available in a system, it should be used as much as possible for less complexity, high accuracy, and fast convergence. Several algorithms have been very generally described in Annex B. Chosen algorithms are just examples of different approaches to the beamforming problem, because the variety of approaches is very rich. In the next section, the CG is described in more detail: fast convergence, acceptable computational complexity, and simple application set this algorithm suitable for simulations and analysis, and useful in real beamforming systems.

2.3.3 Conjugate Gradient Algorithm

The Conjugate Gradient (CG) can be applied to adjust the weights of an antenna array [GiMC01]. The method in general is useful for solving the linear system:

$$\mathbf{Rw} = \mathbf{b} \tag{2.8}$$

where $\mathbf{R}$ is a $N \times N$ known symmetric positive-definite matrix, representing the correlation matrix of the input data vector, $\mathbf{b}$ is a known $N \times 1$ cross-correlation vector between the input data and desired signal, and $\mathbf{w}$ is an unknown weights vector.

The direct solution of (2.8), i.e. $\mathbf{w} = \mathbf{R}^{-1}\mathbf{b}$ requires a matrix inversion, which is computationally expensive. In many applications, when the dimension of the matrix $\mathbf{R}$ is large, or when $\mathbf{R}^{-1}$ should be calculated periodically, the problem becomes more severe. In order to solve (2.8) and yet avoid matrix inversion, an iterative method should be used. This can be achieved by minimising the cost function $f(\mathbf{w})$ of the following equation:

$$f(\mathbf{w}) = \frac{1}{2}\mathbf{w}^H\mathbf{Rw} - \mathbf{b}^H\mathbf{w} \tag{2.9}$$

where $(\square)^H$ denotes *Hermitian* (to account for complex nature of input data). Thus, a residual vector,

$$\mathbf{r} = \mathbf{b} - \mathbf{Rw} = -\nabla f(\mathbf{w}) \tag{2.10}$$

denotes the error between the desired signal and the array output, and ∇f denoting the gradient of the function f.

The method starts with an initial guess $\mathbf{w}(0)$ of the weight, obtains a residual $\mathbf{r}(0)$ and initial direction vector $\mathbf{g}(0)$,

$$\mathbf{g}(0) = \mathbf{r}(0) = \mathbf{b} - \mathbf{Rw}(0) \tag{2.11}$$

and moves the weights in this direction to yield a weight update equation

$$\mathbf{w}(i+1) = \mathbf{w}(i) + \alpha(i)\mathbf{g}(i) \tag{2.12}$$

where i denotes number of iteration, and a is the step size, defined as

$$a(i) = \frac{\mathbf{r}(i)^H\mathbf{r}(i)}{\mathbf{g}(i)^H\mathbf{Rg}(i)} \tag{2.13}$$

The residual $\mathbf{r}(i)$ and the direction vector $\mathbf{g}(i)$ are updated using:

$$\mathbf{r}(i+1) = \mathbf{r}(i) - a(i)\mathbf{Rg}(i) \tag{2.14}$$

and

$$\mathbf{g}(i+1) = \mathbf{r}(i+1) + b(i+1)\mathbf{g}(i) \tag{2.15}$$

with

$$b\left(i+1\right)=\frac{\mathbf{r}\left(i+1\right)^{H}\mathbf{r}\left(i+1\right)}{\mathbf{r}\left(i\right)^{H}\mathbf{r}\left(i\right)} \tag{2.16}$$

In the CG algorithm, factor $b(i)$ ensures that the R-orthogonality is preserved between new search directions.

If a rough estimate of the value **w** exists, it can be used as the starting value **w**(0) in the beginning of calculations, if not, it can be set to 0 [Shew94]. The algorithm is stopped when the residual falls below a certain predetermined level, or after a fixed number of iterations. It should be noted that the direction vector points in the direction of the gradient of the error surface $\mathbf{r}(i)^H\mathbf{r}(i)$ at the i^{th} iteration, which the algorithm is trying to minimise. The method converges to the minimum of the error surface within at most N iterations for an N-rank matrix, thus it provides the fastest convergence of all the iterative methods [ChWi00], [Goda97].

Two types of implementation of the CG algorithm exist, depending on the data acquisition method used: sample-by-sample and block processing.

For sample-by-sample processing, it is important to periodically reset the direction vector to the true gradient in order to ensure the convergence of the algorithm. The convergence may not be reached in N steps, because of the loss of orthogonality between search directions, caused by, e.g., finite fixed-point precision. How often the algorithm is reset influences its performance: if using a certain set of direction vectors does not increase the cost function, then global convergence can be assured, since a true steepest-descent step is taken every time the algorithm is reset.

Block-by-block CG implementation requires that both **R** and **b** be firstly calculated. The computational complexity of this implementation depends on *K (K£N),* the number of iterations. For large N the computational complexity of the algorithm is K times of the complexity of the sample-by-sample CG algorithm [Bagh99]. The reason is the independent calculation of each solution, where the search directions and residuals have to be calculated for each cost function [GiMC01].

2.4 Antenna Arrays

2.4.1 Introduction

Usually, the radiation patterns of single-element antennas are relatively wide, i.e. they have relatively low directivity (gain). In many type of communications, antennas with very high directivity are often required. It is possible to construct this type of antenna by enlarging the dimensions of the radiating element (maximum size much larger than λ), however, this may lead to the appearance of multiple side lobes, and technologically inconvenient shapes and dimensions. Another way to increase the electrical size of an antenna is to construct it as an assembly of radiating elements in a proper electrical and geometrical configuration - *antenna array*. Usually the array elements are identical; this is not necessary, but it is more practical, simple and convenient for design and fabrication, and the individual elements may be of any type (wire dipoles or loops, apertures, etc.). The total field of an array is a vector superposition of the fields radiated by the individual elements, hence, in order to provide a very directive pattern, it is necessary that the partial fields (generated by the individual elements) interfere constructively in the desired direction and interfere destructively in the remaining space. In an array of identical elements, there are five controls that can be used to shape the overall antenna pattern [Bala97]:

a) the geometrical configuration of the overall array (linear, circular, spherical, etc.)
b) the relative displacement between elements
c) the excitation amplitude of individual elements
d) the excitation phase of each element
e) the relative pattern of each element

A remarkable property of the antenna arrays is the simplicity of changing the field distribution in the system's aperture. This property is useful for electronic antenna pattern steering.

The far field of an array of identical elements is equal to the product of the field of a single element, at a selected reference point (usually the origin), and the Array Factor (AF) of that array.

$$\mathbf{E}(total) = \mathbf{E}(single\,element\,at\,reference\,point) \times [Array\,Factor] \tag{2.17}$$

The AF is a function of the number of elements, their geometrical arrangement, their relative magnitudes, their relative phases, and their spacing. Since the AF does not depend on the directional characteristics of the radiating elements themselves, it can be formulated by replacing the actual elements by isotropic point sources. The pattern multiplication rule is valid for arrays with any number of identical elements, which do not necessarily have identical magnitudes, phases, and/or spacing between them [Bala97].

2.4.2 Uniform M-element Linear Array

It is assumed that each succeeding element has a γ progressive phase lead current excitation relative to the preceding one (γ represents the phase by which the current in each element leads the current of the preceding element). A linear array of identical elements with identical magnitudes and with a progressive phase is called a Uniform Linear Array (ULA), Figure 2.14. In the case of adaptive beamforming, elements can be fed with different magnitudes and phases respectively to the weights vector provided by adaptive processor. If the elements are of any other than isotropic pattern, the total field pattern can be obtained by simply multiplying the AF by the normalised field pattern of the individual element [Bala97].

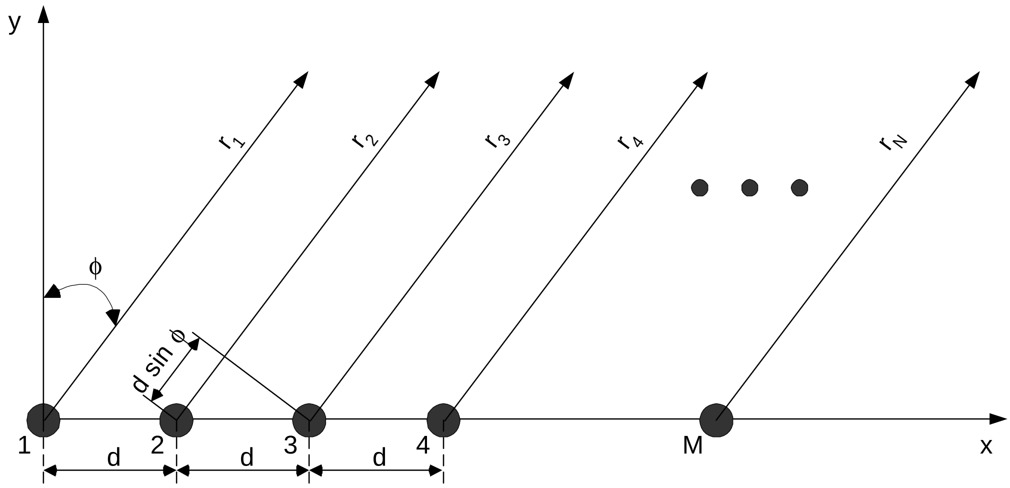

Figure 2.14 – Far-field geometry of M-element linear array of isotropic sources.

The AF of an *M*-element uniform linear array of isotropic sources is:

$$AF = 1 + e^{j(kd\sin f + g)} + e^{j2(kd\sin f + g)} + \mathbf{K} + e^{j(M-1)(kd\sin f + g)} \tag{2.18}$$

which can be rewritten as

$$AF = \sum_{n=1}^{M} e^{j(n-1)y} \tag{2.19}$$

where $y = kd\sin f + g$, or yet as a closed form, which is more convenient for pattern analysis

$$AF = e^{j\left(\frac{M-1}{2}\right)y} \cdot \frac{\sin\left(\frac{M}{2}y\right)}{\sin\left(\frac{y}{2}\right)} \tag{2.20}$$

The phase factor $e^{j\left(\frac{M-1}{2}\right)y}$ is not important, unless the array output signal is further combined with the output signal of another antenna. It represents the phase shift of the array's phase centre relative to the origin, and it would be identically equal to one if the origin were to coincide with the array's centre [Bala97]. Neglecting the phase factor, and for small values of y, (2.20) can be reduced to:

$$AF = \frac{\sin\left(\frac{M}{2}y\right)}{\sin\left(\frac{y}{2}\right)} ; \frac{\sin\left(\frac{M}{2}y\right)}{\frac{y}{2}} \tag{2.21}$$

The maximum value of the magnitude of the AF is equal to M. To normalise the array factor so that the maximum value is equal to unity, (2.21) is written in normalised form as

$$\left(AF\right)_n = \frac{1}{M}\left[\frac{\sin\left(\frac{M}{2}y\right)}{\sin\left(\frac{y}{2}\right)}\right] \tag{2.22}$$

or

$$\left(AF\right)_n ; \frac{1}{M}\left[\frac{\sin\left(\frac{M}{2}y\right)}{\frac{y}{2}}\right], \text{ for small } y \tag{2.23}$$

Several ULA properties have been introduced in Annex C.

2.4.3 Uniform Circular Array

A circular array consisting of M identical isotropic elements evenly spaced in a circle of radius $r_{a,}$ is shown in Figure 2.15, which is referred to as Uniform Circular Array (UCA).

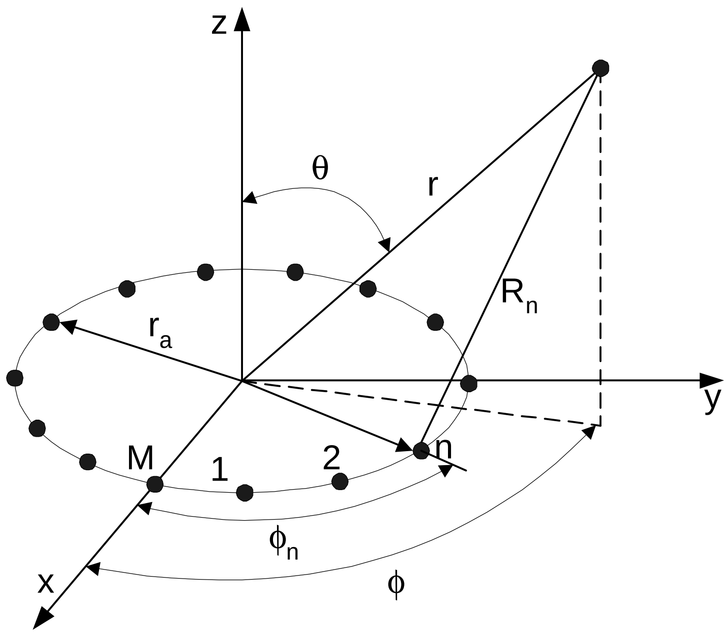

Figure 2.15 – Geometry of an M-element circular array

AF can be expressed in the case of a uniform configuration as

$$AF(q,f)=\sum_{n=1}^{M} e^{j\left[kr_a \sin q \cos(f-f_n)+y_n\right]} \tag{2.24}$$

where $f_n = 2p\left(\dfrac{n}{M}\right)$ is the angular position of nth element on x-y plane, and y_n is phase excitation (relative to the array to the centre) of the nth element.

To direct the peak of the main beam in the (q_0, f_0) direction, the phase excitation of the nth element can be chosen to be

$$y_n = -kr_a \sin q_0 \cos(f_0 - f_n) \tag{2.25}$$

thus the array factor of (2.24) can be written as

$$AF(q,f)=\sum_{n=1}^{M} e^{jkr_a\left[\sin q \cos(f-f_n)-\sin q_0 \cos(f_0-f_n)\right]} \tag{2.26}$$

An example of $AF(q,f)$ for sixteen-element circular array with radius r_a=0.5λ, in q=π/2 plane with antenna beam steered towards various f_0 is given in Figure 2.16.

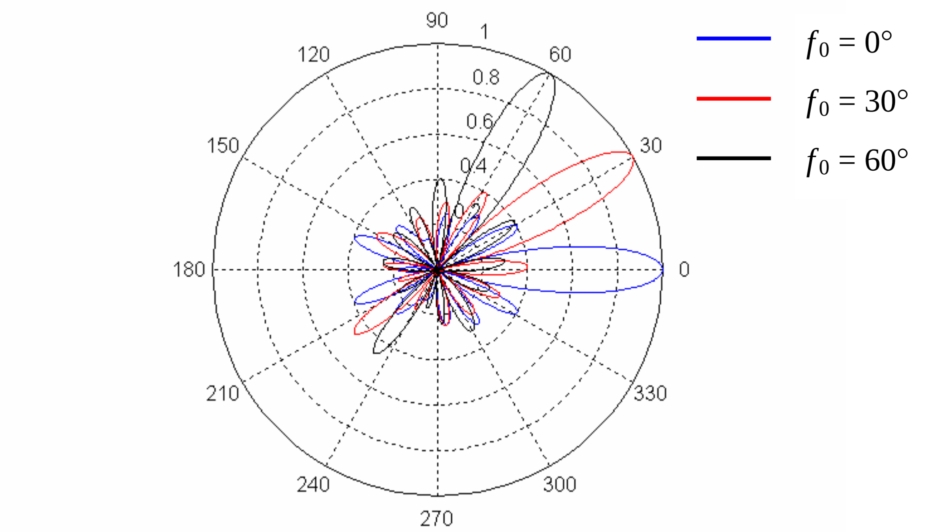

Figure 2.16 – AF patterns of 16-element circular array.

As far as optimum element spacing is concerned, 1.4l radius in 12-element case, which corresponds to element spacing d=0.7247l, minimises the mutual coupling of the elements. Furthermore, a broadside array does not have a full-size grating lobe if d is less than l, and an endfire array must have d smaller than l/2 to avoid a full-size grating lobe [Goda02].

2.4.4 Non-Uniform Arrays

In this section, linear and circular arrays have been described. In case of linear array, broadside case has been investigated in more detail. Some most important equations i.e. for finding nulls, maxima, HPBW (Half Power Bandwidth) of main and maxima of side lobes have been introduced in Annex C. Also in Annex C, one can find examples and figures of beam steering and some proposals of corresponding solutions to achieve comparable HPBWs for both ULA and UCA. The circular array, which has the main advantage of having the ability of beam steering in the whole angular range of $[0; 2\pi[$, has been also presented.

It is worth to mention that the main ULA characteristic is its symmetry, i.e., the radiation pattern is the same to the front of the array and to the rear, while in UCA there is no such symmetry, so the beam is pointed to the specific direction. These two types of antenna arrays are introduced, being most convenient and simple for the adaptive implementation to the Wideband Directional Channel Model (WDCM) simulations scenarios.

Non-uniform arrays enlarge the number of degrees of freedom in beamforming by making the amplitude of each element excitation also variable. In the case of the beamformer, a proper algorithm can set not only the phase but also the amplitude of each element, and thus form the main lobe and the nulls more precisely, which gives increased gain and additional possibilities.

3 Implementation

3.1 General Description

The problem presented in this work deals with implementation of beamforming for the UMTS FDD mode and analysis of the impact that the WDCM has on the convergence of beamforming algorithm. The CG algorithm has been applied to control the beamforming process, by choosing the weight vector and optimising it in sense of MMSE.

In Figure 3.1, a flowchart presents the general concept of performing the simulations.

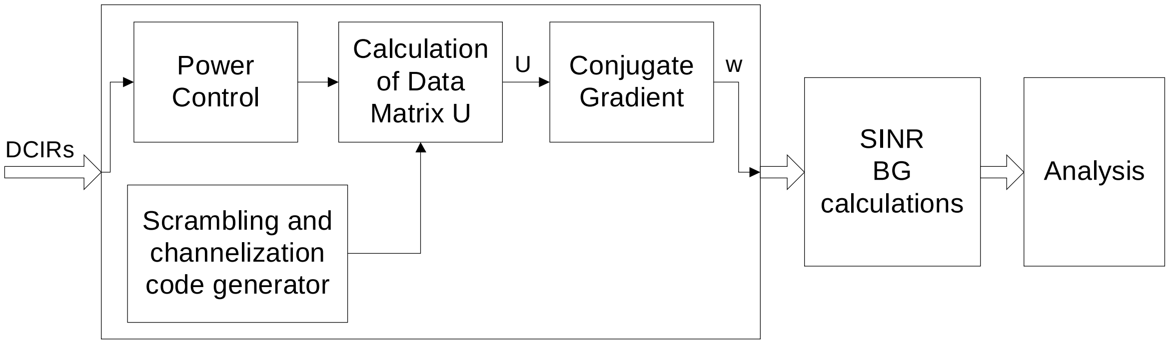

Figure 3.1 – Simulation flowchart.

The main blocks of Figure 3.1 have been described in detail further in this chapter.

As it is shown, the main input parameters are Directional Channel Impulse Responses (DCIRs) obtained from [ZoMa00], [MPKZ01], which will be described in detail in Section 3.5. These DCIRs provide the information on ToA, AoA, modulus and phase of incoming signals, which are required from the wideband system perspective and also to take into account directional requirements of beamforming.

As outputs of simulations one obtains several values and parameters, which are further used for a variety of analysis, comparisons and conclusions. To obtain the reference source for the non-blind adaptive algorithm implementation, UTRA FDD scrambling and channelisation code sequences combination is generated. To make the simulations as close to the real system as possible, also a simple PC mechanism has been applied.

It should be mentioned that the general structure and some components of the simulations have been derived on the basis of [GiCo02d], with the following changes for the UMTS FDD mode application:

- Scrambling sequences and channelisation codes generator has been added.

  In order to obtain reference signal in the UMTS FDD UL mode, for distinguishing different MTs, an adequate generator has been added. As it was already mentioned, for this mode of UMTS, a combination of both, scrambling and channelisation, codes is needed. Moreover, to change the number of users dynamically in the FDD simulations, the program has been written to change this parameter easily.

- Programs have been changed to work automatically for given number of users

  In the case of UMTS FDD mode, there are more users predicted to make use of the system. For this reason, programs have been changed to calculate consecutive values automatically for a given, but changeable, number of users. The previous version of the program made calculations "manually" for constant number of users, without the possibility of changing this number and not affecting the structure of the whole program in the same time. The changes made to the program allow changing parameters for different scenarios in a quick and simple way, making simulation easier.

- CG algorithm has been applied as a MATLAB® internal function (*pcg.m*)

  To make simulations faster, the manual CG algorithm has been replaced by the *pcg.m* internal MATLAB® Optimisation Toolbox function. Consistence of algorithm and *pcg.m* function has been accurately verified. Algorithms have been compared in the sense of the results, as well as in the sense of the theoretical information contained in MATLAB® manual.

- A number of minor changes to tune the program for maximum performance

  In UMTS FDD mode, codes length used for simulation and the number of users are larger than in TDD mode. As a consequence, the sizes of the matrixes and memory are also much more demanding. There were some possibilities to free some memory, make some calculations faster, or avoid repeating calculations, which have been discovered, allowing to increase performance.

3.2 Code Generation

In the case of UMTS, CDMA is especially favourable for providing a signal reference closely correlated to the Desired Signal (DesS), but very weakly correlated to the orthogonal or closely orthogonal interfering sources, referred to as Non-Desired Interference (NDesI) – a code. It is known that such a referential source existing, it should be used to its maximum extent, providing best convergence and final error performance [LiLo96]. Consequently, as mentioned in Section 2.1.3, to perform beamforming, a combination of both channelisation and scrambling codes should be used. Channelisation codes are built according to the code tree, as it is shown in Figure 2.6 and/or generation algorithm (2.3).

The method of reference signal generation is shown in Figure 3.2. It is assumed that each user transmits one Dedicated Physical Control Channel (DPCCH) and one Dedicated

Physical Data Channel (DPDCH), as data seems to be the most common signal to be transmitted. Weights b_c and b_d have been set to unity, because PC between DPCCH and DPDCH is not implemented; it should not affect the simulation results, and makes the problem simpler. According to [3GPP01b], DPCCH is spread by code $c_c = C_{ch,256,0}$, and DPDCH (when only one DPDCH is to be transmitted) is spread by code $c_{d,1} = C_{ch,SF,k}$, where SF is the spreading factor of $DPDCH_1$ and k = SF/4; SF is assumed to be constant and equal to 128. It is also assumed that each user uses the same channelisation codes and MTs are distinguished by their unique scrambling code.

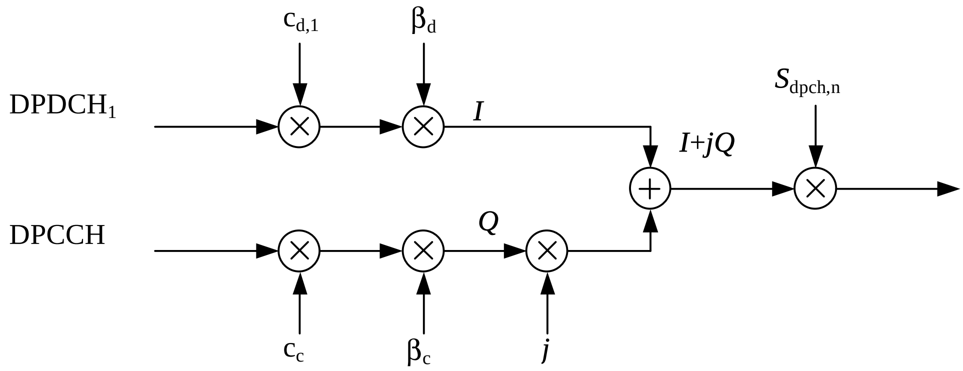

Figure 3.2 – Reference signal generation (according to [3GPP01b]).

The stream of real-valued chips on the I- and Q-branches are then summed and treated as a complex-valued stream of chips. This complex-valued signal is then scrambled by the complex-valued scrambling code $S_{dpch,n}$. The scrambling code is applied, aligned with the radio frames, i.e. the first scrambling chip corresponds to the beginning of a radio frame [3GPP01b].

All UL physical channels are subject to scrambling with a complex-valued scrambling code. The DPCCH/DPDCH/High Speed DPCCH (HS-DPCCH) may be scrambled by either long or short scrambling codes. There are 2^{24} long and 2^{24} short uplink scrambling codes. The long scrambling sequences, $c_{long,1,n}$ and $c_{long,2,n}$, are constructed from position wise modulo 2 sum of 38400 chip segments of two binary m-sequences generated by means of two generator polynomials of degree 25; the resulting sequences constitute segments of a set of Gold sequences, which are $2^{25} - 1$ chips long, hence, being too long for simulation purposes. The scrambling code, $S_{dpch,n}$, to be used is the short scrambling sequence as it is shorter, thus easier to generate and to be used in the simulations. The short scrambling sequences $c_{short,1,n}(i)$ and $c_{short,2,n}(i)$ are defined from a sequence from the family of periodically extended S(2) codes; the generation method for the short scrambling code is defined in detail in [3GPP01b].

Though scrambling codes are not orthogonal, they have good auto- and cross-correlation properties, for any temporal shift. These properties are good only for periodic correlations, i.e., if the spreading factor is equal to the period of the sequence, and if the two information symbols used (with cross-correlation with no time shifts between to sequences) are equal.

In practice these are ideal and not probable situations, therefore, the use of the sequences will not lead to the extreme correlation values [RaMe01]. In order to make use of the best possible correlation properties of the scrambling S(2) PN sequences, the full length 256-chip code sequence is required [3GPP01b]. Moreover, it has been verified that cross-correlation values for several number of users remain on acceptable levels, comparing to the auto-correlation values.

A reference signal generator has been implemented, using MATLAB® (file ***code_gen.m***), where the input parameter is the number of users. As it was mentioned before, SF is constant and equal to 128. Firstly, the matrix of channelisation codes is generated for the given SF, and codes for corresponding data channel are chosen. Then, for each user, a scrambling sequence is generated according to [3GPP01b]. Scrambling and channelisation codes are multiplied according to Figure 3.2. Due to periodical nature of codes, only one 256-chip period is generated, leading to 512 complex chips; 512-chip sequences are put together into a matrix and saved as an output parameter, to be used as inputs to the CG.

3.3 Channel Matrix Calculations

In this work, a block-by-block CG algorithm has been applied, which requires that the Channel Matrix, $\mathbf{U}$ ($N_s \times M$), be firstly calculated to create a positive-definite Correlation Matrix, $\mathbf{R} = \mathbf{U}^H \mathbf{U}$ ($M \times M$), as an input to calculate each weight vector. In the simulations, this operation results in high computational complexity, highly dependent on number of L active BS-MT links and number of antenna elements M [GiMC01].

For each array element, for all active BS-MT links, L, and for each time and angle sample of the DCIR, each element of $\mathbf{U}$ is a product of:

- combination of scrambling and channelisation code
- DCIR magnitude
- DCIR phase
- antenna Array Factor

As a result of this multiplication, channel matrices are obtained for all, L, active links. These results are added with antenna thermal noise, N, creating a single $\mathbf{U}$ matrix.

The CG implementation follows [GiCo02a]. For each link *l*, the CG is applied to minimising the quadratic form:

$$\mathbf{f}_l(\mathbf{w}_l) = \frac{1}{2}\mathbf{w}_l^H \mathbf{R}\mathbf{w}_l - \mathbf{d}_l^H \mathbf{w}_l \tag{3.1}$$

where $\mathbf{R} = \mathbf{U}^H\mathbf{U}$ ($M\times M$) is the correlation matrix, $\mathbf{d}_l = \mathbf{U}^H\mathbf{c}_l$ ($M\times 1$), and $\mathbf{c}_l$ ($N_s\times 1$) is the *l*th DesS code or sequence, whose elements correspond to each chip. All the *L* cost functions are minimised independently. The CG Normal Equation Residual (CGNR) problem:

$$\mathbf{U}^H\mathbf{U}\mathbf{w}_l = \mathbf{U}^H\mathbf{c}_l \tag{3.2}$$

leads to a solution $\mathbf{w}_l$, minimising the residual error, $\left\|\mathbf{U}\mathbf{w}_l - \mathbf{c}_l\right\|$, i.e., towards MMSE [Shew94], [GoLo96]. In other words minimising this error leads towards a beamformer output that is as correlated as possible to the corresponding DesS code [GiCo02a]. The rank *M* **R** matrix is symmetric and positive-definite, guaranteeing the CG convergence to the minimum residual error in at most *M* steps, theoretically.

CG algorithm has been applied as a MATLAB® internal function (*pcg.m*), which is consistent with description in Section 2.3.3. It was verified that Gram-Schmidt orthogonalisation is applied in *pcg.m* MATLAB® function to assure the U-orthogonality between consecutive search directions, in order to reduce round-off errors [HeBK99].

3.4 Implementation of Power Control

Power Control mechanism has been applied according to [GiCo02b], [GiCo02d]. The method hereby applied approximates a CLPC in the UL, where each MT would respond to a Transmit Power Control (TPC) command sent by the BS, here being independent of any outer loop PC. CLPC is predicted to be the most common PC mechanism in the UMTS FDD mode, since OLPC is used only to provide a coarse initial power setting of the MT at the beginning of a connection.

In Figure 3.3, a flow chart summarily describes the PC algorithm that has been applied.

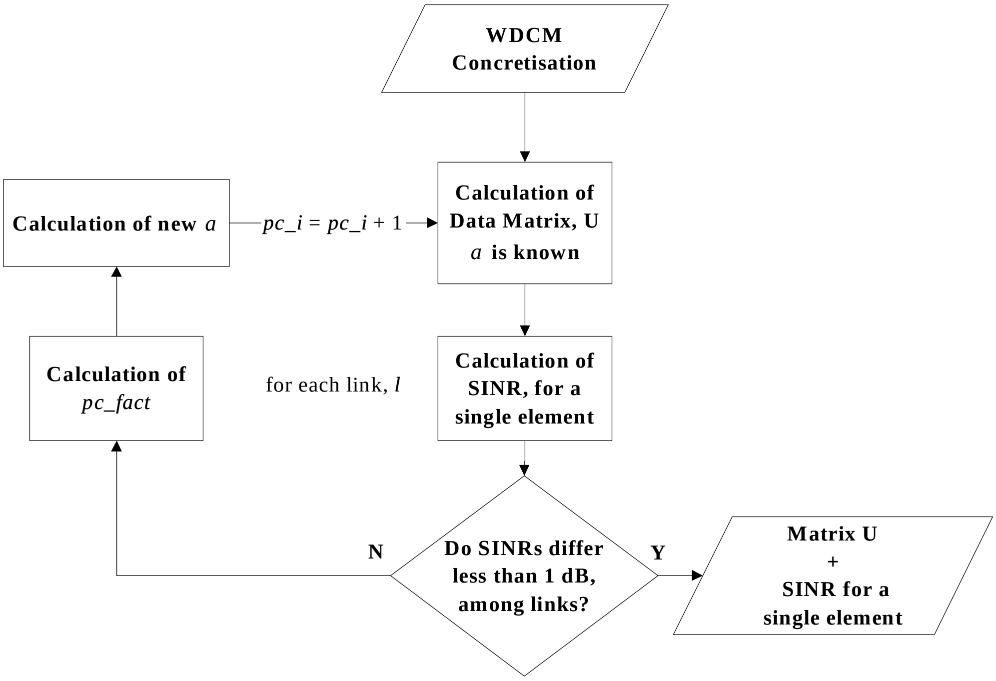

Figure 3.3 – Flow chart of the PC process (extracted from [GiCo02d]).

Before any beamforming action takes place, the SINR is calculated for each link, for a single receiving antenna only. After such calculation, for each iteration *pc_i*, a PC factor is found for each *l*th link's SINR, $SINR^{(l)}_{(pc\_i)}$:

$$pc\_fact^{(l)}_{(pc\_i)} = \frac{Const.}{SINR^{(l)}_{(pc\_i)}} \tag{3.3}$$

At each array element, *m*, from user *l* a sequence of P_l impulses will arrive at $t=t_{l,p}$, with complex amplitude $a^{(l)}_{pc\_i,p}$ and azimuth $f^{(l)}_p$, with *p* corresponding to each path. An impulse response vector, $\mathbf{h}_l(t)$, due to transmitter *l*, can be considered:

$$\mathbf{h}_l(t) = \sum_{p=1}^{P_l} \mathbf{a}(f^{(l)}_p) a^{(l)}_{pc\_i,p} d(t - t_{l,p}) \tag{3.4}$$

where $\mathbf{a}(f^{(l)}_p)$ is the steering vector corresponding to each *p*th path from the *l*th link. Then, each incoming ray amplitude, $a^{(l)}_{pc\_i,p}$, is affected by the corresponding PC factor, calculating the next iteration value:

$$a^{(l)}_{pc\_i+1,p} = a^{(l)}_{pc\_i,p} \times \sqrt{pc\_fact^{(l)}_{(pc\_i)}} \tag{3.5}$$

Afterwards, the resulting $SINR^{(l)}_{(pc\_i+1)}$ is calculated, and the process is repeated, for all links [GiCo02d].

In Figure 3.4, it is exemplified how SINR values, for all active links, get closer, along iterations in the case of FDD. As expected, for the case of 32 users, the values' spread is larger than for less users. Nevertheless, even for such case, the total SINR interval is reduced from near 22 dB to less than 1 dB at the first iteration. For such reason, no more than single iteration has been needed for all simulations.

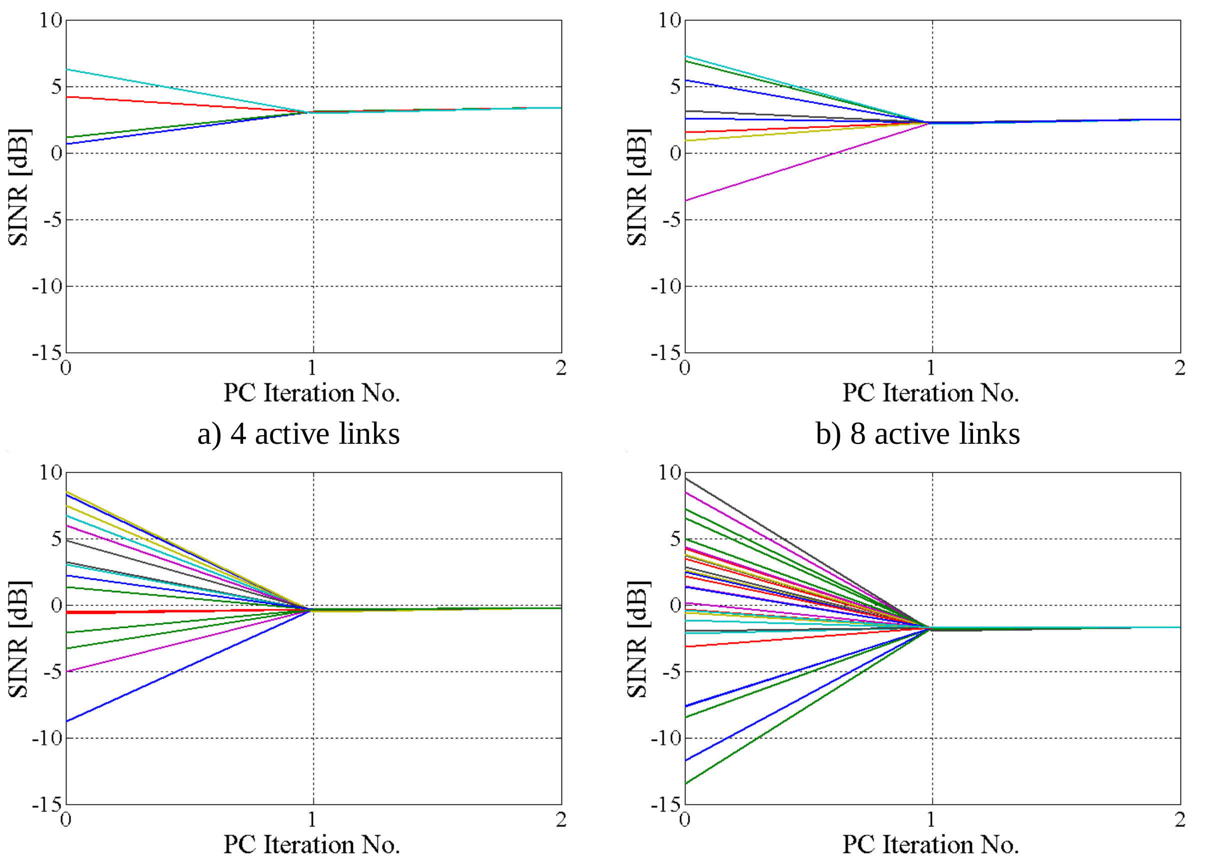

a) 4 active links
b) 8 active links
c) 16 active links
d) 32 active links

Figure 3.4 – Examples of SINR progression along the PC iterations.

Figure 3.5 presents the SINR values before or after PC, for 4 active MTs, considering the single antenna. It is again visible, in Figure 3.5b, how close all links' SINR values are after a single PC iteration, where all active links' results are visually superimposed. The SINR range also decreases due to PC, from more than 22 dB to 8 dB. It must be noticed that the implemented PC process is totally independent from the beamformer operation, meaning that the process does not lead to an optimum final solution in the sense of minimum transmitted power together with the optimum beamformer.

The PC mechanism, following the above description, has been implemented and verified for FDD, accounting for the variable number of users, using MATLAB® (file *power_control.m*), based on the already available TDD implementation [GiCo02d], [GiCo02b].

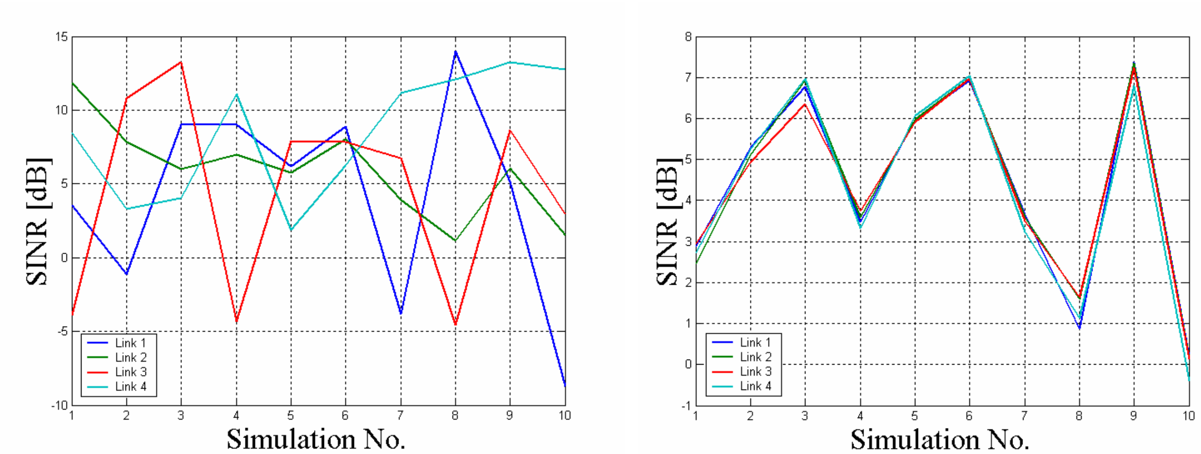

a) Before PC. b) After PC, single iteration.

Figure 3.5 – SINR among 4 active links, for 10 independent DCIR concretisations.

3.5 WDCM Description

The WDCM implemented is described in detail in [ZoMa00], [MPKZ01]. As it was mentioned before in Section 2.2.2, this model is based on GBSBCM. It consists of a set of clusters of scatterers, uniformly distributed in a circular area centred at each MT in a horizontal plane. It is assumed that there are no scatterers near the BS vicinity, according to fact that BS is placed higher than any MT in macro-cell scenario.

Main parameters of the channel have been pointed out in Section 2.2.2. Some of these parameters are scenario specific, and some are scenario independent and common for all. Cluster distribution is uniform within the scattering region and cluster density is 0.001/m^2. Distribution of scatterers within clusters is Gaussian, with average number of scatterers per cluster of 10. These values try to match with observed reality and physical phenomena. The former is accounting for traffic flow or tree density, while the latter is sufficiently large to assume cluster fading. [Marq01], [MPKZ01]. Relative delays are considered as integer multiples of the chip duration, 0.26 μs, for a chip rate of 3.84 Mchip/s, and all incoming signals are assumed to arrive at the same instant of time, only allowing for inter-cluster delays [GiCo02c].

Each l^{th} link (from the total L active links) has been characterised by such WDCM. A *link* is defined as an active MT-BS pair, identified by a code, spatial and temporally independent of any other active MT-BS pair [GiCo02c].

Propagation channels are independent among all links. The DCIR is kept the same for all links at the same BS-MT distance, and independency is assured by generation of uniformly distributed phases for each link. In case of several MTs existing in the same scenario position, a few metres' separation is assumed and independent generation of phases is also performed to account for fast fading effects.

As it was mentioned before, the output parameters of the channel, obtained from the WDCM and referred to DCIRs, are used for simulations and provide information on moduli, phase, AoA and ToA of incoming signal. Angular spread of the WDCM used in simulations has been set to 0.5°.

The antenna used in the simulations is an 8-element ULA with element spacing of $\lambda/2$, oriented with its normal in the direction considered as 0°, which is coincident with the LoS direction, on the same horizontal plane as the WDCM, and a 12-element UCA with element spacing of 3/4 λ. It is assumed that in both cases elements are omnidirectional, ideally matched, weighted and calibrated, with no inter-element coupling. It is also considered that ULA has a ground backplane, ideally not receiving any signals from behind.

The figures of examples of DCIRs, Figure 3.6, have been taken as an average among 100 concretisations for different BS-MT distances of 1000 and 2000 m. One can notice that for 1000 m angle spread is larger than for 2000 m, while keeping the scattering circle radius constant (200 m in case of these examples). The number of rings corresponds to the number of chips of delayed signals, which is mainly dependent on the radius of the scattering circle (increases by enlarging the radius). In Figure 3.7, one can observe the dependency of AoA spread and ToA spread on the scattering circle radius; it is visible that by increasing radius from 50 to 400 m AoA spread widens and ToA increases. It is worth to notice that the relation is very strong and can be put as one of the major objectives to analyse while investigating the beamformer performance. The 50 m scattering circle radius may be the critical case in terms of very weak angular freedom for the beamformer to locate nulls or lobes efficiently.

In Table 3.1, average properties of DCIRs have been put together, and issues that are visible on the figures above have been put in numbers. It shows ToA spread, Δt, and narrowband (NB) and wideband (WB) AoA spreads, Δf_{NB} and Δf_{WB}, respectively. Δf_{NB} is the total angular spread, without temporal distinguishing any signals, calculated for 180° ULA sector. Δf_{WB} is the angular spread, taking into account ToA of arriving signal; two wideband AoA spreads have been distinguished: $\Delta f_{\mathrm{WB},=0}$ where t = 0, for non-delayed signals, and $\Delta f_{\mathrm{WB},>0}$ where $t > 0$, for all remaining delayed ones [GiCo02c]. Noticeable is that scatterers circle radius, r_{max}, affects both AoA and ToA spreads more significantly than the BS-MT distance does. It is obvious that the growth of ToA spread carries also more delayed NDesI power within received signal, but on the other hand larger angular spread ensures more freedom for effective location of nulls and lobes to improve NDesI reduction capacity. Concluding, it can be seen that these two issues can reduce each other's impact on final system performance.

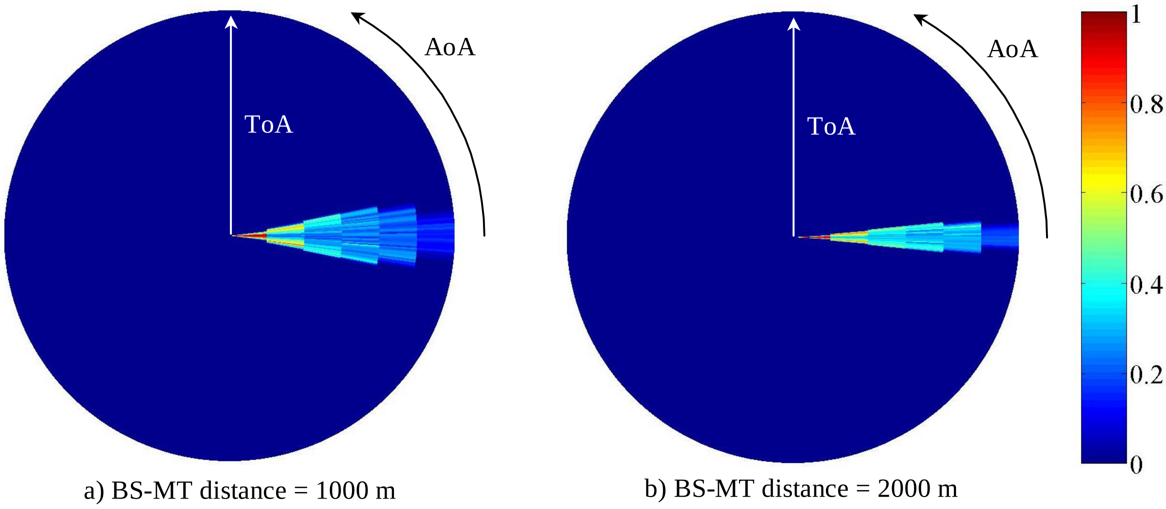

Figure 3.6 – Average signal intensity for 1000 and 2000 m BS-MT distance with 200 m scattering radius normalised to each maximum.

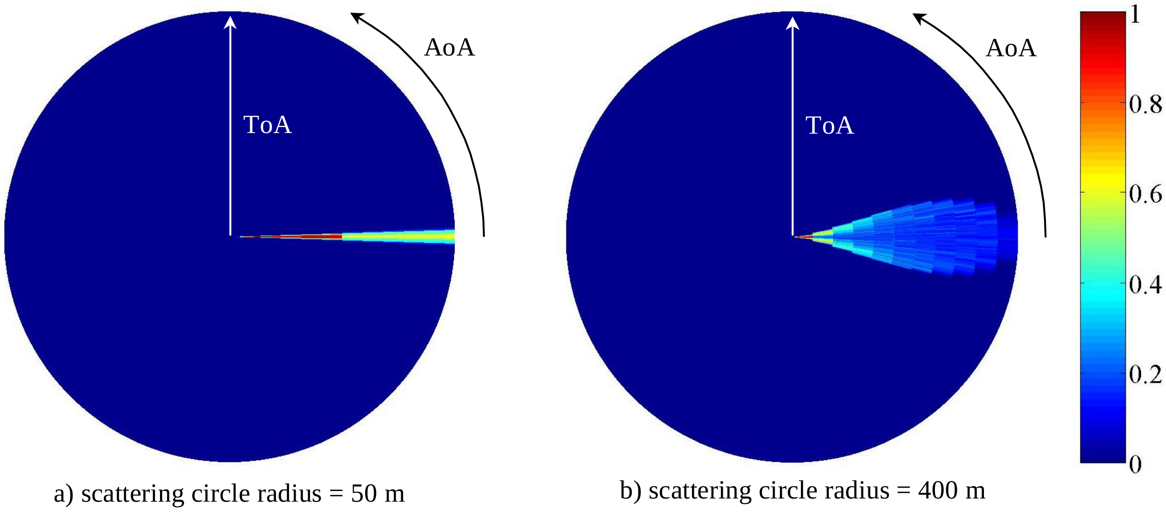

Figure 3.7 – Average signal intensity for 50 and 400 m scattering circle radius for BS-MT distance of 1500 m normalised to each maximum.

Table 3.1 – The ToA and AoA average spreads as a function of r and d_{MT_l} [based on GiCo02c].

r_{max} [m]	d_{MT_l} [m]	Δt [ms]	Δf_{NB} [°]	$\Delta f_{\mathrm{WB,=0}}$ [°]	$\Delta f_{\mathrm{WB,>0}}$ [°]
50	1500	0.102	0.5	<0.5	<0.5
200	1000	0.362	5.6	3.1	6.4
	1500	0.365	3.7	2.0	4.2
	2000	0.377	2.8	1.5	3.1
400	1500	0.678	7.4	3.1	8.4

3.6 Specific Scenarios

The macro-cell scenarios that have been chosen for simulations differ in angular positioning of MTs, their distance from BS, number of users or scattering region radius. All calculations have been performed for 4, 8, 16 and 32 users for scenarios shown in Table 3.2 (scenarios M_b and M_e for 50 and 400 m only for 8 and 16 users), and for 16, 32 and 64 users for scenarios from Table 3.3.

In Table 3.2 and Table 3.3 all scenarios have been set together. They have been divided into two groups: the first one consists of scenarios where either all active MTs are in the same position at the 0° angular reference, or are spread uniformly within the sector; the second group distinguishes one MT on a separate position, while the others are again either all together or randomly spread within the half-sector.

Scenarios presented in Table 3.2 have been identified to verify the dependence of beamformer performance on BS-MT distance, or scatterer circle radius, for two kinds of MTs groupings: together or randomly spread. The former gives also the opportunity to observe if the beamformer is able to work in environments of many signals arriving from common angles, very close to each other. Moreover, the dependency on the number of links can be evaluated giving an overall view on the beamformer behaviour towards high MT density.

Table 3.2 – WDCM macro-cell scenarios, for all MTs together or all angularly spread (based on [GiCo02c]).

Sc #	**d_{MT_l} [m]**	**r_{max} [m]**	**Scenario (not to scale):**
M_a	1 000	200	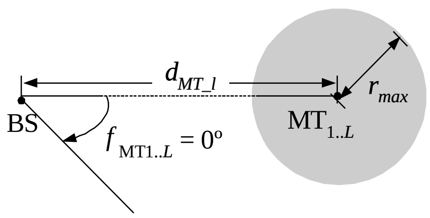
M_b	1 500	50 200 400	
M_c	2 000	200	
M_d	1 000	200	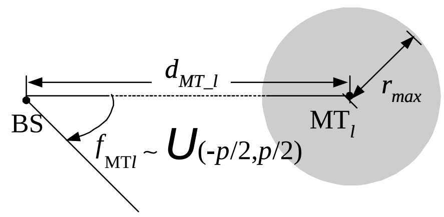 with independent f_{MTl}, among links
M_e	1 500	50 200 400	
M_f	2 000	200	

Taking into account that in scenarios M_a-M_c all MTs are placed in one location, one can compare this situation to e.g. BS being placed at a border crossing point. One can imagine many people being there in the same location (with possible a few metres spacing) far below the BS level. Scenarios M_d-M_f can be compared to a situation where the BS is located by the highway at the city entrance in the rush hours. If there is a traffic jam, one can observe a line of cars standing or slowly moving (temporary stationarity is assumed) at a comparable distance from the BS.

Table 3.3 – WDCM macro-cell scenarios, where a single MT is kept angularly separated from the rest (based on [GiCo02c]).

Sc #	d_{MT_l} [m]	r_{max} [m]	Scenario (not to scale):
M_g	1 500	200	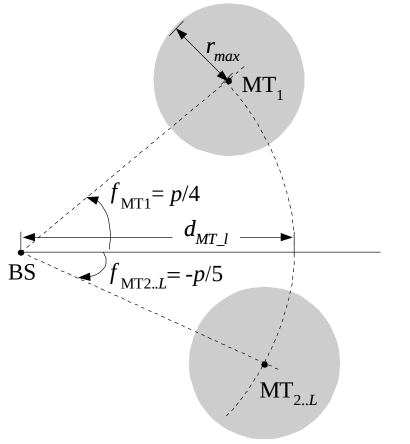
M_h		200	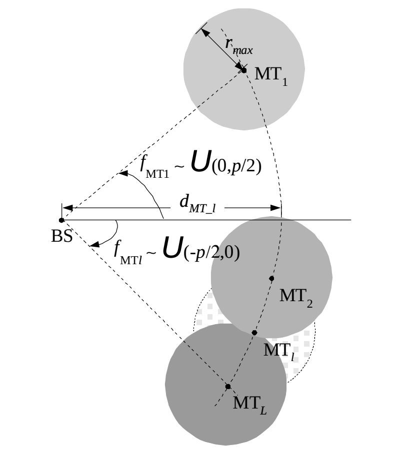

Scenarios from Table 3.3 assume constant BS-MT distance of 1500 m, scatterer circle radius of 200 m, and two MTs groupings, both with one MT separated from the rest. The first scenario places one MT at the angle of 45° with all others at –36°, and the other one considers a separate MT being placed at a random angle in the first quadrant, while the rest are placed separately at random fourth quadrant angles. These types of scenarios aim at verifying how the beamformer performs when one of MTs is placed separately from others, i.e., DesS comes from one specific direction, and all NDesI come from one or more other directions; these can also show better if the beamformer sets weights to form a visually clear array pattern, while directions of DesS and NDesI are well distinguished.

Scenarios M_g and M_h can be treated as variations of scenarios described above. For instance, one can imagine that scenario M_g corresponds to M_a-M_c grouping the sense that one user is on a gas station, placed at some angle in respect to the border crossing point, being separated from the grouping of the other users. Scenario M_h can represent a variation of M_d-M_f grouping, with one user, for instance an unfortunate owner of a broken car, is still in some distance from the rest of the cars staying in the traffic jam at the city entrance, calling for a road service to fix the car.

3.7 Analysis Approach

Due to the size of the matrices **R** and vectors **d**, leading to large computational time, most of the average calculations involve 100 totally independent DCIRs, with spatial cluster/scatterer distributions and reflection coefficients being independent between each DCIR concretisation. Anyhow, the number of required independent concretisations is still being accessed, especially taking into the account the larger processing time due to the larger sequence lengths required. SINR and BGs are, thus, averaged among concretisations, grouping MTs in the same situations, i.e., averaging together all that are dispersed or all those that exist within the same group.

The results on the SINR and BG dependency on the WDCM and scenario characteristics are evaluated as a function of the number of active users, distance between MT and BS, grouping and/or displacement of MTs, iteration number, and scenario specific parameters. Additionally, the several power components that are involved in the process, i.e., DesS, NDesI components, noise and cross-correlation contributions have been analysed as a function of scenario and iteration number, e.g., [GiCo02b] and [GiCo02c], for TDD. Array patterns have also been used for the analysis of results.

The calculation of SINR for the lth link follows (3.6) [GiCo01a]:

$$SINR^{(l)} = \frac{P_{DesS}{}^{(l)}}{\frac{1}{G_p}\left(\sum_{l_T=1}^{L_T} P_{NDesI}{}^{(l)} + N_{th}\right)} \tag{3.6}$$

where:

- G_p - CDMA processing gain (equal to the spreading factor, in this case, 128),
- P_{DesS} - DesS power,
- P_{NDesI} - NDesI power,
- N_{th} - total thermal noise power.

The noise power calculation assumes a matched circuit for each antenna. The maximum available power to a matched load, per Hertz, at T=290ºK, is given by:

$$N_0(f) = \mathrm{k}_{Boltz} \cdot T \cdot B_w \quad [W] \tag{3.7}$$

where:

- k_{Boltz} – Boltzmann constant,
- B_w = 5 MHz, UMTS FDD bandwidth.

The total noise available power for a noise equivalent bandwidth, B_w, will be equal to –107.02 dBm. Moreover, it is assumed that at each antenna element the low-noise amplifier has a noise factor of 3 dB. As the result additive noise power at each element is equal to –104.02 dBm [GiCo01a].

The Beamforming Gain (BG), G_{bf}, is defined as the SINR gain relative to the SINR achieved with a single omnidirectional antenna at the BS, for each of the L active links:

$$G_{bf}^{(l)} = SINR^{(l)}\Big|_{\mathrm{beamformer}} - SINR^{(l)}\Big|_{\mathrm{single}} \quad [dB] \tag{3.8}$$

As it was mentioned before, for all WDCM scenarios, 100 independent DCIRs, with independent spatial cluster/scatterer distributions and reflection coefficients between each DCIR concretisation, are calculated. As the results of these calculations, SINR and BG are obtained for every link l in every concretisation. These values are then averaged either together or in groups, depending on simulated scenario.

$$X = \frac{1}{KL}\sum_{k=1}^{K}\sum_{l=1}^{L} x_{k,l} \tag{3.9}$$

where:

- X – average SINR or BG,
- K- number of concretisations,
- L - number of active links,
- $x_{k,l}$ – SINR or BG of lth link at kth concretisation.

Similarly to calculating the mean value (among links and among concretisations), the standard deviation is also calculated among links as well as among concretisations, giving a view on the whole distribution of values, and to ensure that the number of concretisations is sufficient.

After preliminary simulations, it was verified that the standard deviation reaches the order of magnitude of several dBs (depending on scenario), which seams to be a large value. On the other hand, by changing the number of concretisations (10, 100) results remained nearly at the same level, varying by some fractions of dB.

As a consequence, the number of concretisations has been set to 100, also taking into account the very high computational burden. This choice of concretisations number was constrained by computational complexity on the one hand, and by a credibility of the statistical probe, on the other. 100 concretisations was considered to be the lower limit in the sense of statistics, but also the upper limit in the sense of acceptable time of simulations (single to several hours for a scenario, reaching dozens for most complicated ones).

All average calculations have been implemented using MATLAB® (file *ch_gbsb_av.m*). Implementation also included extension of the program to the FDD case, accounting for a variable and large number of users.

4 Analysis of Results

4.1 Initial Considerations

In this chapter, simulation results and their analysis are presented, separated into three levels. The first analysis level, intra-scenario analysis, considers detailed description of phenomena observed in each group of scenarios, further referred to as grouped MTs scenarios (M_a-M_c), randomly spread MTs scenarios (M_d-M_f) and "separate-others" MTs scenarios (M_g and M_h); on the second level of analysis, inter-scenario analysis, and a comparison between different groups of scenarios has been performed; finally the last level compares ULA and UCA simulation results. At the end some general conclusions are presented.

Before describing all scenarios, it is worth to present some general observations that are common for all simulations. It is worth to notice, Figure 4.1, that it has been verified that the CG algorithm is working properly on setting the final values of weights (resulting in corresponding BG values in BS) not later than after the 8^{th} iteration (usually after 4^{th}-6^{th} iteration) for 8-element ULA and 12-element UCA as well, which is consistent with theory. It is also visible that the evolution of CG is starting from small values (0-5dB), and then reaches a stable level, which can suggest that the initial guess may be important in increasing the speed of convergence of the algorithm. In cases where BG values are high, the evolution is starting from low value, and increasing, but for cases where BG is small, the behaviour of BG evolution is harder to predict.

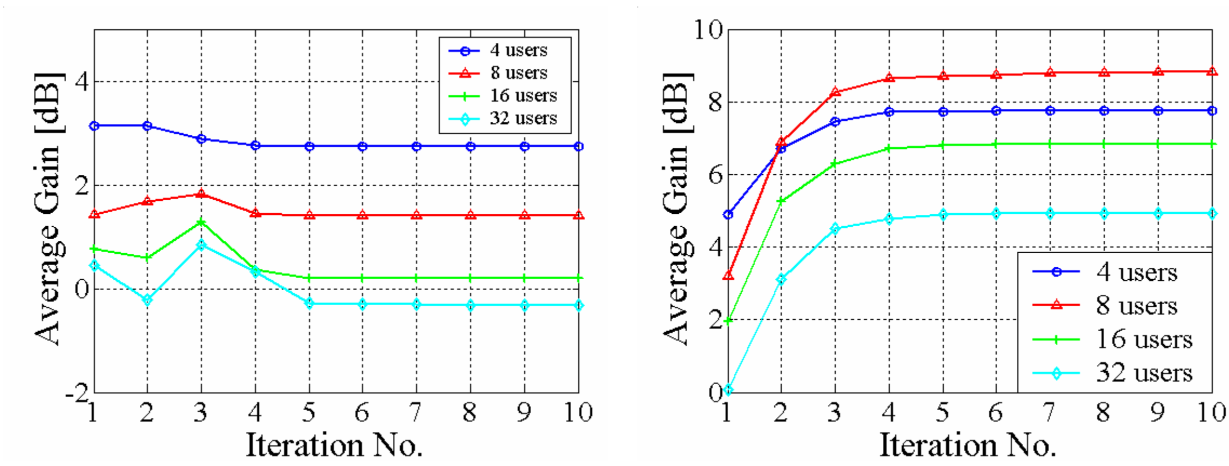

a) scenario M_b　　　　b) scenario M_d

Figure 4.1 – Examples of BG evolution as a function of iteration number.

In the following part of this chapter, the evolution of CG will be no longer presented, and only the final BG values will be used. Moreover, it is common for all scenarios that SINR falls more quickly with the increasing number of users than BG. Primarily, it can be explained by how BG is calculated (3.8). It seems logical that array SINRs decrease with the number of users, and that for the omnidirectional antenna the same phenomenon occurs (interference level from other users increases); the difference between this two, which is in fact BG, decreases slower of course.

Although the simulations have been done for 100 concretisations of DCIRs, it has been compared to the results achieved after averaging only 10 concretisations, Figure 4.. Numbers indicated in legends (SINR 10, Gain 100) indicate the number of DCIR concretisations used to calculate average and standard deviation. It is observable that differences between 10 and 100 are so insignificant that 100 concretisations have been acknowledged as a number large enough to make important conclusions. As one can observe, mean values are well inside the standard deviation borders of each other, which implies that simulations are reliable and precise enough. However, one should be aware that the difference or inaccuracy can happen for smaller number of iterations, as one can see in Figure 4.a; for 1000 m, the difference between gain obtained after averaging 10 simulations is around 1 dB less than for averaging 100 simulations. Moreover simulations with 100 independent DCIRs are already very time-consuming so increasing the number of concretisations does not seem adequate. In Figure 4.c,d, comparisons of standard deviations in respect to 100-concretisation standard deviation are presented, where:

- $\Delta = \left| \dfrac{average\,result\;\;from 10\,concretisations - average\,result\;\;from 100\,concretisations}{average\,result\;\;from 100\,concretisations} \right|$
- $e = \left| average\,result\;\;from 10\,concretisations - average\,result\;\;from 100\,concretisations \right|$
- $s10$ – standard deviation from 10-concretisation simulation
- $s100$ – standard deviation from 100-concretisation simulation

One can observe that error values are well below 10%, which confirms convergence between 10- and 100-concretisations results. Large value of relative error, *D*, in Figure 4.d is a result of proximity of values to zero, which in turn gives large *D* when calculating the difference; this is well known “subtraction of close to zero values” problem when calculating relative errors. To analyse the error value, the absolute error, *e*, has been calculated, and its result, lying below 10%, shows that vicinity of zero is the main reason for the large *D* value.

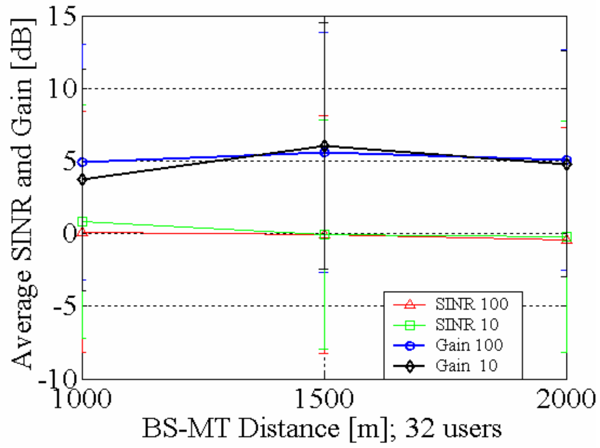

a) scenarios M_d-M_f

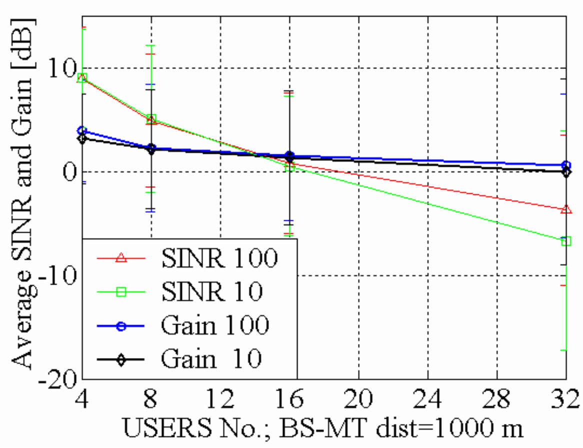

b) scenario M_a

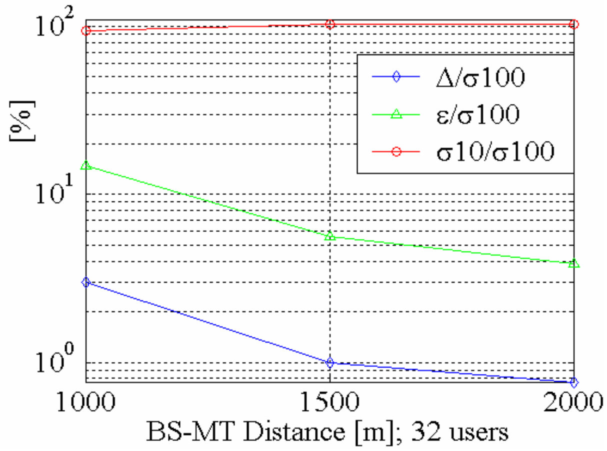

c) errors for scenarios M_d-M_f

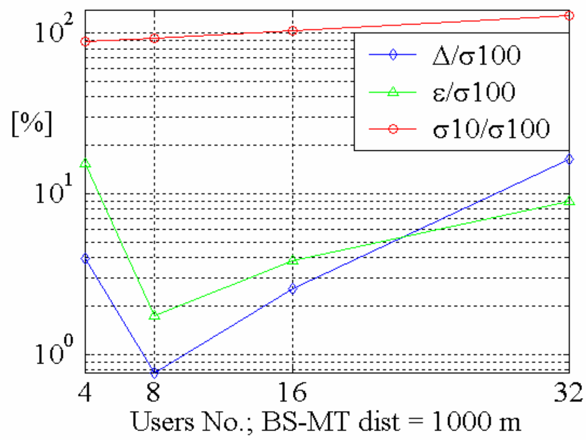

d) errors for scenario M_a

Figure 4.2 – Comparison of 10 and 100 concretisation averaging with mean values.

As an additional explanation for the number of simulations performed for each scenario, number of scenarios, and numbers of users chosen, one should be aware of computational complexity that results in the very large value of calculation time for each scenario. Examples of calculation times for 100 concretisations of UCA, which in case of ULA are more or less 2/3 shorter, because of less antenna elements used, have been put together in Table 4.1. For scenarios M_a-M_f, one can estimate 1 calculation unit, which is equal to calculation time for 100 concretisations for 4 users, which makes 2 Calculation units for 8 users, 4 calculation units for 16 users, and 8 for 32 users. That implies that one scenario, for 4, 8, 16 and 32 users, takes some 15 calculation units, which multiplied by the number of scenarios, and taking into account fact that scenarios M_g and M_h involve 64 users, it already seems to be quite large value. Increasing scattering circle radius, results in lengthening calculation time by several times, because DCIRs are much longer then. Taking into consideration the available resources (PC with Celeron 1.2 GHz processor and 256 MB RAM), chosen number of users, simulations and scenarios seemed to be the largest possible to be performed.

Table 4.1 – Calculation times for UCA simulations.

Scenario	Simulation time [hh:mm]				
	4 users	8 users	16 users	32 users	64 users
M_a	4:33	9:05	18:14	36:58	-
M_b (50 m)	-	0:42	1:27	-	-
M_b	3:43	7:22	14:47	29:56	-
M_b (400 m)	-	91:18	51:56	-	-
M_c	3:07	6:14	12:31	25:23	-
M_d	4:30	8:59	18:01	37:22	-
M_e (50 m)	-	0:42	1:35	-	-
M_e	3:40	7:19	14:43	29:48	-
M_e (400 m)	-	25:47	51:54	-	-
M_f	3:07	6:14	12:29	25:19	-
M_g	-	-	14:32	29:26	60:30
M_h	-	-	14:35	29:32	60:47

4.2 ULA Analysis

4.2.1 Intra-scenario Analysis

Grouped MTs scenarios

The first group of scenarios (M_a-M_c) consists of all MTs placed together in one position at 0° angle. It is worth to note that such placement is extremely difficult in the sense of beamforming, while, as it was mentioned before, in simulations DCIRs are the same for all MTs (only with changed phase to take into account the few metres spacing among them); moreover, especially in the macro-cell case, angle spread in these scenarios is extremely narrow. This results in fact that all signal contributions from all links arrive to the BS from exactly the same angles, so it is impossible for the beamformer to reduce NDesI components and place lobes in the directions of DesS. Results of simulations confirm that this placement is in fact very difficult for the beamformer to solve, and one can observe that BG is not reaching values more than 4 dB, Table 4.2, Figure 4.3. These values tend to decrease a little with the number of users, Figure 4.4, which is logical, since the gain is achieved because of code distinction of signals (CDMA). The more users are in the channel, the harder it is to distinguish them (additionally the codes are not fully orthogonal, which makes the problem more complex in order to increasing cross-correlation values). For 4 links the gain is low, but it is above the 0 dB level, but for 8 users and more, BG values for all scenarios of this group oscillate around 0 dB, which implies that there is no gain comparing to an omnidirectional antenna.

Table 4.2 – Simulation results for grouped MTs scenarios.

Scenario	No users	SINR			BG		
		Max value [dB]	CG Iteration number	Average value [dB]	Max value [dB]	CG Iteration number	Average value [dB]
M_a	4	9.12	3	8.94	4.09	3	3.90
	8	5.26	3	4.87	2.64	3	2.26
	16	1.33	4	0.77	2.05	4	1.50
	32	-2.97	4	-3.71	1.28	4	0.55
M_b	4	7.06	1	6.67	3.14	1	2.75
	8	3.74	3	3.31	1.83	3	1.40
	16	-0.03	3	-1.12	1.28	3	0.19
	32	-4.24	3	-5.41	0.85	3	-0.32
M_c	4	6.93	1	5.96	2.75	1	1.78
	8	3.03	2	2.07	1.22	2	0.27
	16	-0.76	1	-2.24	0.49	1	-0.99
	32	-5.18	1	-6.91	0.33	1	-1.40

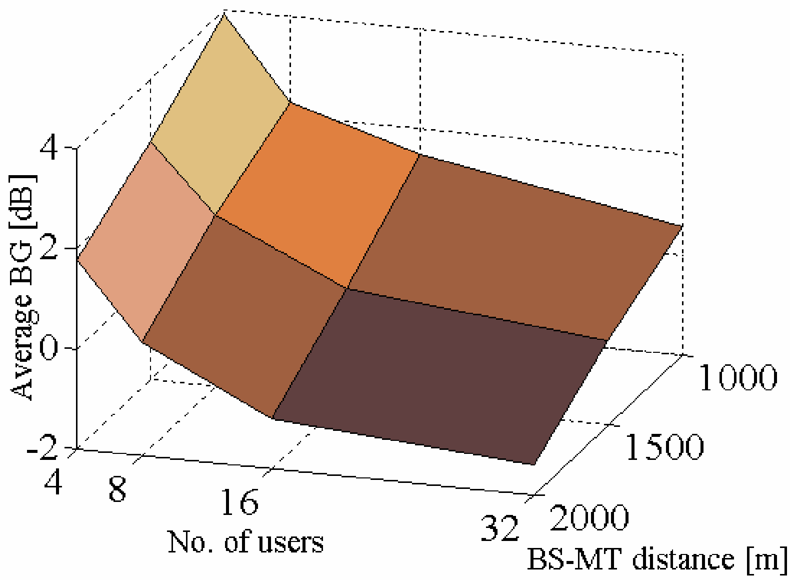

Figure 4.3 – BG and SINR as a function of BS-MT distance and number of users; scenarios M_a-M_c.

As a function of distance, Figure 4.5, BG shows a slight tendency to decrease with distance, which is probably caused by the equal suppression of all links, since they are all in the same place. It will be shown later that this phenomenon is not observed when the MTs are spread randomly around the BS (scenarios M_d-M_f), because then more visible effects are caused by MTs superimposing each other and signal suppression with distance is not visible.

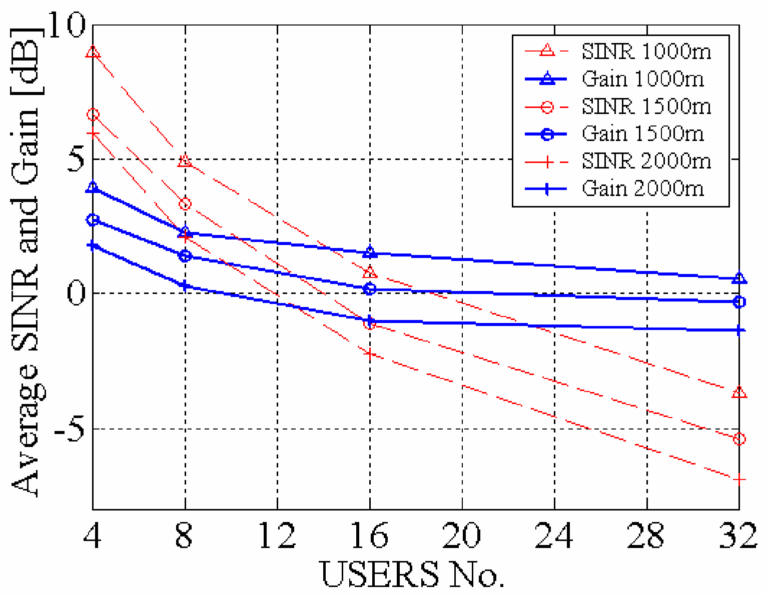

Figure 4.4 – BG and SINR as a function of number of users; scenarios M_a-M_c.

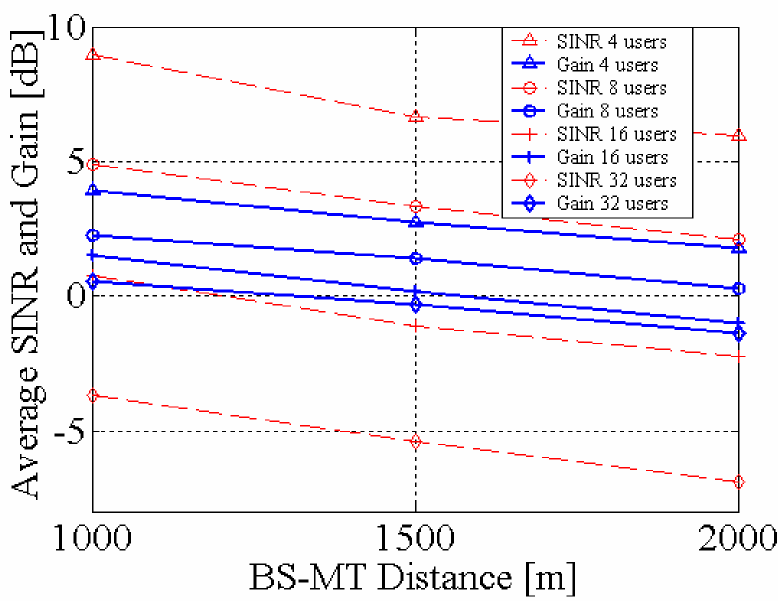

Figure 4.5 – BG and SINR as a function of BS-MT distance; scenarios M_a-M_c.

Randomly spread MTs scenarios

In the second group of scenarios (M_d-M_f), obtained gains are significantly higher (reaching more than 8 dB), Table 4.3, Figure 4.6. The main reason for that is the spatial spread of MTs, and what follows the spatial (angular) spread of DesS and NDesI contributions, because in opposition to the latter case, in these scenarios, AoAs of each link are independent of each other, which gives more freedom for the beamformer to place lobes in the direction of DesS and nulls in the direction of NDesI if possible. It is worth to notice that for this scenario the relation between the BG and BS-MT distance is very weak, Figure 4.7.

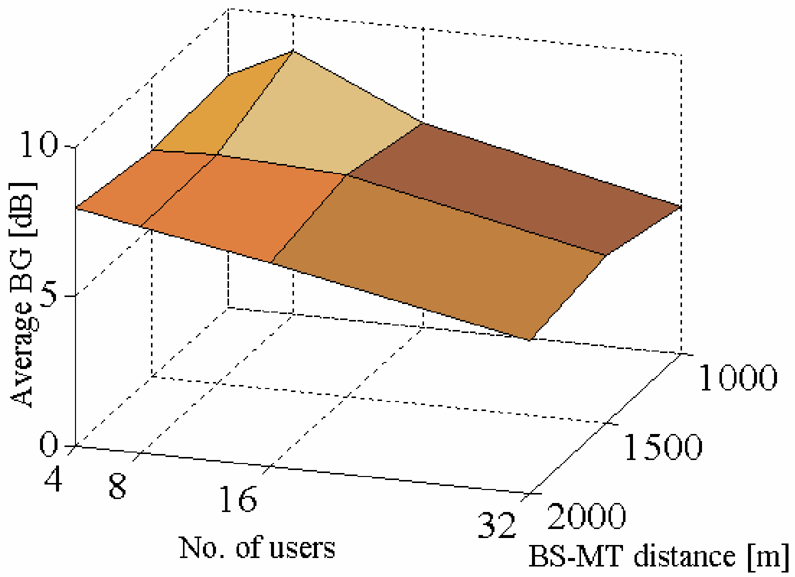

Figure 4.6 – BG and SINR as a function of BS-MT distance and number of users; scenarios M_d-M_f.

For the constant number of users, BG is practically independent of the distance. The probable reason is, as it was mentioned before, that the random nature of MT placement results in superimposing, adding and subtracting signals from different links. Also the relation between BG and number of links is not very visible, Figure 4.8. Only between 16 and 32 users one can observe a small tendency of BG to decrease. Between 4 and 16 users, the BG level remains almost constant for each BS-MT distance.

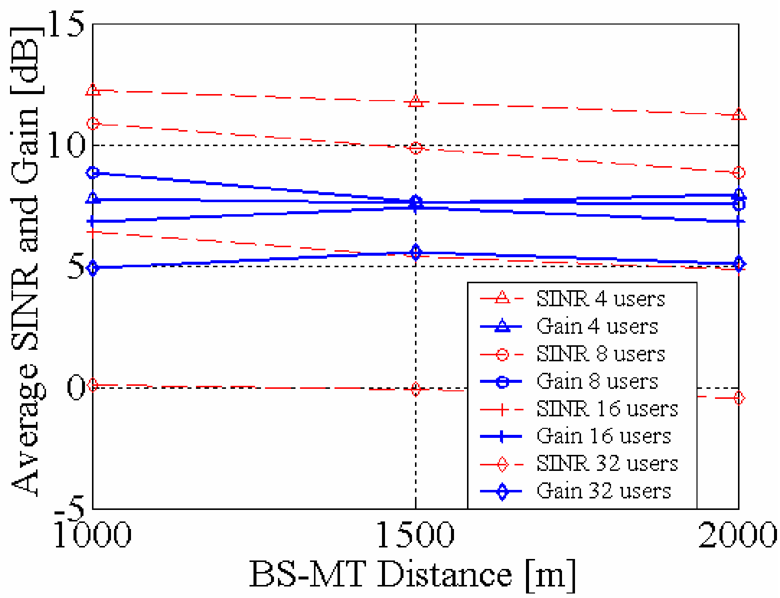

Figure 4.7 – BG and SINR as a function of BS-MT distance; scenarios M_d-M_f.

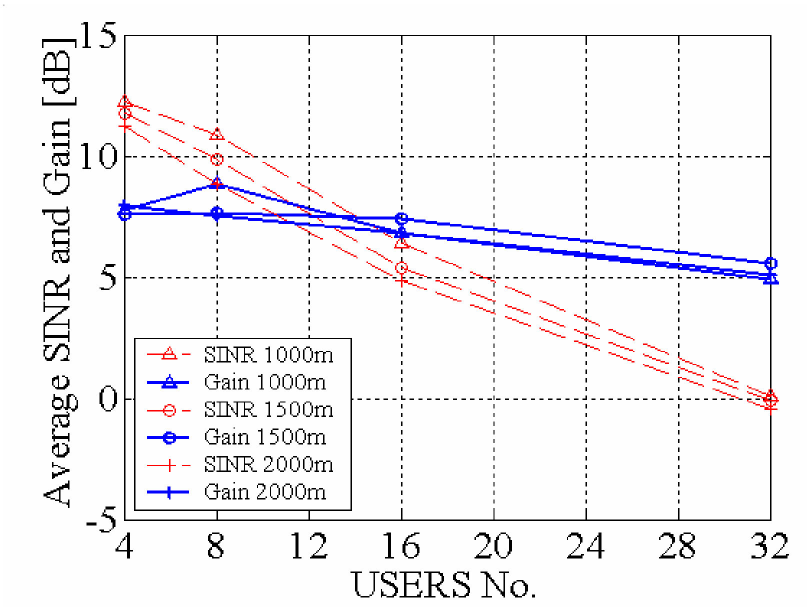

Figure 4.8 – BG and SINR as a function of number of users; scenarios M_d-M_f.

Table 4.3 – Simulation results for randomly spread MTs scenarios.

Scenario	No users	SINR			BG		
		Max value [dB]	CG Iteration number	Average value [dB]	Max value [dB]	CG Iteration number	Average value [dB]
M_d	4	12.21	10	12.21	7.76	10	7.76
	8	10.86	9	10.86	8.81	9	8.81
	16	6.41	6	6.41	6.83	6	6.83
	32	0.11	6	0.11	4.92	6	4.92
M_e	4	11.75	6	11.75	7.58	6	7.58
	8	9.88	10	9.88	7.66	10	7.66
	16	5.41	9	5.41	7.39	9	7.39
	32	-0.05	4	-0.06	5.61	4	5.59
M_f	4	11.22	10	11.22	7.94	10	7.94
	8	8.85	7	8.84	7.56	7	7.56
	16	4.85	8	4.85	6.80	8	6.80
	32	-0.44	6	-0.45	5.09	6	5.08

“Separate-others” MTs scenarios

The last group of scenarios consists of one MT placed separately from other MTs; other MTs are placed either together in one location (similarly to scenarios M_a-M_c) or spread randomly among fourth quadrant angles (similarly to scenarios M_d-M_f).

One can observe, Figure 4.9, that in scenario M_g gain of separate MT is well over 20 dB than grouped MTs, and that the difference increases with increasing number of users, Table 4.4. The position of MTs, separate as well as others, is well defined and constant, which lets placement of lobes and nulls to be performed precisely. Grouped MTs are in the same position, so the contributions of NDesI from that direction, can be reduced easily (probably with just one null) no matter how many users are there and the BG of separate MT grows in respect to other MTs, which all are cancelled at one time.

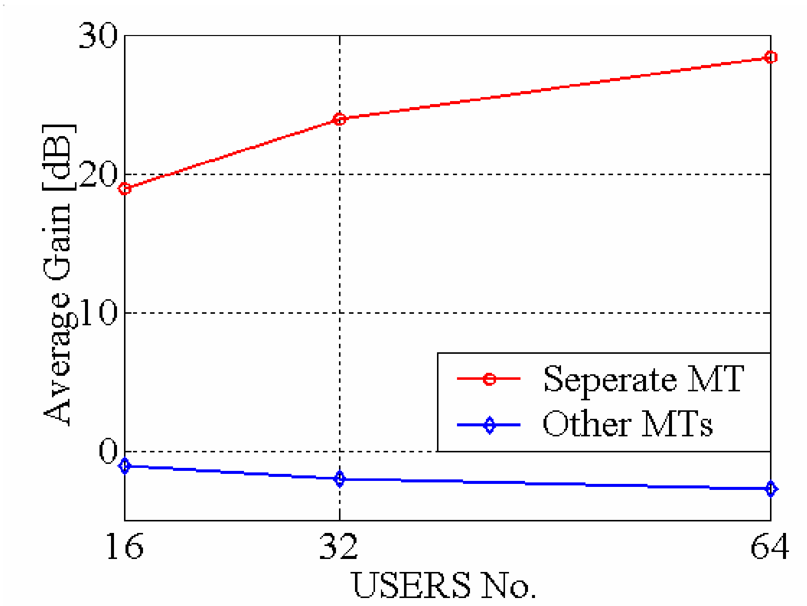

Figure 4.9 – Dependency of BG on number of users; scenario M_g.

The scenario M_h presents quite similar behaviour, Figure 4.10. In general still separate MT’s gain is dominating over other MTs’ average gain. Increasing the number of users makes the difference bigger, by increasing separate MT’s gain and decreasing other MTs gains. For 16 users the difference is less than 10 dB, than achieves almost 15 dB, reaching finally nearly 20 dB for 64 users.

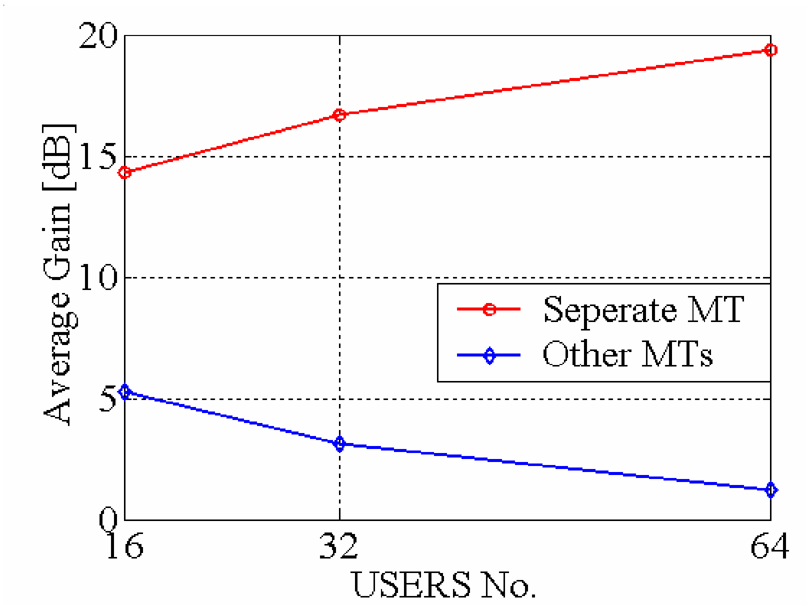

Figure 4.10 – Dependency of BG on number of users; scenario M_h.

Table 4.4 – Simulation results for “separate-others” MTs scenarios.

Scenario	No users	SINR		BG	
		Separate MT [dB]	Other MTs [dB]	Separate MT [dB]	Other MTs [dB]
M_g	16	17.60	-2.43	18.90	-1.12
	32	18.83	-7.14	23.91	-2.05
	64	19.74	-11.41	28.34	-2.81
M_h	16	12.64	3.58	14.30	5.24
	32	11.89	-1.67	16.68	3.13
	64	11.02	-7.14	19.40	1.24

4.2.2 Inter-scenario Analysis

As one can see, scenarios used in these simulations split generally into three groups: grouped MTs, randomly spread MTs, and “separate-others” MTs scenarios. Each of them has been described separately, but in this section they will be compared among each other.

Firstly, it is worth to emphasize that grouped MTs scenarios (M_a-M_c) are extremely difficult for the beamformer to solve, and it is hard to notice significant impact of smart antenna technology on receiving capability, Figure 4.11. Gain in these situations remains not larger that 5 dB, even for a very small number of users. For more users, it tends to be negative, which indicates that in fact there is no gain at all, in comparison to an omnidirectional antenna. It is important also to underline regularity in behaviour of the BGs, as well as a function of BS-MT distance and number of users. This regularity gives basis to predict with a good reliability that for more than 64 users and any distance, or for any number of users and distances more than 2000 m, BG would be negative. It also lets to estimate rough borders for sensibility of use of beamforming in above-mentioned conditions.

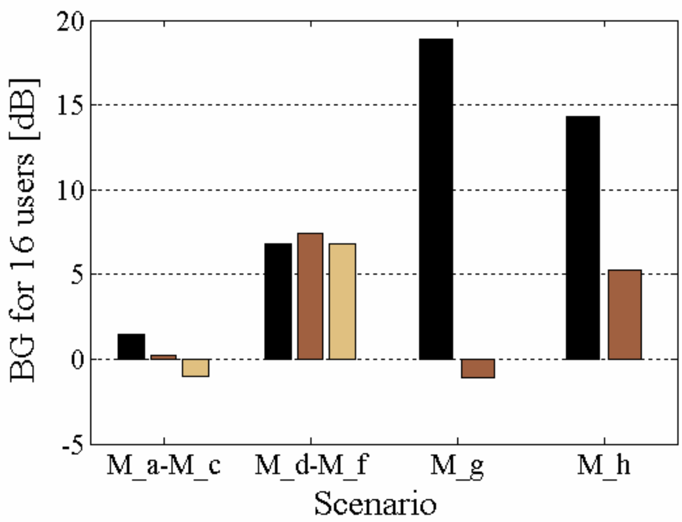

Figure 4.11 – Comparison of BG for different scenarios.

Randomly spread scenarios bring BG to the order of 8 dB for the smallest number of users, slightly decreasing when the number of users increases (5 dB for 32 users). In this group of scenarios, gains are much higher than in the former one. Moreover, they are independent of BS-MT distance, and only weakly dependent on the number of users; combined with the random nature of scenarios comprising this group it gives a more general view on the behaviour of BG when users are spread around BS, which is more likely in real world. These results indicate that it is easier to perform beamforming for users randomly spread than for all grouped together, which has been previously explained.

Between scenarios M_b and M_e, also dependency of BG on the scattering circle radius has been examined. Results have been put together in Table 4.5 and Figure 4.12. At first sight, one can notice the opposite behaviour in Figure 4.12 a) and b), particularly for extreme values. For scenario M_b, there is visible trend of BG to go up for 400 m, after nearly constant values for 50 and 200 m, while for M_e one can observe gain improvement for 50 m radius and falling values for 200 and 400 m. This behaviour can be explained by pointing that for 400 m, radius angle and temporal spread is much larger than for 50 and 200 m; it is easier then to place lobes in the directions of incoming signals. Of course, as it has been mentioned earlier, DCIRs for all MTs in this scenario are at the same position, and DesS and NDesI arrive from the same directions, but one can also gain from large time spread and reject all signals that are not correlated. Then probably, it is code orthogonality (or quasi-orthogonality) that gives gain from remaining contributions.

Table 4.5 – Results of dependency of BG on scattering circle radius.

Scenario	No users	BG [dB]		
		r_{max}=50 m	r_{max}=200 m	r_{max}=400m
M_b	8	1.46	1.40	2.52
	16	0.61	0.19	1.23
M_e	8	8.95	7.66	7.63
	16	9.11	7.39	5.96

Gain is not much, which suggests that this gain is really the matter of code distinction like in scenarios M_a-M_c where the gains were also small. In Figure 4.12b one can observe the behaviour of BG for different scattering circle radius for scenario M_e. The reason for this behaviour is very different from the former case. When all MTs are spread around the BS one can gain from narrowing angle spread, which happens for smaller radii, it allows to collect all DesS contributions with one narrow lobe, and it is relatively easy to null all or most of NDesI signals, because they also arrive in narrow angle spreads. Moreover, time spread is small, so there is also comparatively less not correlated signals that can add their contributions to NDesI.

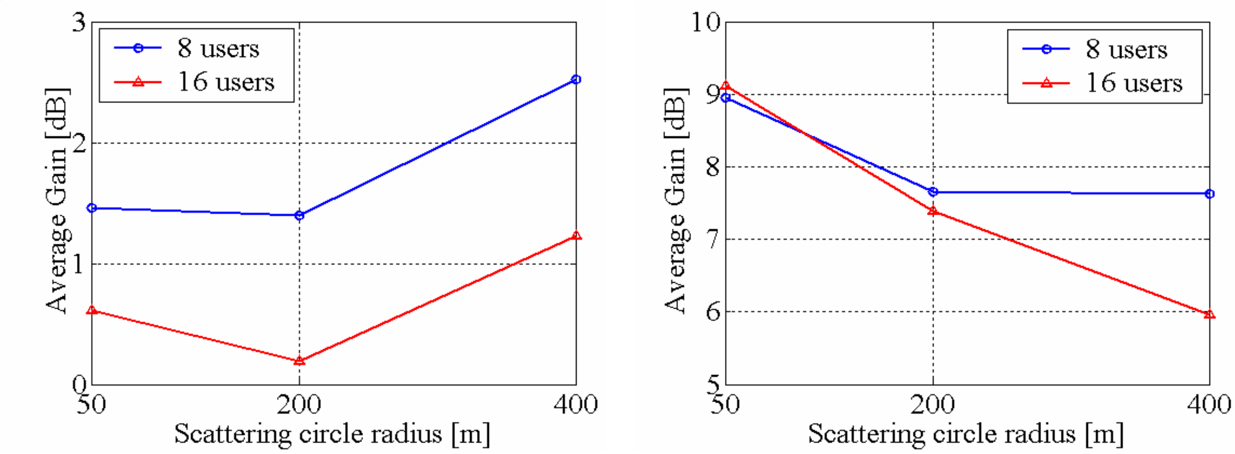

a) scenario M_b   b) scenario M_e

Figure 4.12 – Dependency of BG on scattering circle radius.

The characteristic feature for the last group of scenarios is the presence of a separate MT, which gives the beamformer the opportunity of placing the main lobe precisely in the direction of the DesS. The rest of MTs are either grouped together or spread randomly among the angles of the fourth quadrant. Comparing to other scenarios, it is visible that gains achieved in these ones are well above the gains present in other groupings, which shows that having one separate MT is a big advantage, letting the beamformer to reach good performance. One should also notice that other MTs follow the behaviour of the scenario, which are similar to, in the meaning that in scenario M_g, other MTs are grouped together like in scenario M_a-M_c, and in scenario M_h, other MTs are spread randomly like in scenario M_d-M_f. Even the values of BG of other MTs are not very far from the corresponding scenarios, however, with visible influence of separate MT lowering these values.

4.3 UCA Analysis

4.3.1 Intra-scenario Analysis

Grouped MTs scenarios

The behaviour of BG for this group of scenarios is quite similar as it was for ULA. One can still notice gains not higher than 5 dB for the whole range of distances, Figure 4.13, and numbers of MTs, Figure 4.14, used in simulations. Gains are falling with increasing number of users and increasing BS-MT distance, but in the sense of users’ number this trend attenuates and gains fall very slowly for 16 and 32 users, Figure 4.15. The main feature of this scenario is low level of achievable gains. Like it has been previously explained, the reason for that lies in particular in placement all MTs in same location, which makes the environment very demanding as far as beamforming is concerned. Firstly, all signals, both DesS and NDesI, arrive from the same AoAs, which makes beamforming useless, and most of the gain is achieved from code distinction of signals and results in BGs around 0 dB in almost all situations. Decreasing BG with distance shows also that beamforming system is more sensitive for distance changes than omnidirectional antenna for such users placement, which can be an important conclusion in opposition to gaining range with use of beamforming. The whole set of results for this scenario has been put together in Table 4.6.

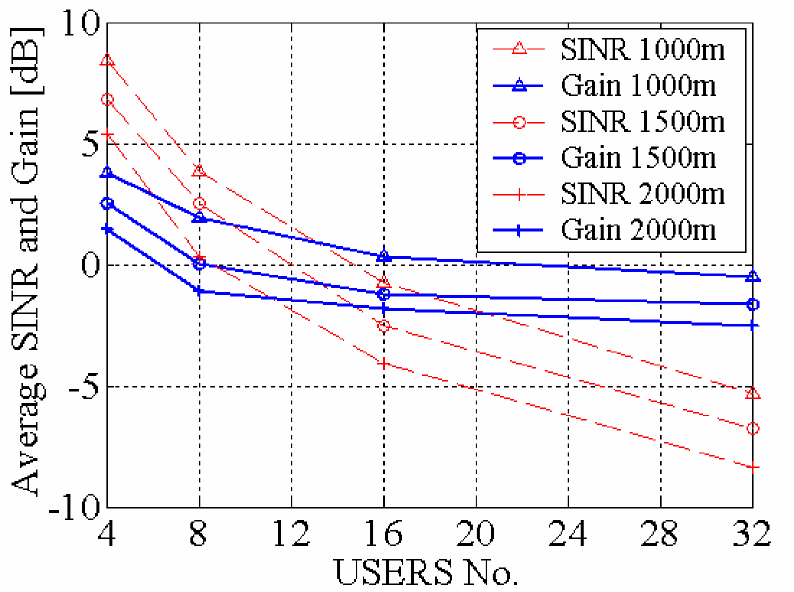

Figure 4.13 – BG and SINR of UCA as a function of number of users; scenarios M_a-M_c.

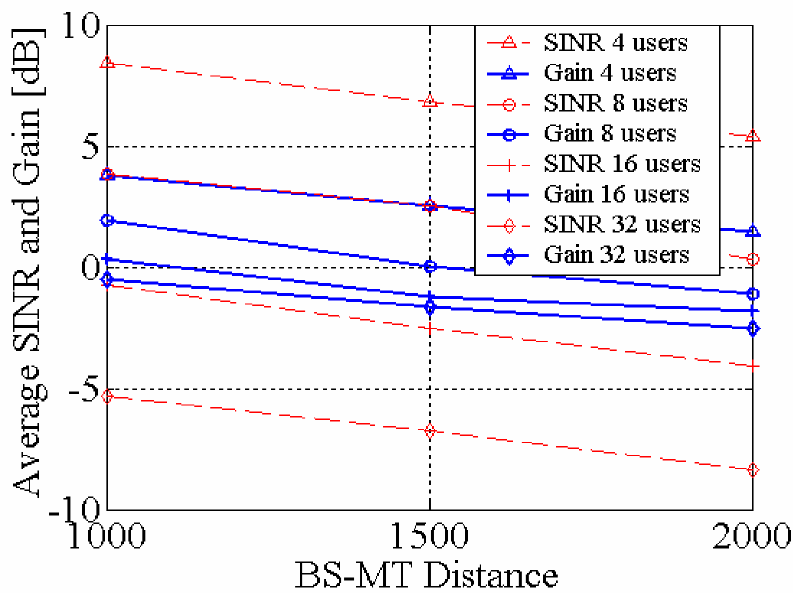

Figure 4.14 – BG and SINR of UCA as a function of BS-MT distance; scenarios M_a-M_c.

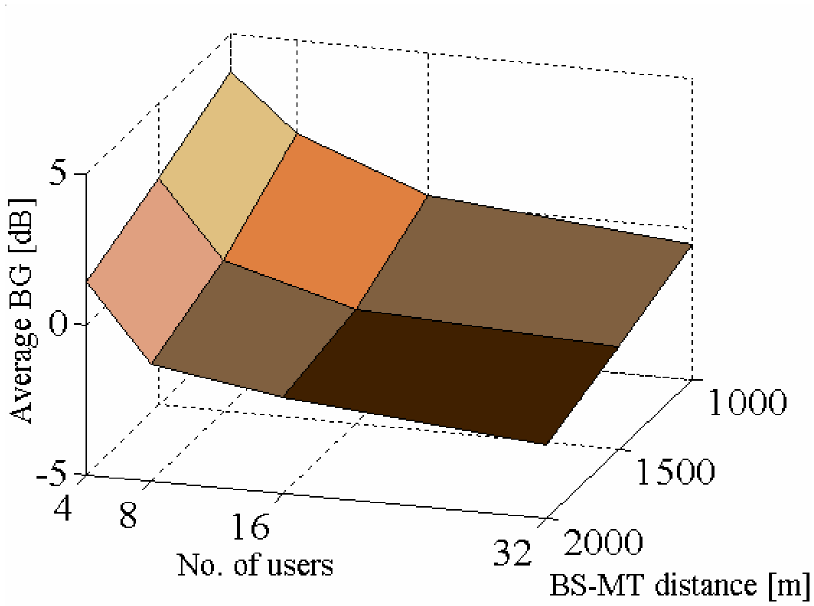

Figure 4.15 – BG and SINR of UCA as a function of BS-MT distance and number of users; scenarios M_a-M_c.

Table 4.6 – Simulation results for UCA for grouped MTs scenarios.

Scenario	No users	SINR			BG		
		Max value [dB]	CG Iteration number	Average value [dB]	Max value [dB]	CG Iteration number	Average value [dB]
M_a	4	8.63	3	8.40	3.98	3	3.76
	8	4.85	3	3.82	2.97	3	1.94
	16	0.81	3	-0.77	1.88	3	0.30
	32	-3.82	4	-5.31	0.99	4	-0.50
M_b	4	7.80	2	6.79	3.56	2	2.54
	8	3.97	2	2.52	1.48	2	0.03
	16	-0.40	1	-2.52	0.93	1	-1.19
	32	-4.31	3	-6.77	0.85	3	-1.61
M_c	4	6.52	1	5.38	2.57	1	1.43
	8	2.44	2	0.35	1.00	2	-1.09
	16	-1.74	1	-4.08	0.53	1	-1.81
	32	-5.35	1	-8.37	0.47	1	-2.54

Randomly spread MTs scenarios

In scenarios M_d-M_f one can observe gains of the order of 10 dB, Table 4.7, Figure 4.16. BG changes are not very large, oscillating around 7-11 dB. The relation between BG and number of users or BS-MT distance is not distinct. Again, the explanation for this type of behaviour should be found in the large freedom to place lobes and nulls by the beamformer, because of wide angular spread of MTs, and their DesS and NDesI. In Figure 4.17, dependency of BG on number of users for different BS-MT distances is shown. It is visible that while SINR fall almost linearly for the simulated numbers of users, BG remains nearly constant, which suggests that SINR of omnidirectional antenna falls probably in the same way, since BG is the difference between the two. Dependency of BG on the BS-MT distance is shown in Figure 4.18, where lack of relation in simulated range of distances is depicted.

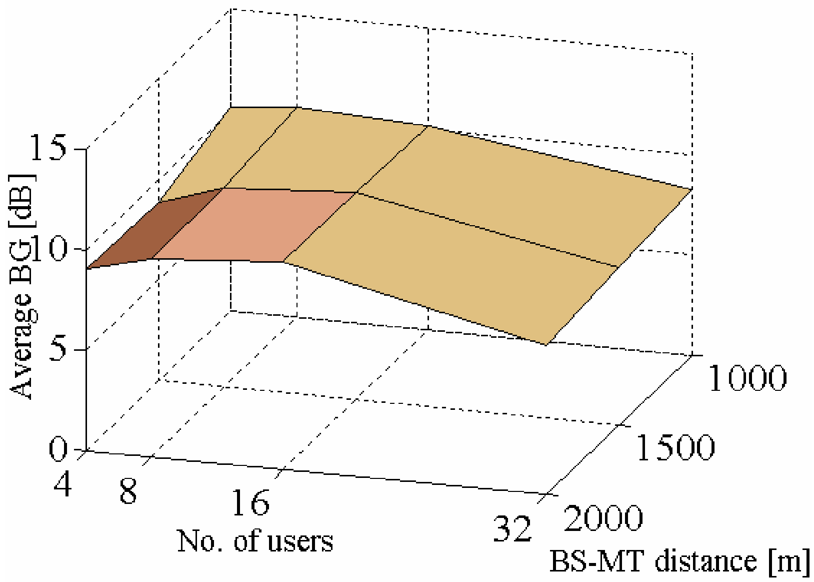

Figure 4.16 – BG and SINR of UCA as a function of BS-MT distance and number of users; scenarios M_a-M_c.

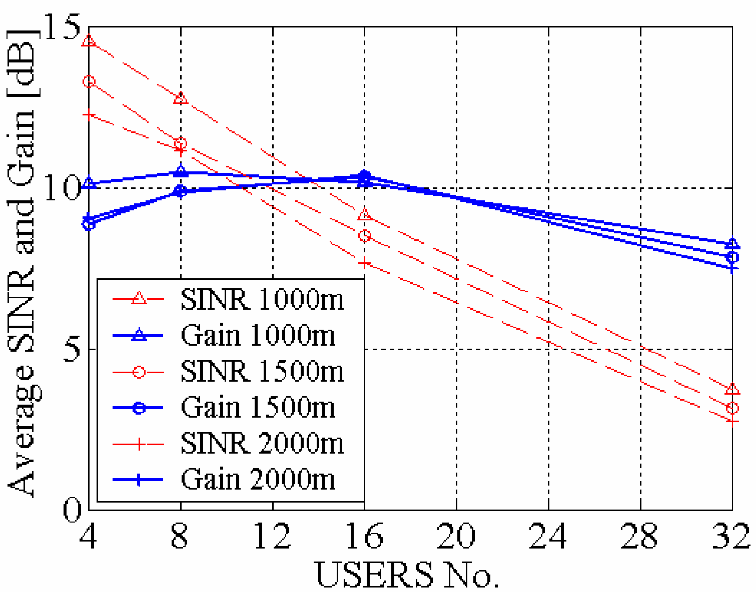

Figure 4.17 – BG and SINR of UCA as a function of number of users; scenarios M_d-M_f.

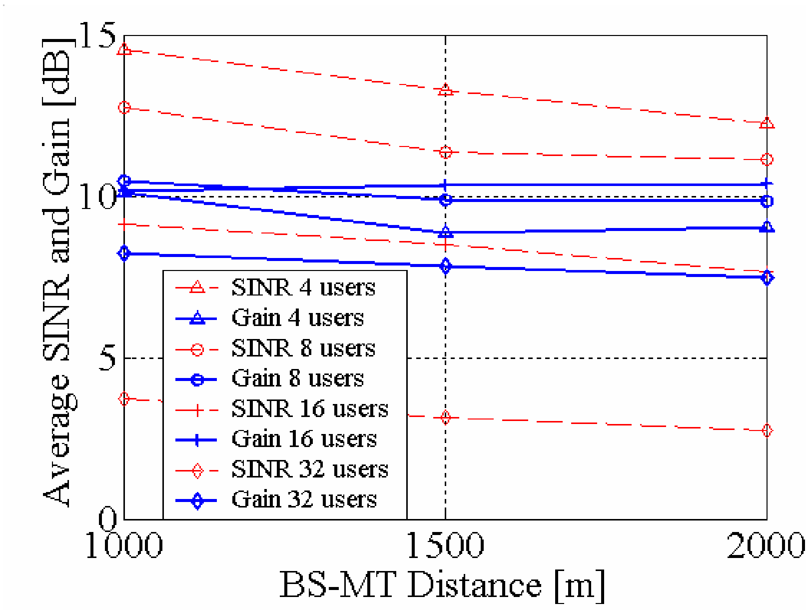

Figure 4.18 – BG and SINR of UCA as a function of BS-MT distance; scenarios M_d-M_f.

Table 4.7 – Simulation results for UCA for randomly spread MTs scenarios.

Scenario	No users	SINR			BG		
		Max value [dB]	CG Iteration number	Average value [dB]	Max value [dB]	CG Iteration number	Average value [dB]
M_d	4	14.55	10	14.55	10.12	10	10.12
	8	12.75	10	12.75	10.48	10	10.48
	16	9.13	10	9.13	10.16	10	10.16
	32	3.73	10	3.73	8.22	10	8.22
M_e	4	13.27	4	13.26	8.86	4	8.85
	8	11.36	9	11.36	9.90	9	9.89
	16	8.50	10	8.50	10.32	10	10.32
	32	3.13	10	3.13	7.84	10	7.84
M_f	4	12.25	10	12.25	9.05	10	9.05
	8	11.15	7	11.13	9.88	7	9.86
	16	7.63	10	7.63	10.37	10	10.37
	32	2.73	10	2.73	7.48	10	7.48

“Separate-others” MTs scenarios

The gain of a separate user is much higher than others reaching 20-30 dB for scenario M_g, Figure 4.19, and 15-20 dB for M_h, Figure 4.20. BG of other MTs remains nearly constant in scenario M_g, being independent on number of users, because all are suppressed by the same null. Well specified position of all NDesI (from separate MT point of view) lets beamformer to place null precisely. On the other hand, it is hard for the beamformer to achieve larger BG values for any other MT, because of their difficult placement, which has been described earlier in case of grouped MTs scenarios. In scenario M_h, BG of other MTs decreases probably as a result of superimposing signals when the number of users becomes large. The more users one has in the scenario, the harder it is to distinguish them and the stronger this effect is. At the same time separate MT remains at constant and well known position so the ratio between DesS and NDesI gets higher. Results obtained in this group of scenarios are presented in Table 4.8.

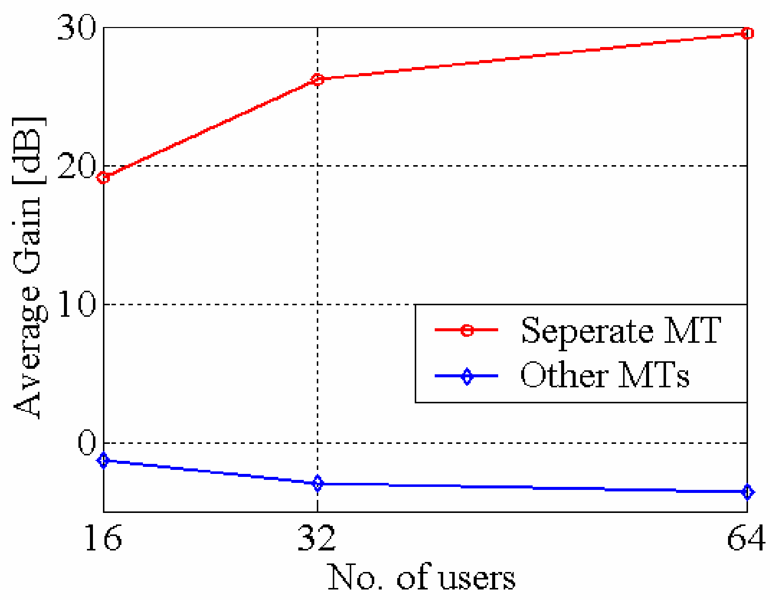

Figure 4.19 – Dependency of BG for UCA on number of users; scenario M_g.

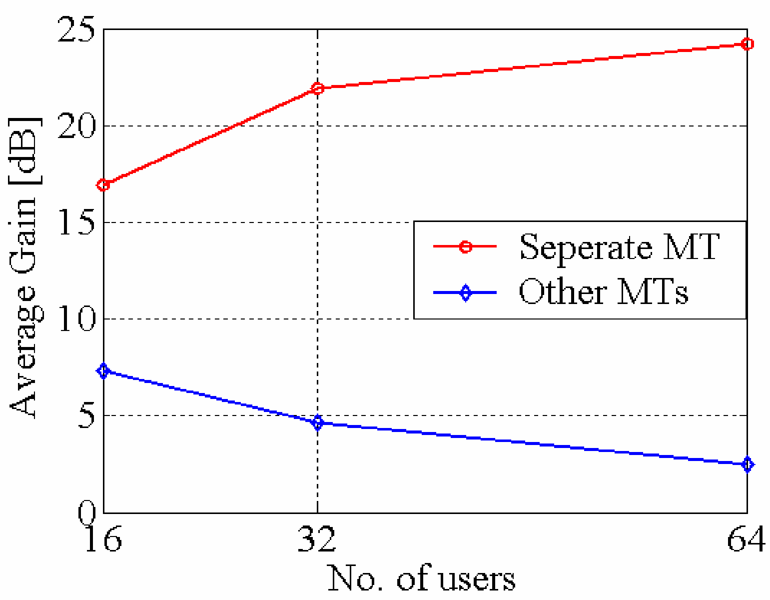

Figure 4.20 – Dependency of BG for UCA on number of users; scenario M_h.

Table 4.8 – Simulation results for UCA for “separate-others” MTs scenarios.

Scenario	No users	SINR		BG	
		Separate MT [dB]	Other MTs [dB]	Separate MT [dB]	Other MTs [dB]
M_g	16	17.87	-2.47	19.07	-1.26
	32	20.52	-8.59	26.17	-2.94
	64	21.02	-12.05	29.49	-3.58
M_h	16	15.67	6.08	16.94	7.35
	32	17.13	-0.12	21.94	4.69
	64	16.11	-5.65	24.21	2.46

4.3.2 Inter-scenario Analysis

One can notice that in scenarios M_a-M_c profit of using beamforming is very low or even none, Figure 4.21. The main reason for this has been previously introduced and is a result of difficult placement of MTs for the beamformer to solve. Scenarios M_d-M_f present much larger BG values and seem much more sensible to the use of beamforming, especially taking into account their stability at least in the ranges of MT numbers and BS-MT distances that have been simulated. Best possible results have been achieved in scenarios M_g and M_h, for which reasons have also been clarified.

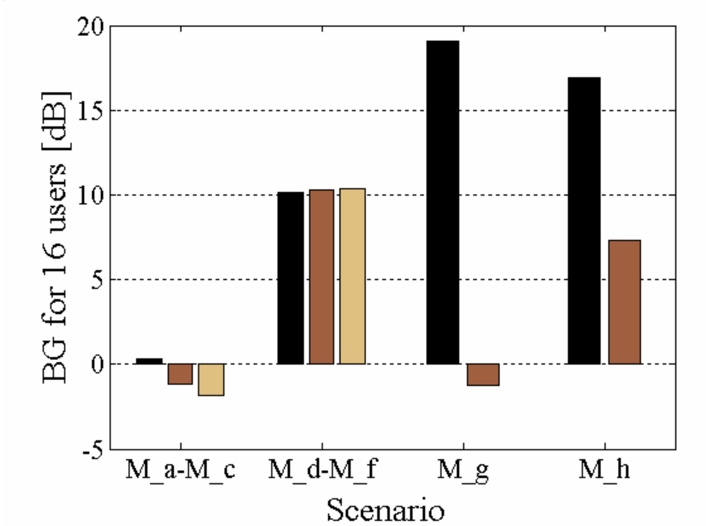

Figure 4.21 – Comparison of BG for different scenarios.

Like in the case of ULA, for scenarios M_b and M_e relation between BG and scattering circle radius have been examined, Table 4.9. Results of simulations are presented in Figure 4.22. Increase of BG values for some radii that has been wider explained for ULA, is in this case also visible. Particularly for scenario M_e difference between 50 m and other radii is noticeable, because it is easier for the beamformer to resolve angularly spread MTs. In case of scenario M_b difference to the advantage of 400 m is not that large, but it is still present. The reason has been previously clarified in the case of ULA. The fact that in Figure 4.22b BG for 16 users is slightly higher than for 8 users is of no importance for considering dependency of BG on scattering radius, and as it was already described in scenarios M_d-M_f BG remains nearly constant for different numbers of users (in this case it is not more than 1 dB).

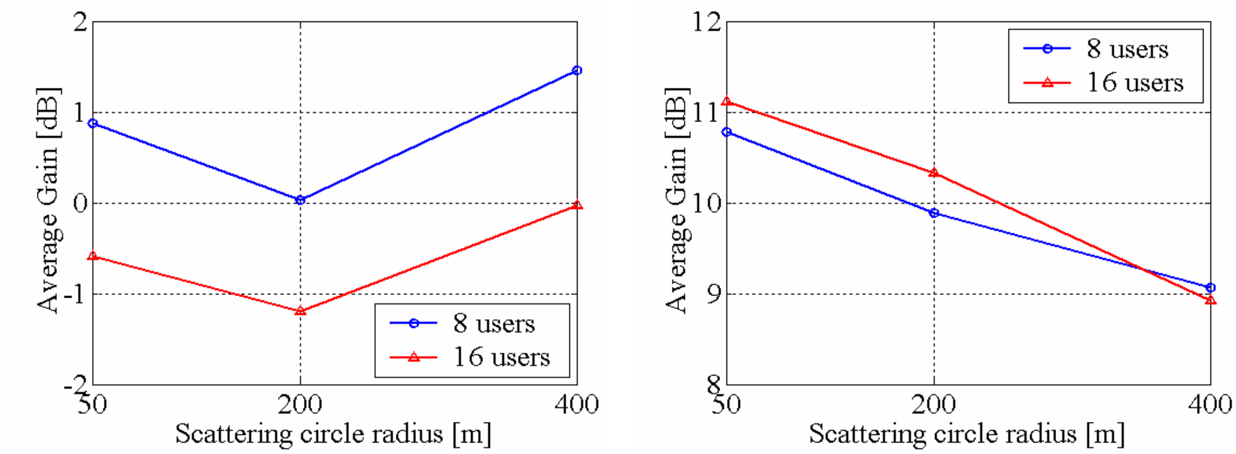

a) scenario M_b b) scenario M_e

Figure 4.22 – Dependency of BG on scattering circle radius for UCA.

Table 4.9 – Results of dependency of BG on scattering circle radius for UCA.

Scenario	No users	BG [dB]		
		r_{max}=50 m	r_{max}=200 m	r_{max}=400m
M_b	8	0.87	0.03	1.46
	16	-0.58	-1.19	-0.03
M_e	8	10.78	9.89	9.06
	16	11.11	10.32	8.92

4.4 Comparison of ULA and UCA

The previous analyses show, when comparing ULA and UCA, that behaviour of these two is very similar in each of simulated scenarios. Qualitatively both arrays behave in the same way, the only difference, in fact not that big, being in the quantitative comparison. Usually, when it happens, it is to the advantage of UCA, of which the clearest example is in scenario M_h, where the difference reaches nearly 5 dB. However, one should be still aware of large standard deviation values, which should suggest that these simulations have more qualitative meaning than quantitative one.

To compare directly ULA and UCA, a simulation for the same conditions have been performed. One concretisation, with the same DCIRs, the same random noise and phases has been used to analyse thoroughly the behaviour of both antennas. The scenario chosen for this comparison is M_g with the scattering circle radius of 50 m, since it guarantees the most precise placement of nulls and lobes, and is the most suitable, and easiest for beamforming, thus for comparison also. Firstly, the evolution of the BG along CG iterations has been examined, and results are shown in Figure 4.23.

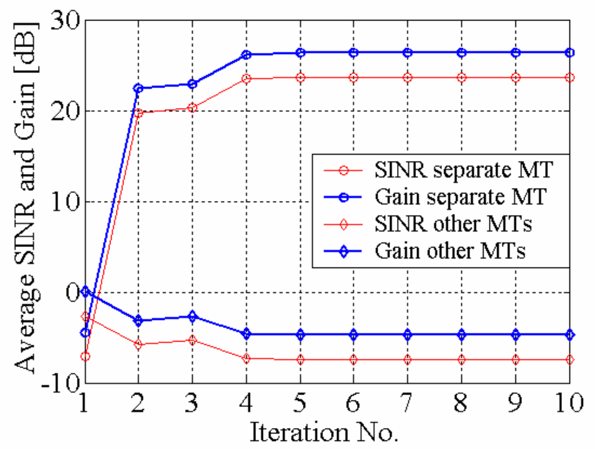

a) ULA

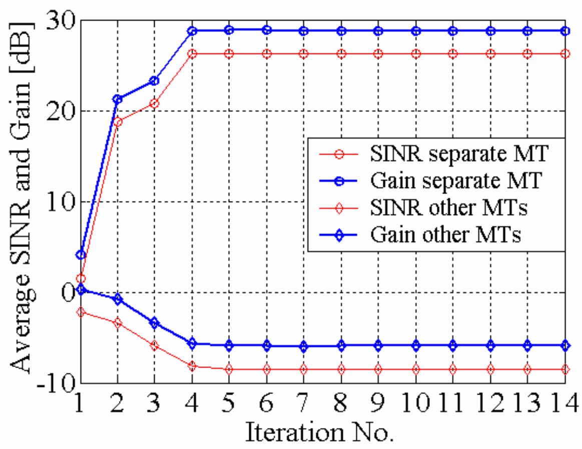

b) UCA

Figure 4.23 – Comparison of BG evolution for ULA and UCA.

One can observe that the behaviour is indeed very similar, even along CG iterations, but reaching slightly different values to the advantage of UCA, which has just been mentioned. In the 8-element ULA case, the evolution is presented along 10 iterations, since CG should obtain solution not later than after 8^{th} iteration, the same justification is for 14 iterations for 12-element UCA where solution should be reached before 12^{th} iteration, nevertheless one can see that in both cases BG reaches stable value after 4^{th} – 5^{th} iteration.

It is also worth to observe how array patterns behave for each of arrays, which is depicted in Figure 4.24. In Figure 4.24a,b only 180° angle sector between -90° and 90° is important, since the sectorisation, has been applied there. ULA pattern seems to be better than UCA, but it should be pointed that all patterns have been normalised to its maximum value, hence, they should not be compared quantitatively. One can also notice that for separate MT, ULA pattern has very well formed main lobe in the direction of DesS, small side lobes, and well placed null in the direction of NDesI. UCA has slightly worse main lobe in terms of direction, also well placed null in the direction of NDesI, but it has several big side lobes. To explain this, one should again remember that values are normalised to the pattern's maximum value, which means that the gain from main lobes does not has to be the same even if both have the same values. In terms of side lobes it should be noticed that the target of beamforming is to gain as much as possible from the DesS, and cancel as much as possible of NDesI. At this level of analysis it is assumed that all other directions are of no meaning, so the presence of side lobe, e.g., in the direction of 270° either does not improve or worsen BG, since DesS arrives from 45° and NDesI from –36°.

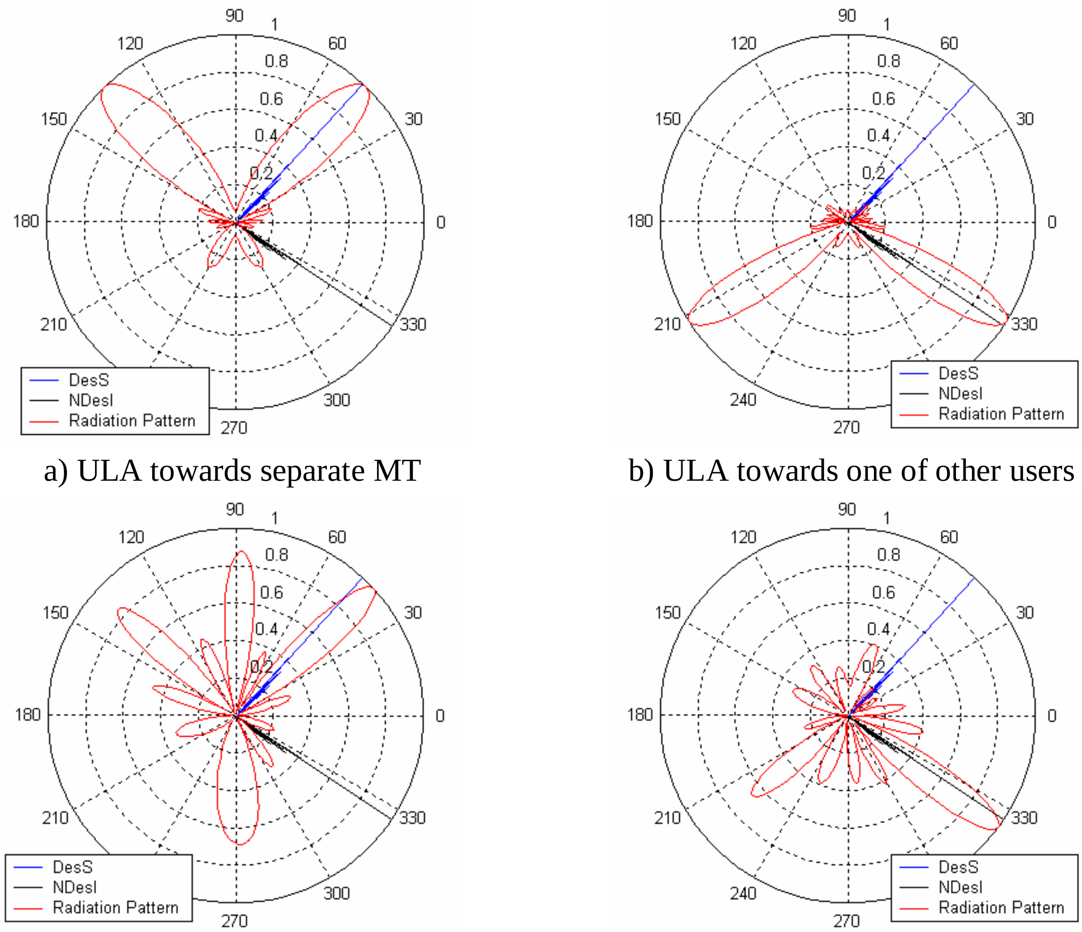

a) ULA towards separate MT

b) ULA towards one of other users

c) UCA towards separate MT

d) UCA towards one of other users

Figure 4.24 – Comparison of radiation patterns for ULA and UCA.

The array patterns of all grouped MTs are very similar, with similar main lobes, thus, leading to very low BGs, which was previously referred.

It has been verified that for most of situations, the best array patterns one can observe for 3^{rd}-4^{th} CG iteration. This phenomenon can be explained with the difference between MMSE and optimum SINR or BG solutions. In MMSE solution, the $\mathbf{w}^{\mathbf{H}}\mathbf{R}\mathbf{w}$ term in the cost function (2.9) involves not only the powers used in calculation of SINR, but also ones that do not contribute to the calculation of SINR. Several involved powers evolve differently, which implies that the MMSE may not lead to the best SINR and BG. Detailed analysis of the problem and composition of **R** can be found in [GiCo02b].

It is worth also to address the problem of sectorisation. All simulated scenarios are meant for 180° angle sectors, which does not allow to derive profits from the advantage of UCA, which is the ability to place the main lobe around 360°. It would be interesting e.g. to compare performance of both arrays at the borders of the sector, where ULA starts to radiate in the end fire direction. Also, some analysis of omnidirectional performance of UCA beamforming could be useful. All of these are predicted for future work and probably will be soon addressed.

Analysis of the results obtained in simulations allow to draw some general conclusions, however still being aware of the issues mentioned several times in this section, which are: quite large standard deviation leading to analyse the results rather qualitatively than quantitatively, limited number of scenarios in terms of numbers of users, distances and types of scenarios, which are the result of large computational complexity causing that simulations were very time taking, and finally characteristics of the scenarios favouring ULA and not letting UCA to show its all capabilities.

One can see from the obtained results, that the biggest impact on BG was the spatial placement of MTs, and depending on it BG values can vary from negative ones to well above 25, or even nearly 30 dB. Other factors like BS-MT distance, number of users or scattering circle radius are highly scenario dependent, and these have no general impact on BG. In some scenarios use of beamforming gives no gain at all, and these scenarios should be examined particularly in deep, to learn why is that, and if there is anything to do to improve the situation. In other scenarios the gain is very high, which should be also well studied to gain as much as possible from these.

Generally, results show that there is nearly no difference between the two used antenna arrays, so it is very hard to say which one is more suitable. From this point of view, the deciding issue can be economy, in the sense that it should be calculated if it compensates to use 12-element UCA or just 8-element ULA is enough. In the future one of the arguments can be possibility to use one UCA instead of using 2 or 3 ULAs.

5 Conclusions

At the beginning of this work, general characteristic of UMTS has been described, with the emphasis put on some very important aspects. One can find more detailed information on system architecture to identify the domain of further work. Frequency bands have been introduced with explanation of difference between FDD and TDD modes. Furthermore, coding issues have been described, and finally power control, to give an overall view on all aspects one should know, when dealing with beamforming in UMTS.

Later on, one can find the preview of several channel models; various channel models have been put together and briefly described. It can be noticed that the choice of the channel model to be used in simulations should be tuned to specific scenario that will be simulated or analysed. It has been identified that some of the models were developed to provide analytical models of the spatial correlation function, while others are intended primarily for simulation purposes. The models have varying complexity, and the set of assumptions underlying each approach depends on environments or geometries with varying deepness, or do not depend at all on them. Some can be applied to specific environments (macro- or micro-cells), while others are more general. It should be noticed that general assumptions are often similar for many models, e.g., to simulate multipath and wideband nature of radio-channel a number of scatterers are being used. The models are also different in details, e.g., in geometrical placement of scatterers. Some of them put more attention from a geometrical point of view, while others do it from a statistical one. Some models tend to be more precise, but more complex in calculating and obtaining results, while others, meant for simulation purposes, are simpler, remaining still comparable with measurement data.

Finally, some of the approaches are mixed ones resulting in hybrid models taking into account geometry and statistics of the model. Usually it results in simple, but quite precise models, such as GBSBMs, and these are considered the best for the simulation purposes, thus both have been described in detail.

Having already specific system (UMTS) and transmission medium (GBSBC and GBSBE) models, one should consider which adaptive algorithm to choose. There are various criteria described in this work. Inputs and outputs of each criterion have been identified, which is the most important issue, when choosing the specific one. MMSE criterion seems to be the best for the purpose of this work, because although one has to generate reference signal (which in CDMA systems is already generated), the DoA can be unknown.

Several algorithms have been also described. The choice of algorithm is crucial in terms of performance. One should always consider a constant trade-off between speed of convergence and computational complexity. The CG algorithm has been chosen and described in detail, because of its fast convergence, good stability, and acceptable computational complexity. All these features are combined with its simplicity, which makes simulations and analysis easy.

Theory of linear and circular arrays has been also presented, since these two types of antenna arrays are simple and useful for analysis, being at the same time good for beamforming purposes. A linear array is easy to implement and to feed with proper currents, but it radiates power to the front as well as to the back. A circular array does not have this symmetry, can steer the main beam to any direction in angular range of $[0; 2\pi[$, but is more difficult to implement and to feed.

Simulation environments have been mainly implemented in MATLAB®, and have been described in Chapter 3. Part of the work is based on [GiCo02d], but it required several changes, mostly concerning automation of the code caused by use of large numbers of users. Moreover, as a result of using a different UMTS mode in respect to [GiCo02d], some changes have been applied; these changes caused increase of computational complexity, and again required some changes to tune up performance. Long code sequences used in UMTS FDD mode and large number of users used in simulations, made some matrices very big, which also became a problem to solve, since the computers used did not have enough memory. Sets of scenarios have also been defined and described with a brief explanation of crucial terms, and relation to real-world situations. After undergoing all these problems, and optimising the code to be most efficient, simulations have been started.

Simulation results have been analysed in three levels; the most detailed one, intra-scenario level, includes an accurate analysis of each scenario/group of scenarios. Second level, inter-scenario analysis, considers relations between different scenarios/groups of scenarios, but still for the same array, ULA or UCA. At last, results obtained for ULA and UCA have been compared and overall conclusions have been drawn.

Generally, MT grouping has been identified as the issue being most important, and having the major impact on beamforming. Other issues, like scattering circle radius, BS-MT distance, or number of users does not have that much impact, modifying BG only by the order of magnitude of several dB. Analysis also showed that some scenarios have no or nearly no gain at all, while others have gains of 25-30 dB. These observations show that beamforming can really have very positive impact on receiving/transmitting, but one should be aware that is not always the case.

It should be noticed that in future work downlink beamforming should be addressed, to investigate which is its impact on BG, when BS is transmitting to MT. One of the possibilities is to use weights estimated in UL, and to simulate DL transmission just by changing reflection coefficients as a result of 190 MHz duplex offset between UL and DL, and changing spreading/scrambling sequence for the proper for DL transmission. BG should be then measured at MT antenna, considered for simplicity as an omnidirectional. The channel model used to generate DCIRs in UL direction has also ability to perform simulations in reverse direction, allowing to measure signals arriving to the centre of scattering circle from BS. As a result of different transmitting and receiving frequencies, interferences from other MTs can be omitted. In first approach the same scenarios should be analysed, and compared with results obtained in UL simulations.

Also some more scenarios should be examined. Especially in case of UCA, 360° randomly angular spread MTs results can be important, giving the possibility to resign from sectorisation, which is needed in case of ULA, as a result of ULA radiation symmetry. Possibly, if gains would be high enough using UCA, then one UCA could be used instead of using two ULAs to cover the 360°-angle area.

Worth to address in the future work seem to be also scenarios based on M_a-M_c or M_d-M_f groups, but with mixed BS-MT distances, e.g., group of users at 1000 m, and other group of users at 1500 or 2000 m. Some scenarios similar to M_g or M_h can be simulated, keeping one MT separated from others in distance or in distance and position at one time.

Finally some problems should be studied better: existence of large standard deviations in obtained results, and relation between MMSE and BG optima.

Annex A – Directional Channel Models

Lee's Model

In Lee's model [LiRa99], scatterers are evenly spaced on a circular ring about the MT, Figure A.1. Each of the scatterers is intended to represent the effect of many scatterers within the region and, are referred to as effective scatterers. The model was originally used to accurately predict the correlation between signals received by two sensors as a function of element spacing at the BS or MT. However, since the correlation matrix of the received signal vector of an antenna array can be determined by considering the correlation between each pair of elements, the model has application to any arbitrary array size. Measurements of the correlation observed at both the BS and the MT are consistent with a narrow angle spread at the BS and a large angle spread at the MT. Correlation measurements made at the BS indicate that the typical radius of scatterers is from 100 to 200 wavelengths [LiRa99].

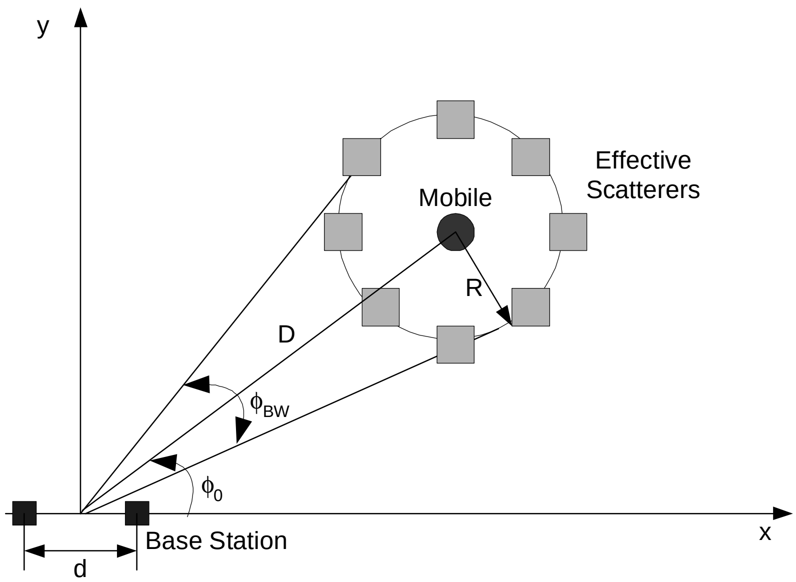

Figure A.1 – Lee's Model (extracted from [LiRa99]).

Motivated by the need to consider small-scale fading in diversity systems, Stapleton et al. [LiRa99] proposed an extension to Lee's model that accounts for Doppler shift by imposing an angular velocity on the ring of scatterers. For the model to give appropriate maximum Doppler shift, the angular velocity of scatterers must equal v/R, where v is the vehicle velocity and R is the radius of the scatterer ring. Stapleton refers that this model can be used to simulate the BER for π/4-DQPSK (π/4-Differencial Quadrature Phase Shift Keying) systems in a manner, which closely matches measured data [LiRa99]. While the model is quite useful in predicting the correlation between any two elements of the array (thus the array correlation matrix), it is not well suited for simulations requiring a complete Vector Channel Impulse Response (VCIR) model of wireless channel.

Discrete Uniform Distribution

The Discrete Uniform Distribution model [LiRa99] is similar to Lee's model in terms of both motivation and analysis. The model evenly spaces *N* scatterers within a narrow beamwidth centred about the bearing to the MT as shown in Figure A.2. The model is useful for predicting the correlation between any pair of elements in the array (which can be used to calculate the array correlation matrix), but it fails to include all the channel phenomena, such as delay spread and Doppler spread, required for certain types of simulations.

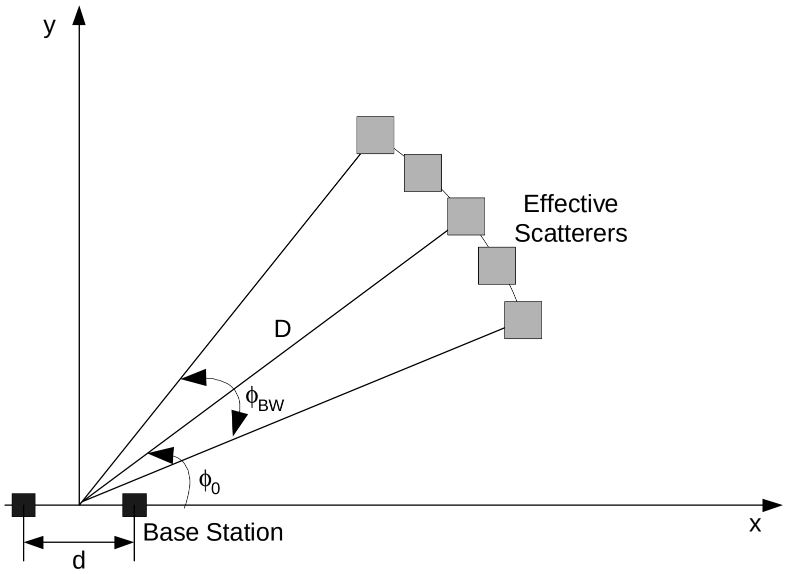

Figure A.2 – Discrete Uniform geometry (extracted from [LiRa99]).

Geometrically Based Single Bounce Statistical Channel Models

The Geometrically Based Single Bounce Statistical Channel Models [LiRa99] are developed by defining a spatial scatterer density function, and are useful for both simulation and analysis purposes. Use of the models for simulation involves randomly placing scatterers in the scatterer region according to the spatial scatterer density function. From the location of each of the scatterers, the DoA, ToA, and signal amplitude are determined. From the spatial scatterer density function it is possible to derive the joint and marginal ToA and DoA probability density functions. Knowledge of these statistics can be used to predict the performance of an adaptive array. Furthermore, knowledge of the underlying structure of the resulting array response vector may be exploited by beamforming and position location algorithms.

Two variations of the GBSB model are considered. The GBSBCM is applicable to high tier, macro-cellular scenarios where the base station is very high relative to scatterers, and is based on a circular distribution of scatterers near the mobile unit. A second model, a GBSBEM, assumes that scatterers are distributed throughout the transmitter/receiver path. The GBSBEM is more applicable to low tier microcell systems and cases where the base station antenna is at the same height as the surrounding clutter [LiRa99].

The geometry of the GBSBCM is shown in the Figure A.3. It assumes that scatterers lie within radius r_{max} about the mobile. Often the requirement that $r_{max} < D$ is imposed. The model is based on the assumption that in macrocell environments, where antenna heights are relatively high, there will be no signal scattering from locations near the base station. The circular model predicts a relatively high probability of multipath components with small excess along the LoS. From the base station perspective, all of the multipath components are restricted to lie within a small range of angles. The appropriate values for the radius of scatterers can be determined by equating the angle spread predicted by the model (which is a function of r_{max}) with measured values. Typical angle spread for macrocell environments with BS-MT separation of 1 km are approximately two to six degrees [LiRa99].

The GBSBCM can be used to generate sample channels for simulation purposes. Generation of sample channel impulse responses from GBSBCM is accomplished by uniformly placing scatterers in the circular scatter region about the mobile and then calculating the corresponding DoA, ToA, and power levels.

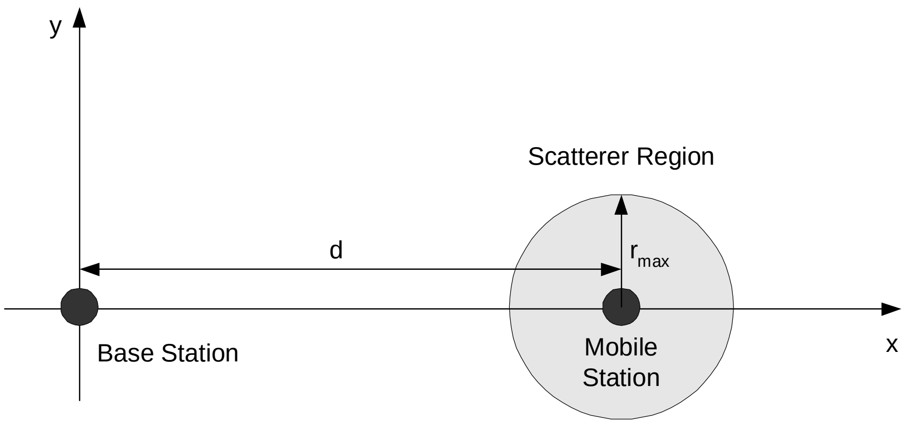

Figure A.3 – Circular scatterer density geometry (extracted from [LiRa99]).

In the GBSBEM model, scatterers are uniformly distributed within an ellipse, as shown in Figure A.4. This model was developed for microcell and picocell environments, where antenna heights are low, so the multipath scattering is just as likely near the BS as it is near the MT. An essential feature of the GBSBEM model is the physical interpretation that only multipath signals that arrive with an absolute delay of less than equal to τ_m are considered. Ignoring components with longer delays is possible because very long delays correspond to long paths, which experience higher path loss. Provided that τ_m is chosen sufficiently large, the model will account for nearly all power and DoA of multipath components.

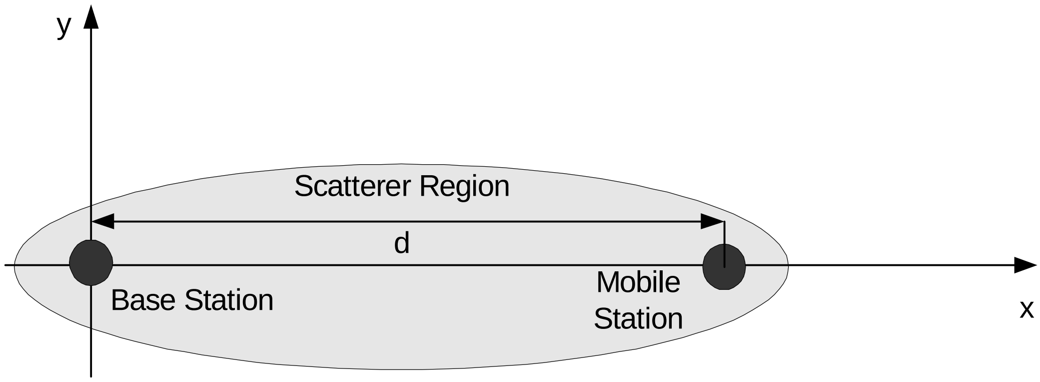

Figure A.4 – Elliptical scatterer density geometry (extracted from [LiRa99]).

The Gaussian Wide Sense Stationary Uncorrelated Scattering Model

The primary motivation of the Gaussian Wide Sense Stationary Uncorrelated Scattering (GWSSUS) model [LiRa99] is to provide a general equation for the received signal correlation matrix, where scatterers are grouped into clusters in space, the delay differences within each cluster not being resolvable within the transmission signal bandwidth. By including multiple clusters, resolvable multipath that introduces frequency selective fading channels is modelled using the GWSSUS. The model provides fairly general results for the form of covariance matrix; however, it does not indicate the number or location of the scattering clusters, hence, the model requires some additional information for application to typical environments [LiRa99].

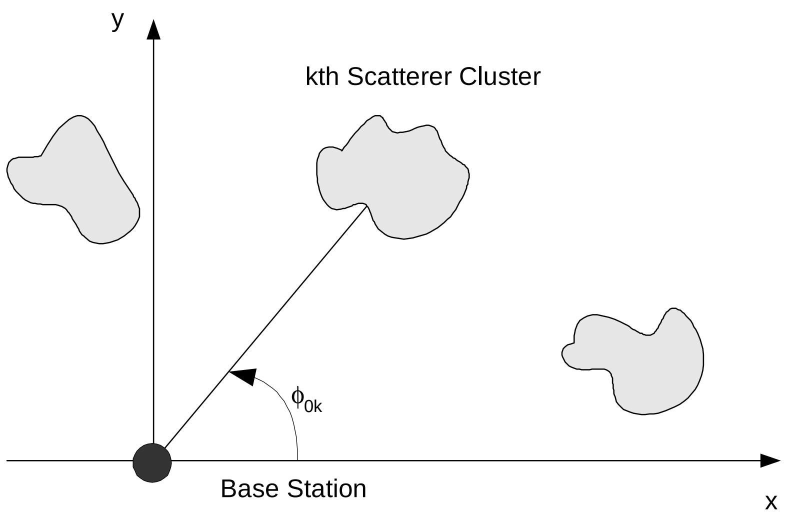

Figure A.5 – GWSSUS geometry (extract from [LiRa99]).

Gaussian Angle-Of-Arrival

The Gaussian Angle-Of-Arrival (GAA) channel model is a special case of the GWSSUS model, where only a single cluster is considered, and the DoA statistics are assumed to be Gaussian distributed around some nominal angle, f_0, as shown in Figure A.6. Since only a single cluster is considered, the model is a narrowband channel model that is valid when the time spread of the channel is small compared to the inverse of the signal bandwidth; hence, time shifts may be modelled as simple phase shifts and the channel is flat fading.

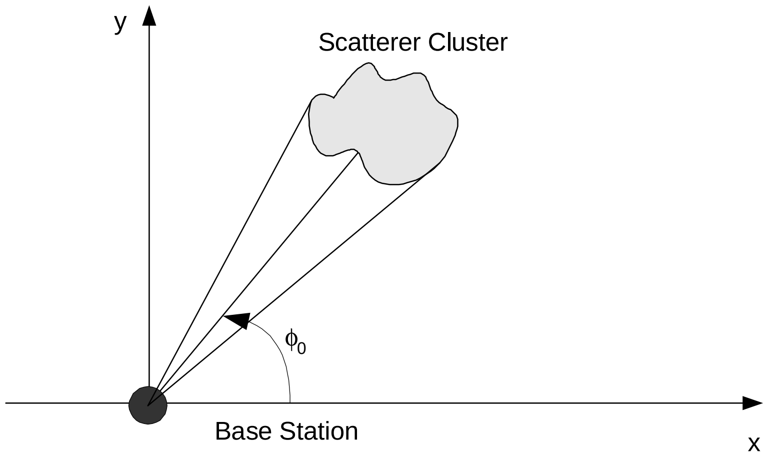

Figure A.6 – GAA geometry (extracted from [LiRa99]).

Time-Varying Vector Channel Model (Raleigh's Model)

Raleigh's time varying vector channel model [LiRa99] was developed to provide both small scale Rayleigh fading and theoretical spatial correlation properties. The propagation environment considered is densely populated with large dominant reflectors, as shown in Figure A.7.

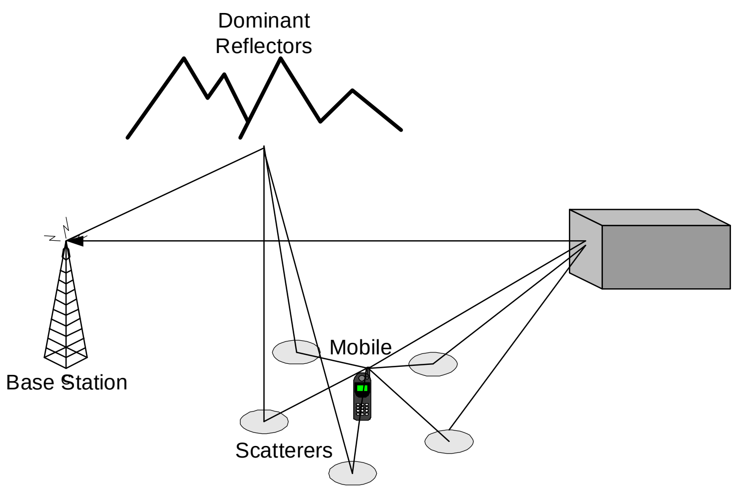

Figure A.7 – Raleigh's model signal environment (extracted from [LiRa99]).

Two GSM Simulation Models

Two spatial channel models [LiRa99] have been developed for simulation purposes in the GSM standard; the Typical Urban (TU) model is designed to have time properties appropriate for large towns in flat environments, while the Bad Urban (BU) was developed to model large delay spread environments with large reflectors that are not in the vicinity of the mobile.

In the TU Model, 120 scatterers are randomly placed within a 1 km radius around the MT. The position of the scatterers is held fixed over the duration in which the MT travels a distance of 5 m; at the end of the 5 m, scatterers are returned to their original position with respect to the MT; at each 5 m interval, random phases are assigned to the scatterers as well as randomised shadowing effects, which are modelled as log-normal with distance with a standard deviation of 5-10 dB. The received signal delay is determined by assuming a ray-traced path from the location of each scatterer. An exponential path loss law is also applied to account for large-scale fading. Simulations have shown that the non-directional TU model and the directional GSM-TU model have nearly identical power delay profiles, Doppler spectrums, and delay spreads. Furthermore, the DoA statistics are approximately Gaussian and similar to those of the GAA model.

The BU model is identical to the TU model, with the addition of a second scatter cluster with another 120 scatterers offset 45° from the first, as shown in Figure A.8. Scatterers in the second cluster are assigned 5 dB less average power than the original cluster, and presence of the second cluster results in increased angle spread, which in turn reduces off-diagonal elements of the array covariance matrix, besides causing an increase in delay spread. The Bad Urban vector channel geometry is shown in Figure A.8.

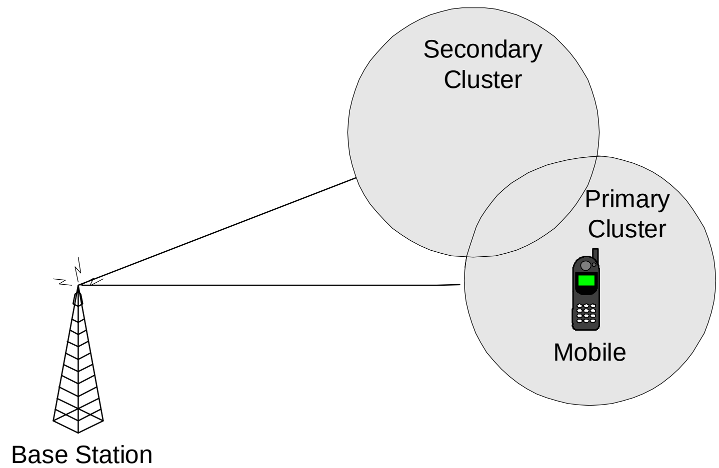

Figure A.8 – Bad Urban vector channel model geometry (extracted from [LiRa99]).

The Uniform Sectored Distribution Model

The Uniform Sectored Distribution model [LiRa99] assumes that scatterers are uniformly distributed within an angle distribution of f_{BW} and radial range of D_R centred about the mobile, the magnitude and phase associated with each scatterer being selected at random from a uniform distribution of [0,1] and [0,2π[, respectively. As the number of scatterers approaches infinity, the signal fading envelope becomes Rayleigh distributed with uniform phase [LiRa99].

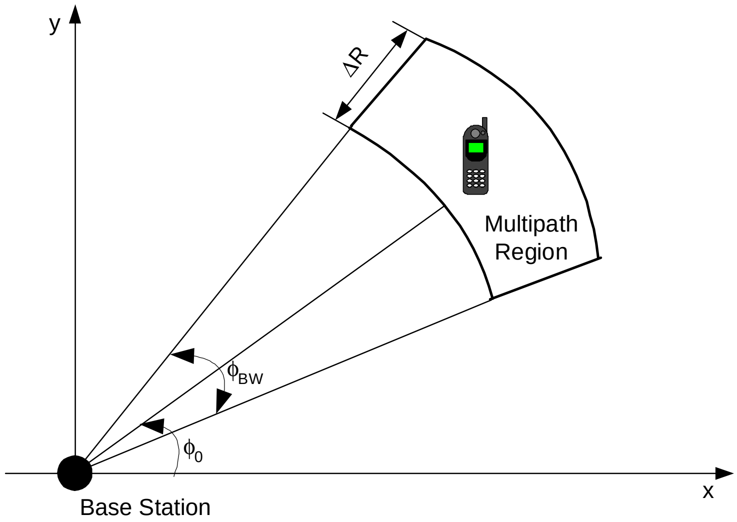

Figure A.9 – Geometry of the uniform sectored distribution (extracted from [LiRa99]).

Modified Saleh-Veneuela's Model

Saleh and Venezuela [LiRa99] developed a multipath channel model for indoor environments based on the clustering phenomenon observed in experimental data. The clustering phenomenon refers to the observation that multipath components arrive at the antenna in groups. It was found that both clusters and rays within a cluster decay in amplitude with time.

Elliptical Subregions Model (Lu, Lo, and Litva's Model)

Lu et al. [LiRa99] proposed a model for multipath propagation based on the distribution of the scatterers in elliptical subregions as shown in Figure A.10, each subregion corresponding to one range of the excess delay time. This approach is essentially the same as the GBSBEM developed by Liberti and Rappaport [LiRa99] in which an ellipse of scatterers is considered. The primary difference between the two models is in the selection of the number of scatterers and the distribution within the entire ellipse, since in Lu, Lo, and Litva's model, the ellipse is first subdivided into a number of subregions, the number of scatterers within each subregion being selected from the Poison random variable, whose mean is chosen to match the measured time delay profile data. It was also assumed that multipath components arrive in clusters due to multipath reflecting points of the scatterers.

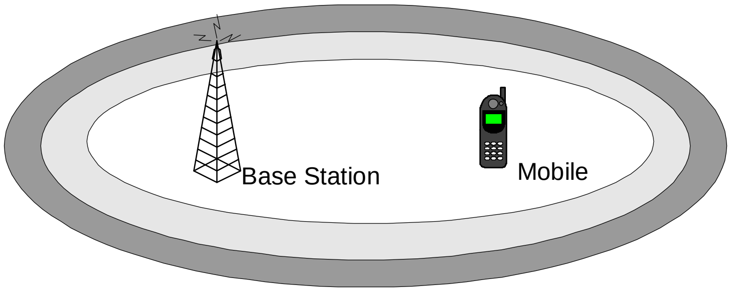

Figure A.10 – Elliptical subregions spatial scatterer density (extracted from [LiRa99]).

Measurement Based Channel Model

Blantz et al [LiRa99] proposed a channel model in which the parameters are based on measurements. The idea behind this approach is to characterise the propagation environment, in terms of scattering points, based on measurement data.

Ray Tracing Models

In recent years, ray tracing techniques have been extensively developed, based on geometric theory, reflection, diffraction, and scattering propagation models. By using site-specific information, such as building databases, this technique deterministically models the propagation channel, including the path loss decay, AoA, and delay spread. However, the high computational burden, and the difficulty in obtaining detailed terrain and building databases, can make ray tracing models difficult to use. Some progress has been made in overcoming the computational burden, and powerful commercial tools that perform site-specific ray tracing coverage analysis are just now becoming available for widespread use.

COST 259 Directional Channel Model

The COST 259 [Corr01] model provides a general and flexible framework that also covers large-scale variations of the channel. The parameter selection relies on previous models as well as recent measurement results. It uses the findings of Hata-Okumura and Walfisch-Ikegami, as well as COST231, for modelling the path loss in different environments, COST207 for global power delay profiles in macro-cells, TSUNAMI-II in respect to the azimuth-delay-power spectrum shape of clusters in macro-cells, and severely influenced by the CODIT radio environment selection in micro- and pico-cells. The approach of distinction between global/local and location-dependent instead of time dependent channel functions stems from the Magic WAND project, while the clustering approach comes from the METAMORP project.

To account for different topographical and electromagnetic features of the surroundings, a 3-level structure has been defined for the COST259 directional channel model (COST259-DCM), Figure A.11. At the top level, a first distinction has been made for the cell type, and for each one, a number of Radio Environments (REs) have been identified. The topographical features of a RE are given by a number of external parameters, such as the frequency bands, the average height of BS and MT, their average distance, average building heights and separations, etc. Furthermore, in micro- and pico-cells, it has been defined whether the propagation has a LoS or Non-LoS property. The propagation conditions encountered in each RE are characterised statistically by a set of PDFs and/or statistical moments. Since the members of this set characterise propagation conditions for the entire RE, they are referred to as Global Parameters (GPs). They serve as key channel parameters that provide the necessary information for the basic system design decisions on modulation technique, burst length, coding scheme, etc, and they have to be extracted from extensive measurement data.

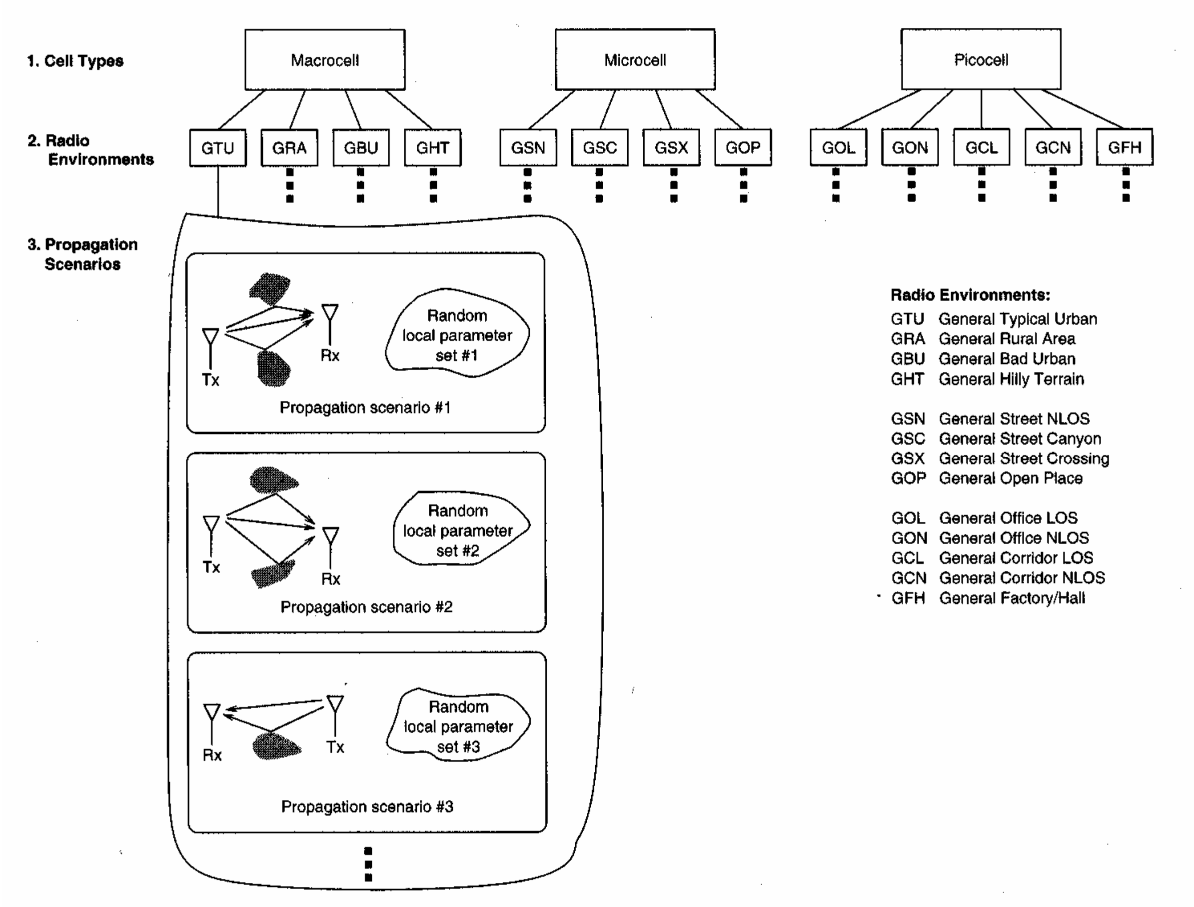

Figure A.11 – Structure of COST259-DCM (extracted from [Corr01]).

The third level of DCM consists of propagation scenarios, which are defined as random realisations of incidence constellations, the latter being specified by random Local Parameters (LPs). A possible set of LPs may be given by parameters of the waves impinging at the location of the receiver antenna, i.e. their number, complex amplitude, delay, and incidence direction, or equivalently, by describing the location of the BS, MT, and the scattering objects interacting with the electromagnetic field. The statistical properties of the LPs are given by a set of global parameters defined in the second level of COST259-DCM.

Annex B – Adaptive Algorithms

Some non-blind algorithms are described in what follows:

- **Least Mean Squares**

The most common adaptive algorithm for continuous adaptation is the Least Mean Squares (LMS) algorithm [LiLo96]. It is based on the steepest-descent method, a well-known optimisation method, that recursively computes and updates the weight vector. It is intuitively reasonable that successive corrections to the weight vector in the direction of the negative of the gradient vector should eventually lead to the MMSE, at which point the weight vector assumes its optimum value. The LMS algorithm is simple to implement, however, it has its drawbacks: in addition to its inherent weak characteristics, the dynamic range over which it operates is quite limited; since received signals in a mobile radio system vary by more than 20 dB, power control is required if the LMS algorithm is to be used; alternatively, the normalised algorithm can be used to overcome the dynamic range limitation.

- **Sample Matrix Inversion**

One way to speed up the convergence rate is to employ the direct inversion of the covariance matrix. If the desired and interference signals are known a priori, then the covariance matrix could be evaluated and the optimal solution for the weights could be computed using Sample Matrix Inversion (SMI) [LiLo96]. The SMI approach offers a relatively fast convergence rate. In practice, the signal environment varies with time due to fading and the desired and interference signals are not known. Thus, the BS must continually update the weight vector to adapt to the change in the channel, the updating rate depending on the fading rate of the channel. There are two major problems of the SMI approach: increased computational complexity that cannot be easily overcome through the use of VLSI, and numerical instability resulting from the use of finite-precision arithmetic and the requirement of inverting a large matrix.

- **Recursive Least Squares**

An important feature of the Recursive Least Squares (RLS) algorithm [LiLo96], [GiMC01] is that the inversion of the covariance matrix is replaced at each step by a simple scalar division. This feature reduces the computational complexity while maintaining a similar performance. The convergence rate of the RLS algorithm is typically an order of magnitude faster than that of the LMS algorithm, provided that the signal-to-noise ratio is high.

- **Conjugate Gradient**

The Conjugate type algorithms, such as CG method [GiMC01], are a family of iterative solvers of linear equation systems. In the CG, the new search direction is selected to be R-conjugate to the previous search directions [HeBK99], thus, it should theoretically converge in at most N steps, where N is the rank of the equation to be solved, the algorithm being based on an MMSE approach. Fast convergence of the algorithm combined with the possibility of block processing and good stability makes it suitable for beamforming purposes [GiMC01].

- **Neural networks**

A neural network is a massively parallel interconnected network of simple elements, and their hierarchical organisations are intended to interact with the objects of the real world in the same way as a biological nervous system [LiLo96]. A neural network may consist of a layered or multilayered non-linear network that tries to reproduce human intellectual capabilities through a "learning" or "adapting" process. It is an ideal tool for use in adaptive signal processing. In particular, a signal-processing problem is represented in terms of optimisation, where a cost function matches the energy function of a particular neural network, the neural network arriving at a solution by minimising its energy function. Recurrent networks are usually suitable for this type of processing, in which the output of a neuron is fed back as inputs to other neurons and/or to itself.

Blind algorithms are also of importance, and some are described next:

- **Constant Modulus Adaptive Beamforming**

The Constant Modulus Adaptive Beamforming approach [LiLo96] exploits the low modulus variation of most communication signals with Frequency Modulation (FM), Phase Shift Keying (PSK), Frequency Shift Keying (FSK), or Quadrature Amplitude Modulation (QAM) modulation formats. Under the assumption that the transmitted signal has a constant envelope, the array output should have a constant envelope as well, however, if multipath is present, there is the multipath fading effect and the array output will not have a constant envelope. The objective of constant modulus beamforming is to restore the array output to a constant envelope signal, on average. This can be accomplished by adjusting the array weight vector in such a way as to minimise the cost function, which measures the signal modulus variation.

- **Decision Directed Algorithm**

In the Decision-Directed Algorithm [LiLo96], the tap weights of the adaptive equaliser are adjusted, via an adaptive process, based on the digital bit stream that is fed back from the hard decision process. A reference signal is generated based on the outputs of the threshold decision device, the beamformer output is demodulated, and based on the demodulated signal, the decision device makes a decision in favour of a particular value in the known alphabet of the transmitted data sequence that is closest to the demodulated signal. Modulation of obtained signal gives the reference signal.

- **Cyclostationary Algorithm**

A number of algorithms make use of the cyclostationary properties of certain types of communication signals [LiLo96]. Signals are said to exhibit cyclostationarity if their cyclic autocorrelation or cyclic conjugate correlation are nonzero either at some time delay or at some frequency shift. The cyclostationarity of signals provides a base for signal selection, that is, a particular signal can be extracted from a signal mixture based on its cycle frequency, provided it has one. There is a number of beamforming techniques that makes use of this selectivity of cyclostationary signals, e.g. Self COherence REstoral (SCORE) algorithm.

Annex C – Antenna Array Parameters

Several ULA parameters have been introduced below:

- **Nulls of the AF**

The nulls of AF are given by:

$$\sin\left(\frac{M}{2}y\right)=0 \Rightarrow \frac{M}{2}y = \pm np \Rightarrow \frac{M}{2}\left(kd\sin f_n + g\right)=\pm np \tag{C.1}$$

$$f_n = \arcsin\left[\frac{l}{2p\,d}\left(-g \pm \frac{2n}{M}p\right)\right],\ n=1,2,3...\left(n\neq 0, M, 2M, 3M...\right) \tag{C.2}$$

When n = 0, M, 2M, 3M… the AF attains its maximum values. The number of nulls that can exist is a function of the element separation ***d*** and the phase excitation difference γ [Bala97].

- **Maxima of the AF**

The maximum values of the magnitude of AF occur when

$$\frac{y}{2}=\frac{1}{2}\left(kd\sin f_m + g\right)=\pm mp \tag{C.3}$$

$$f_m = \arcsin\left(\frac{l}{2p\,d}\left(-g \pm 2mp\right)\right),\ m=0,1,2... \tag{C.4}$$

It is usually desirable to have a single major lobe, i.e. ***m*** = 0, which can be achieved by choosing ***d***/λ sufficiently small, then, the argument of the arcsine function becomes greater than unity for ***m*** = 1, 2… and (C.4) has a single solution:

$$f_m = \arcsin\left(\frac{-g\,l}{2p\,d}\right) \tag{C.5}$$

- **The HBPW of the main lobe**

The half-power beamwidth (HPBW) of the main lobe can be calculated by setting the value of AF_n equal to $1/\sqrt{2}$. For AF_n in (2.23):

$$\begin{aligned}&\frac{M}{2}y = \frac{M}{2}\left(kd\sin f_h + g\right)=\pm 1.391\\ &\Rightarrow f_h = \arcsin\left[\frac{l}{2p\,d}\left(-g \pm \frac{2.782}{M}\right)\right]\end{aligned} \tag{C.6}$$

For a symmetrical pattern around f_m (the angle at which maximum radiation occurs), the HPBW can be calculated as:

$$HPBW = 2\left|f_m - f_h\right| \tag{C.7}$$

- **Maxima of minor lobes (secondary maxima)**

For the array factor of (2.23), there are secondary maxima (maxima of minor lobes), which occur approximately when:

$$\sin\left(\frac{M}{2}\psi\right) = \pm 1$$
$$\frac{M}{2}\left(kd\sin\varphi + \gamma\right) = \pm\left(\frac{2s+1}{2}\right)\pi \tag{C.8}$$

$$\varphi_s = \arcsin\left[\frac{\lambda}{2\pi d}\left(-\gamma \pm \left(\frac{2s+1}{2}\right)\pi\right)\right] \; or \tag{C.9}$$

$$\varphi_s = \frac{\pi}{2} - \arcsin\left[\frac{\lambda}{2\pi d}\left(-\gamma \pm \left(\frac{2s+1}{2}\right)\pi\right)\right] \tag{C.10}$$

- **Broadside array**

A broadside array is one that has maximum radiation at φ = 0° (normal to the axis of the array). For optimal solution, both the element factor and the AF should have their maxima at φ = 0°.

From (C.3), it follows that the maximum of the AF would occur when

$$\psi = kd\sin\varphi + \gamma = 0 \tag{C.11}$$

which implies

$$\psi = \gamma = 0 \tag{C.12}$$

This means that the uniform linear array will have its maximum radiation at φ = 0°, if all array elements have the same phase excitation.

To ensure that there are no maxima in other directions, i.e. grating lobes, the separation between the elements should not be equal to multiples of a wavelength:

$$d \neq n\lambda,\; n = 1, 2, 3... \tag{C.13}$$

Assume that $d = n\lambda$. Then,

$$\psi = kd\sin\varphi = \frac{2\pi}{\lambda} n\lambda \sin\varphi = 2\pi n \sin\varphi \tag{C.14}$$

If (C.14) is true, the maximum condition:

$$\psi_m = 2m\pi,\; m = 0, \pm 1, \pm 2... \tag{C.15}$$

will be fulfilled not only for φ = 0 but also for

$$\varphi_g = \arcsin\left(\frac{m}{n}\right),\; m = 0, \pm 1, \pm 2... \tag{C.16}$$

If , for example, $d = \lambda\ (n = 1)$, (C.16) results in two additional major lobes at:

$f_m = \arcsin(\pm 1) \Rightarrow f_{m_{1,2}} = 90°, 270°$

If $d = 2l$ $(n = 2)$, (C.16) results is four additional major lobes at:

$f_m = \arcsin\left(\pm\frac{1}{2}, \pm 1\right) \Rightarrow f_{m_{1,2,3,4}} = 90°, 150°, 210°, 270°$

The best way to ensure the existence of only one maximum is to choose $d_{max} < l$. Then, in case of broadside array ($\gamma = 0$), equation (C.4) produces no solution for $m \geq 1$ [Bala97].

- **Ordinary end-fire array**

An end-fire is one that has its maximum radiation along the axis of the array $f = \pm 90°$, and it might be required that the array radiates only in one direction – either $f = 90°$ or $f = -90°$, resulting in

$$g = -kd,\ for\, f_{max} = 90° \quad \text{(C.17)}$$

$$g = kd,\ for\, f_{max} = -90° \quad \text{(C.18)}$$

If the element separation is multiple of a wavelength, $d = nl$, then in addition to the end-fire maxima, there are also maxima in the broadside directions. As with the broadside array, in order to avoid grating lobes, the maximum spacing between the element should be less than l,

$$d_{max} < l \quad \text{(C.19)}$$

- **Phased (scanning) arrays**

The maximum radiation can be oriented in any direction to form a scanning array. If the maximum radiation is required to be oriented at an angle f_0 ($-90° < f_0 < 90°$), the phase excitation g between the elements must be adjusted so that

$$y = kd\cos f + g\Big|_{f=f_0} = kd\sin f_0 + g = 0 \Rightarrow g = -kd\cos f_0 \quad \text{(C.20)}$$

Thus, by controlling the progressive phase difference between elements, the maximum radiation can be squinted in any desired direction to form a scanning array (this is the basic principle of electronic scanning for phased array operation). Since the scanning must be continuous, the feeding system should be capable of continuously varying the progressive phase g between the elements [Bala97]. To demonstrate the principle of scanning, the radiation pattern of a 10-element array, with separation of $\lambda/2$ between elements for different pattern directions is plotted in Figure C.1.

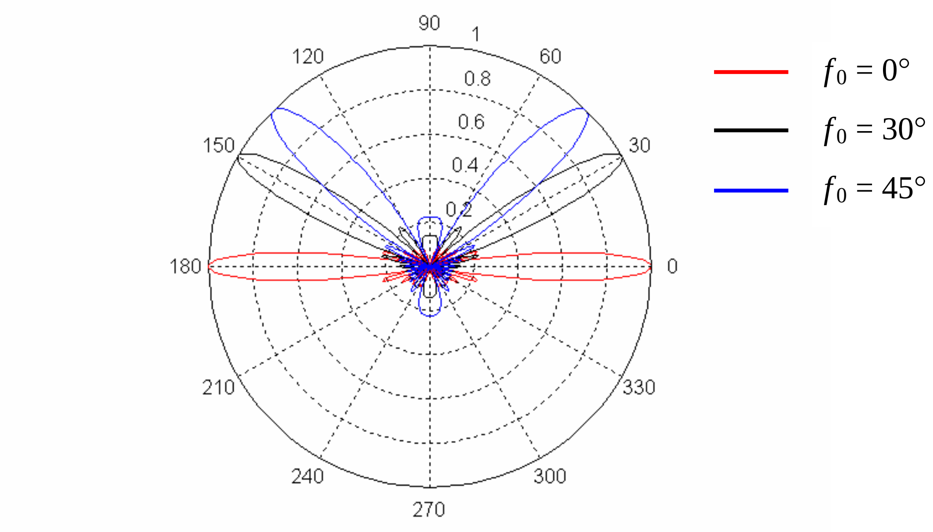

Figure C.1 – Array Factor patterns of a uniform amplitude scanning array.

- **AF for a non-uniform linear array**

If the linear array consists of an even number of elements, located symmetrically along the x-axis, with excitation, which is also symmetrical with respect to x=0, then the array factor is

$$AF^e = \sum_{n=1}^{M} a_n \cos\left[\left(\frac{2n-1}{2}\right) kd \sin q\right] \qquad \text{(C.21)}$$

and for an array consisting of an odd number of elements

$$AF^o = \sum_{n=1}^{M+1} a_n \cos\left[(n-1) kd \sin q\right] \qquad \text{(C.22)}$$

Examples of ULA and UCA patterns

Below some examples of array patterns are presented for different parameters. First, HPBWs of linear and circular array are examined for a fixed number of elements of M=8.

As one can see from Table C.1, HPBW has much larger values, for the same element spacing, for the circular array than linear one.

Table C.1 – Comparison of HPBWs for different element spacings for linear/circular array for fixed number of elements.

Element spacing d	HPBW [°] for M = 8	
	Linear	Circular
$l/2$	12.7	31.5
3/4 l	8.5	20.9
l	6.4	15.6
5/4 l	5.1	12.7
3/2 l	4.2	10.6

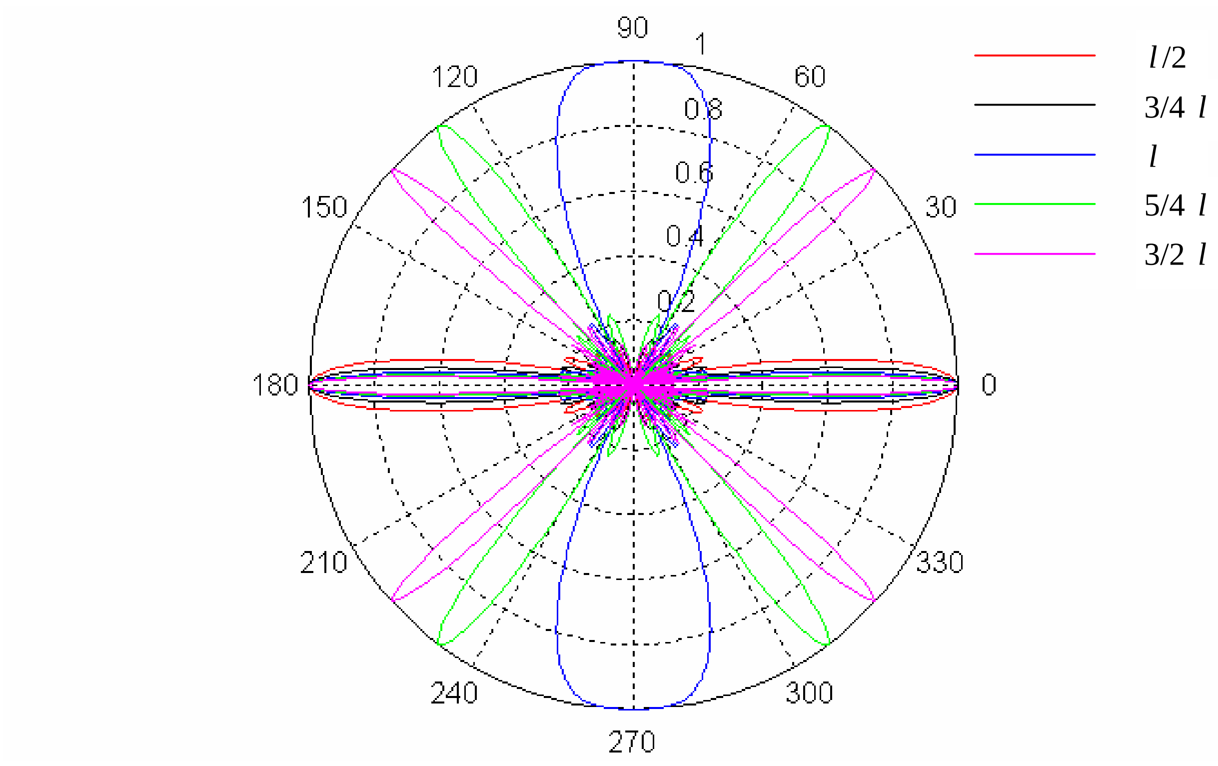

Figure C.2 – Examples of ULA patterns for fixed number of elements and different element spacing.

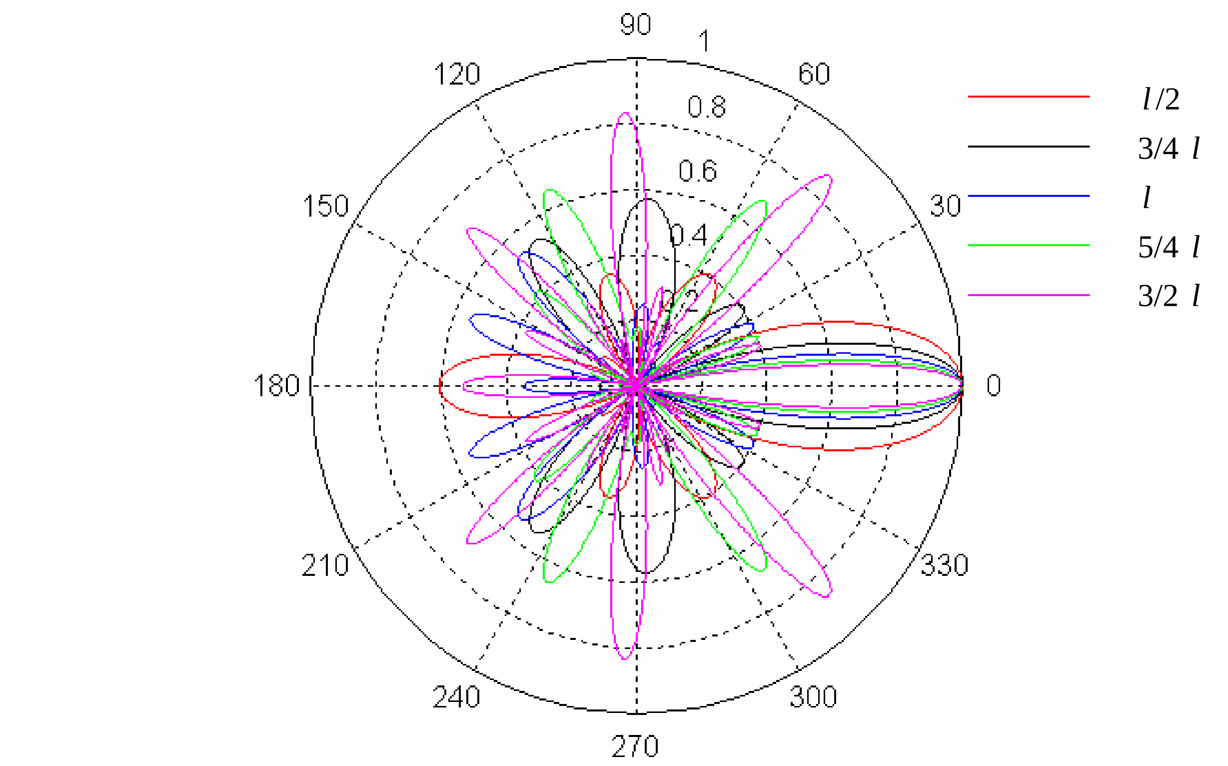

Figure C.3 – Examples of ULC patterns for fixed number of elements and different element spacing.

In Table C.2 different values of HPBW for fixed element spacing ***d*** = *l*/2 and various element number ***M*** have been put together; it is noticeable that one has to use at least twice as much elements in the circular array than in linear array to obtain comparable HPBWs.

Table C.2 – Comparison of HPBWs for different numbers of elements for linear/circular array for fixed element spacing.

Number of elements *M*	HPBW [°] for ***d*** = *l*/2	
	Linear	Circular
2	52.6	52.6
4	25.6	59.1
6	17.0	41.5
8	12.7	31.5
16	6.3	16.6

In Figure C.4 and Figure C.5 one can see some examples of ULA and UCA patterns for fixed element spacing of *l*/2 and different numbers of elements *M*=2,4,6,8.

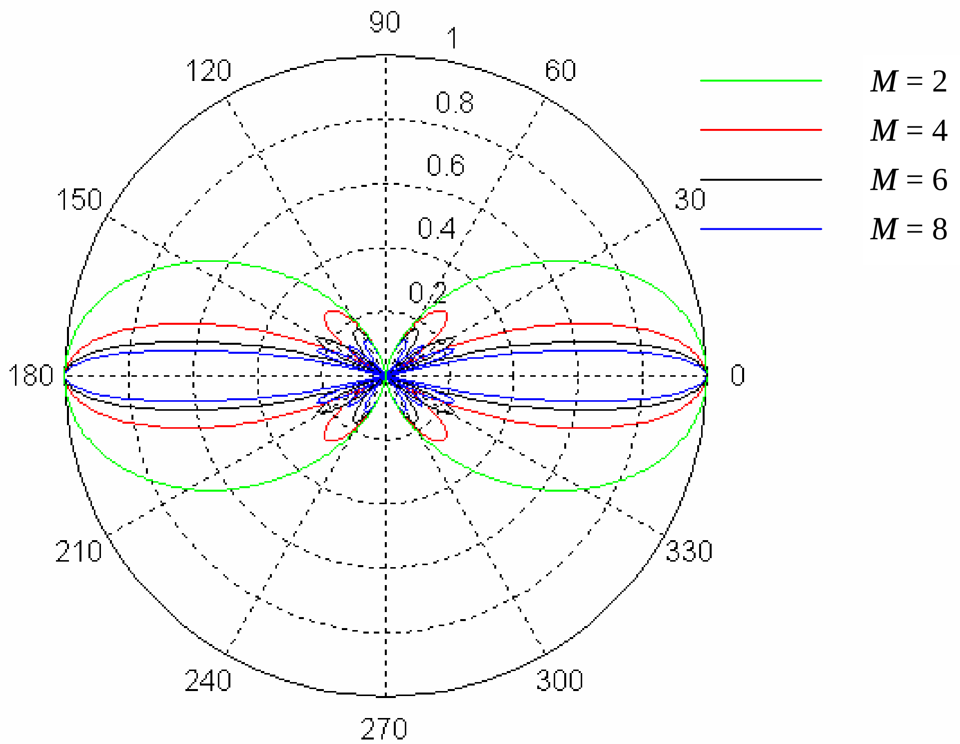

Figure C.4 – Examples of ULA patterns for fixed element spacing and different numbers of elements.

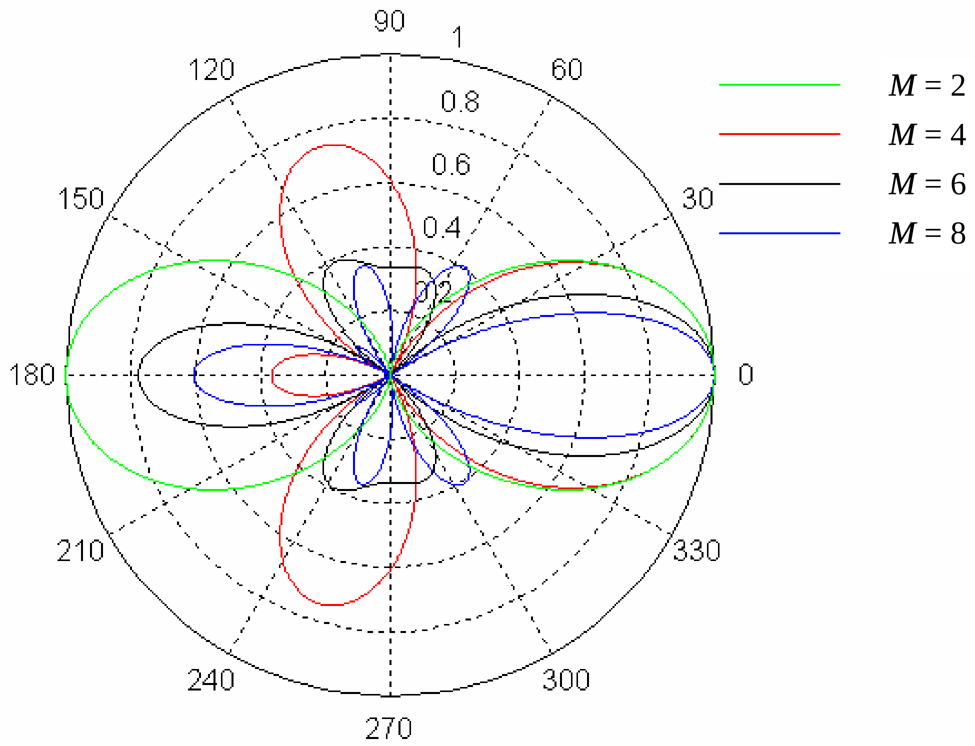

Figure C.5 – Examples of UCA patterns for fixed element spacing and different numbers of elements.

As an example, for circular 12-element array with spacing of 3/4 λ, one has HPBW = 12.7° and the comparable HPBW for a linear array with element spacing of λ/2 should have 8-elements, Figure C.6.

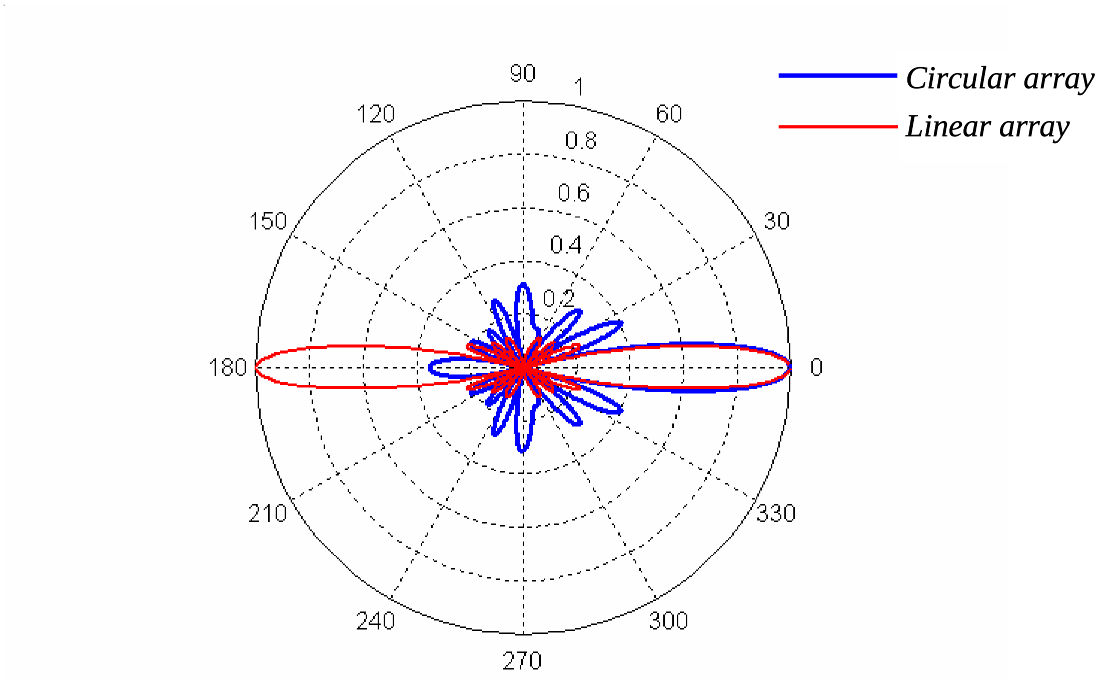

Figure C.6 – Comparison of array patterns for 8-element linear array with λ/2 element spacing and 12-element circular array with 3/4 λ element spacing.

References

[3GPP01a] 3GPP, *General UMTS Architecture*, TS23.101 v4.3.0, Dec 2001, (http://www.3gpp.org)

[3GPP01b] 3GPP, *Spreading and modulation (FDD)*, TS25.213 v5.0.0, March 2001, (http://www.3gpp.org)

[3GPP01c] 3GPP, *Physical Layer – General description*, TS25.201 v4.1.0, Dec 2001, (http://www.3gpp.org)

[Bagh99] Baghaie,R., "Systolic implementation of sample-by-sample conjugate gradient algorithm", in *Proc. of FINSIG'99 – IEEE Finish Signal Processing Symposium*, Oulu, Finland, May 1999

[Bala97] Balanis,C.A., *Antenna Theory: analysis and design*, John Wiley & Sons, New York, USA, 1997

[ChWi00] Chang,S.P. and Willson,A.W., "Analysis of Conjugate Gradient Algorithms for Adaptive Filtering", *IEEE Transactions on Signal Processing*, Vol. 48, No. 2, Feb. 2000, pp. 409-418

[Corr01] Correia,L.M. *Wireless Flexible Personalised Communications*, John Wiley & Sons, Chichester, UK, 2001

[GiCo01a] Gil,J.M. and Correia,L.M., *Application of the RLS and CG Algorithms to Beamforming in TDD and Specific Propagation WDCM Scenarios*, IST-ASILUM Project, Internal Report IST/TUL/IN/Int./057/0.1, IST, Lisbon, Portugal, Sep. 2001.

[GiCo02a] Gil,J.M. and Correia,L.M., "Dependence of Adaptive Beamforming Performance on Directional Channel Modelled Micro-Cell Scenarios", accepted for *PIMRC'2002 – 13th IEEE International Symposium in Personal, Indoor and Mobile Radio Communications*, Lisbon, Portugal, Sep. 2002.

[GiCo02b] Gil,J.M. and Correia,L.M., *Impact of Wideband Directional Propagation Channel Characteristics on Adaptive Beamforming*, submitted to *IEICE Transactions on Communications*, Mar. 2002.

[GiCo02c] Gil,J.M. and Correia,L.M., *Dependence of Adaptive Beamforming Performance on Directional Channel Macro-Cell Scenarios for UMTS*, COST 273, Temporary Document TD(02)050, Espoo, Finland, May 2002.

[GiCo02d] Gil,J.M. and Correia,L.M *Impact of the WDCM on Beamforming*, IST Internal Report, Lisbon, Portugal, Mar. 2002

[GiMC01] Gil,J., Mendez,J., and Correia,L.M., “Comparison of Recursive Least Squares and Conjugate Gradient Applied to Adaptive Beamforming in UMTS”, in *Proc. of IST Mobile Communications Summit 2001*, Barcelona, Spain, Sep. 2001.

[Goda02] Godara,L.C., *Handbook of Antennas in Wireless Communications*, CRC Press, Boca Raton, FL, USA, 2002

[Goda97] Godara,L.C., “Application of Antenna Arrays to Mobile Communications, Part II: Beam-forming and Direction-of-Arrival Considerations”, *Proc. of the IEEE*, Vol. 85, No. 8, Aug. 1997, pp. 1193-1245.

[GoLo96] Golub,G.H. and Loan,C.F. Van, *Matrix Computations*, The John Hopkins University Press, Baltimore, MD, USA, 1996.

[HeBK99] Hernandez, R. I., Baghaie, R. and Kettunen, K., “Implementation of Gram-Schmidt conjugate direction and conjugate gradient algorithms”, in *Proc. of FINSIG’99 – IEEE Finish Signal Processing Symposium*, Oulu, Finland, May 1999

[HoTo01] Holma,H. and Toskala,A., *WCDMA for UMTS*, John Wiley & Sons, Chichester, UK, 2000.

[KALN01] Kaaranen,H., Ahtiainen,A., Laitinen,L., Naghian,S. and Niemi,V., *UMTS Networks*, John Wiley & Sons, Chichester, UK, 2001

[LeMi98] Lee,J.S. and Miller,L.E., *CDMA Systems Engineering Handbook*, Artech House, Boston, MA, USA, 1998.

[LiLo96] Litva,J. and Lo,T., *Digital beamforming in wireless communications*, Artech House, Norwood, MA, USA, 1996.

[LiRa99] Liberti,J. and Rappaport,T., *Smart Antennas for Wireless Communications*, Prentice Hall, Upper Saddle River, NJ, USA, 1999.

[MaCo01] Marques,M.G. and Correia,L.M., “A Wideband Directional Channel Model for UMTS Micro-cells”, in *Proc. of PIMRC’01 – 12th IEEE Personal, Indoor and Mobile Radio Communications Conference*, San Diego, CA, USA, Sep. 2001.

[Marq01] Marques,M.G., *A Wideband Directional Model for Micro-Cells in UMTS*, M.Sc. Thesis, Instituto Superior Técnico, Technical University of Lisbon, Lisbon, Portugal, 2001.

[MPKZ01] Marques,M.G., Pamp,J., Kunisch,J. and Zollinger,E., *Wideband Directional Channel Model and Measurement Campaign*, IST-ASILUM Project, Deliverable D2.3, EC-IST Office, Brussels, Belgium, Oct. 2001 (http://www.nari.ee.ethz.ch/~asilum/).

[RaMe01] Rabanos,J., and Mesquida,C., *Third Generation Mobile Communications* (in Spanish), Telefonica Moviles, Madrid, Spain, 2001

[Shew94] Shewchuk,J.R., *An Introduction to the Conjugate Gradient Method Without the Agonising Pain*, Internal Report, School of Computer Science, Carnegie Mellon University, PA, USA, Aug. 1994, (http://www.cs.cmu.edu/~jrs/jrspapers.html)

[VeBu88] Van Veen,B.D. and Buckley,K.M., ”Beamforming: A Versatile Approach to Spatial Filtering”, *IEEE Acoustics, Speech and Signal Processing Magazine*, Vol. 5, No. 2, Apr. 1988, pp. 4-24.

[ZoMa00] Zollinger,E. and Marques,G., *Wideband Directional Channel Model and Measurement Campaign*, IST ASILUM Project, Deliverable D2.1, IST Central Office, Brussels, Belgium, Nov. 2000.